



**FRIEDRICH-SCHILLER-  
UNIVERSITÄT  
JENA**

---

---

SPATIO-SPECTRAL ENGINEERING OF  
ENTANGLED AND SINGLE PHOTONS IN  
PARAMETRIC DOWN-CONVERSION

---

---

**DISSERTATION**

zur Erlangung des akademischen Grades  
doctor rerum naturalium (Dr. rer. nat.)

vorgelegt dem Rat der  
PHYSIKALISCH-ASTRONOMISCHEN FAKULTÄT  
der  
FRIEDRICH-SCHILLER-UNIVERSITÄT JENA

von

von M. Sc. Baghdasar Baghdasaryan  
geboren am 29.03.1994 in Yeghvard, Armenien

**GUTACHTER:**

1. Prof. Dr. Stephan Fritzsche (Friedrich-Schiller-Universität Jena)
2. Prof. Robert Fickler (Tampere University)
3. Prof. Juan P. Torres (ICFO-Institute of Photonic Sciences )

**TAG DER DISPUTATION: 14.12.2023**

*Dedicated to the memory of my father*



---

## ABSTRACT

---

Engineered photons from spontaneous parametric down-conversion (SPDC) are a valuable tool for studying and applying photonic entanglement, as well as serving as an effective source of single photons. In SPDC, a nonlinear crystal converts a high-energy photon from a laser field into a photon pair, commonly known as *signal* and *idler*. Both the theoretical and experimental research conducted by SPDC has primarily focused on the paraxial regime, where the transverse momentum of photons is referred to as the *spatial* degree of freedom (DOF), and frequency is considered as the *spectral* DOF. Hence, this dissertation also considers the paraxial regime.

Photon pairs generated through SPDC inherently exhibit spatio-spectral coupling, which implies that photons with different spatial DOFs possess varying spectra. While quantum optics applications often focus on either spatial or spectral DOFs independently, the correlation between them poses a fundamental challenge in protocols involving entangled photon sources or single-mode photon states.

Theoretical studies on SPDC, that address both space and spectrum together, are mostly limited to approximate wave functions of photon pairs or involve numerical computations. Such theoretical studies usually consider either monochromatic signal and idler photons (the narrowband approximation), loosely focused pump and collection beams (the plane wave approximation), or infinitesimally thin crystals (the thin crystal approximation).

This dissertation aims to bridge the gap between the fundamental theory of SPDC and its practical applications. In particular, we have developed a comprehensive theory that does not rely on a specific pump beam or nonlinear crystal and goes beyond the common narrowband, plane wave, and thin crystal approximations. The developed approach accurately describes the inseparability of spatial and spectral DOF and applies to a wide range of experimental setups. Furthermore, we show that the origin of the spatio-spectral coupling is closely related to the Gouy phase of the interacting beams.

We utilize the developed theory, taking into account the spatio-spectral coupling insights, to control the entanglement of photon pairs from SPDC. As an application, we shape the spatial distribution of the pump beam to design an efficient source of high-dimensional entangled states in the spatial DOF. In our second application, we tailor simultaneously the effective nonlinearity of the crystal and spatial distribution of the pump, to engineer single-mode photons.



---

## ZUSAMMENFASSUNG

---

Konstruierte Photonen aus der spontanen parametrischen Fluoreszenz (engl. SPDC) sind ein wertvolles Instrument zur Untersuchung und Anwendung der photonischen Verschränkung und dienen außerdem als effektive Quelle für Einzelphotonen. Bei SPDC wandelt ein nichtlinearer Kristall ein hochenergetisches Photon aus einem Laserfeld in ein Photonenpaar um, wobei die erzeugten Photonen als Signal und Idler bekannt sind. Sowohl die theoretische als auch die experimentelle SPDC-Forschung hat sich in erster Linie auf die paraxialen Näherung konzentriert, wobei der Transversalimpuls der Photonen als räumlicher und die Frequenz als spektraler Freiheitsgrad betrachtet wird.

Durch SPDC erzeugte Photonenpaare weisen von Natur aus eine räumlich-spektrale Kopplung auf, d.h. dass Photonen mit unterschiedlichen räumlichen Freiheitsgraden unterschiedliche Spektren besitzen. Während sich Anwendungen der Quantenoptik häufig entweder nur auf die räumlichen oder die spektralen Freiheitsgrade konzentrieren, stellt die Kopplung zwischen ihnen eine grundlegende Herausforderung bei Protokollen dar, die verschränkte Photonenquellen oder Einzelmoden-Photonenzustände beinhalten. Theoretische Studien über SPDC, die sowohl den Raum als auch das Spektrum berücksichtigen, beschränken sich meist auf Näherungen der Wellenfunktion von Photonenpaaren oder beinhalten numerische Berechnungen. In solchen theoretischen Studien werden in der Regel entweder monochromatische Photonen (die Schmalbandannäherung), lose fokussierte Pump- und Sammelstrahlen (die ebene Wellenannäherung) oder unendlich dünne Kristalle (dünne Kristallannäherung) betrachtet.

Ziel dieser Dissertation ist es, die Lücke zwischen der grundlegenden Theorie von SPDC und ihren praktischen Anwendungen zu schließen. Insbesondere haben wir eine umfassende Theorie entwickelt, die sich nicht auf einen bestimmten Pumpstrahl oder nichtlinearen Kristall stützt und über die üblichen Näherungen für Schmalband, ebene Welle und dünne Kristalle hinausgeht. Der entwickelte Ansatz beschreibt genau die Untrennbarkeit von räumlichen und spektralen Freiheitsgraden und ist auf eine Vielzahl von Versuchsanordnungen anwendbar. Darüber hinaus wird in dieser Dissertation gezeigt, dass der Ursprung der räumlich-spektralen Kopplung eng mit der Gouy-Phase der wechselwirkenden Strahlen zusammenhängt.

Wir nutzen die entwickelte Theorie unter Berücksichtigung der Erkenntnisse zur räumlichen und spektralen Kopplung, um die Verschränkung von Photonenpaaren

aus SPDC zu kontrollieren. Als Anwendung manipulieren wir die räumliche Verteilung des Pumpstrahls, um eine effiziente Quelle hochdimensionaler verschränkter Zustände im räumlichen Freiheitsgrad zu schaffen. In unserer zweiten Anwendung passen wir gleichzeitig die effektive Nichtlinearität des Kristalls und die räumliche Verteilung des Pumpstrahls an, um unkorrelierte Einzelphotonen zu erzeugen.



---

## PUBLICATIONS

---

The material presented in this thesis was contributed to the following publications:

- *Enhancing the purity of single photons in parametric down-conversion through simultaneous pump-beam and crystal-domain engineering*  
B. Baghdasaryan, F. Steinlechner, and S. Fritzsche  
*PHYSICAL REVIEW A* **108**, 023718 (2023)
- *Generalized description of the spatio-temporal biphoton state in spontaneous parametric down-conversion*  
B. Baghdasaryan, C. Sevilla-Gutiérrez, F. Steinlechner, and S. Fritzsche  
*PHYSICAL REVIEW A* **106**, 063711 (2022)
- *Spectral properties of transverse Laguerre-Gauss modes in parametric down-conversion*  
C. Sevilla-Gutiérrez, Varun Raj Kaipalath, B. Baghdasaryan, Markus Gräfe, S. Fritzsche, and F. Steinlechner  
*submitted to PHYSICAL REVIEW A*, arxiv: doi: 10.48550/ARXIV.2209.01913

The following publications do not contain thesis work:

- *Maximizing the validity of the Gaussian approximation for the biphoton state from parametric down-conversion*  
B. Baghdasaryan, F. Steinlechner, and S. Fritzsche  
*PHYSICAL REVIEW A* **106**, 063714 (2022)
- *Justifying the thin-crystal approximation in spontaneous parametric down-conversion for collinear phase matching*  
B. Baghdasaryan, F. Steinlechner, and S. Fritzsche  
*PHYSICAL REVIEW A* **103**, 063508 (2021)
- *Enhanced entanglement from Ince-Gaussian pump beams in spontaneous parametric down-conversion*  
B. Baghdasaryan and S. Fritzsche  
*PHYSICAL REVIEW A* **102**, 052412 (2020)



---

## ACKNOWLEDGMENTS

---

I would like to express my deep gratitude and appreciation to all those who have contributed to the successful completion of this thesis.

First and foremost, I am immensely grateful to Prof. Stephan Fritzsche, who provided me with the opportunity to immerse myself in the world of science within his research group. Even back during my bachelor's, he encouraged me to write a scientific paper instead of a regular thesis. This gave me a taste of what real scientific work looks like beyond just studying in class. At this point, I want to especially mention Birger Böning, who guided me in writing my first-ever research paper during my bachelor's studies.

Prof. Fritzsche not only improved my scientific writing during my Ph.D. time but also guided me on how to present a paper's story to capture the community's attention. Our discussions on understanding physics, especially the significance of small details, were invaluable. He also made sure our group had a good balance of work and fun, like the hiking trips we enjoyed together.

I extend my gratitude to Dr. Fabian Steinlechner, who generously shared research ideas with me. Our discussions on current trending topics and potential solutions were invaluable. He not only enhanced my theoretical understanding but also provided insights into practical aspects. He also introduced me to his Ph.D. student, Carlos Sevilla-Gutiérrez, whom I'd like to thank as well. Carlos was always ready to clarify my queries on experimental physics.

And I cannot forget the valuable suggestions, I got from Fabian Steinlechner, René Sondenheimer, Romain Soguel, Darvin Wanisch, Shreyas Ramakrishna, Richard Bernecker, and Carlos Sevilla-Gutiérrez who made major contributions to the readability of the dissertation by proofreading large parts of the manuscript. Their input helped me make my thesis better. I also want to thank Danish Furekh Dar, Yuancheng Wang, Zhongwen Wu, and Andrey Bondarev for their suggestions on how to improve the abstract of the thesis.

I extend my appreciation to everyone in the Atomic Theory Group in Jena, with whom I shared my Ph.D. journey. Our group meetings were very useful for me. The questions from group members guided me in identifying gaps in my understanding and areas for further learning. Also, the time that we spent together outside work, was very enjoyable for me.



---

## CONTENTS

---

|       |  |    |
|-------|--|----|
| 1     | Introduction   | 1  |
| 2     | Mathematical framework and notations   | 7  |
| 2.1   | Basic concepts . . . . .   | 7  |
| 2.2   | Separability and entanglement of bipartite states . . . . .                    | 8  |
| 2.3   | Schmidt Number and Purity . . . . .  | 10 |
| 2.4   | Reduced density operator and purity . . . . .                                  | 11 |
| 2.4.1 | Density operator of a pure state . . . . .                                     | 11 |
| 2.4.2 | Density operator of a mixed state . . . . .                                    | 12 |
| 2.4.3 | Reduced density operator . . . . .   | 13 |
| 3     | Theory of spontaneous parametric down-conversion                               | 15 |
| 3.1   | Nonlinear optics . . . . .   | 15 |
| 3.2   | Hamiltonian of parametric down-conversion . . . . .                            | 17 |
| 3.3   | Paraxial approximation . . . . .   | 19 |
| 3.4   | Biphoton state . . . . .   | 20 |
| 3.4.1 | Time evolution of the biphoton state . . . . .                                 | 20 |
| 3.4.2 | Phase mismatch in the z direction . . . . .                                    | 23 |
| 3.5   | Biphoton state decomposed in Laguerre-Gaussian basis . . . . .                 | 25 |
| 3.5.1 | Laguerre Gaussian decomposition . . . . .                                      | 25 |
| 3.5.2 | Derivation of coincidence amplitudes . . . . .                                 | 26 |
| 3.6   | Experimental verification . . . . .  | 29 |
| 4     | Spatio-spectral coupling in spontaneous parametric down-conversion             | 33 |
| 4.1   | Spectral filtering . . . . .   | 34 |
| 4.2   | Spatio-spectral coupling and the Gouy phase . . . . .                          | 36 |
| 5     | High-dimensional entangled states in the spatial degree of freedom             | 39 |
| 5.1   | Pump beam engineering . . . . .  | 40 |
| 5.1.1 | Narrowband regime . . . . .  | 40 |
| 5.1.2 | Broadband regime . . . . .   | 42 |
| 5.2   | Schmidt number and the purity of the subspace state . . . . .                  | 43 |
| 5.3   | Schmidt number and the purity of the full state . . . . .                      | 44 |
| 5.4   | N-dimensional state in the OAM basis . . . . .                                 | 45 |
| 6     | Spatially indistinguishable single mode photons from domain-engineered crystal | 49 |
| 6.1   | Spatial biphoton state . . . . .   | 50 |

|       |  |    |
|-------|--|----|
| 6.2   | Optimal parameters for high purity . . . . .   | 51 |
| 6.2.1 | Bulk and periodically poled crystals . . . . . | 52 |
| 6.2.2 | Gaussian nonlinear response . . . . .          | 55 |
| 6.3   | Crystal engineering . . . . .                  | 56 |
| 6.3.1 | Optimal susceptibility function . . . . .      | 56 |
| 6.3.2 | Custom poling . . . . .                        | 58 |
| 6.4   | Pump engineering . . . . .                     | 60 |
| 6.5   | Efficiency of pump engineering . . . . .       | 61 |
| 7     | Conclusions and Outlook                        | 65 |
|       | Bibliography                                   | 71 |
|       | Declaration                                    | 87 |

---

## LIST OF FIGURES

---

|            |   |    |
|------------|---|----|
| Figure 1.1 | Introduction to the spontaneous parametric down-conversion (SPDC) process . . . . .     | 3  |
| Figure 3.1 | Geometry of the pump and collection beams with respect to the crystal. . . . .          | 22 |
| Figure 3.2 | Mode correlation matrix of the Laguerre-Gaussian (LG) decomposition . . . . .           | 30 |
| Figure 3.3 | Spectra of different spatial modes of the LG decomposition . . . . .                    | 31 |
| Figure 4.1 | Spatio-spectral coupling as a function of the bandwidth of spectral filters . . . . .   | 35 |
| Figure 4.2 | Trade-off between the brightness and the bandwidth of spectral filters . . . . .        | 36 |
| Figure 4.3 | Interplay of the Gouy Phase and the spectrum of spatial modes . . . . .                 | 38 |
| Figure 5.1 | High-dimensional entangled states in the orbital angular momentum (OAM) basis . . . . . | 42 |
| Figure 5.2 | A three-dimensional entangled state in the OAM basis . . . . .                          | 47 |
| Figure 5.3 | A five-dimensional entangled state in the OAM basis . . . . .                           | 48 |
| Figure 6.1 | Periodically poled crystal . . . . .  | 52 |
| Figure 6.2 | Purity as a function of the pump beam waist and the crystal length . . . . .            | 53 |
| Figure 6.3 | Pair collection probability as a function of the beam parameters . . . . .              | 54 |
| Figure 6.4 | Custom poled crystal . . . . .  | 55 |
| Figure 6.5 | Comparison of a Gaussian with an optimized nonlinearity . . . . .                       | 57 |
| Figure 6.6 | Convergence of the cosine series . . . . .  | 58 |
| Figure 6.7 | phase matching function of the custom poled crystal . . . . .                           | 59 |
| Figure 6.8 | Enhanced purity by pump beam engineering . . . . .                                      | 62 |
| Figure 7.1 | Selection rule for the radial mode correlations . . . . .                               | 67 |
| Figure 7.2 | Broad spectrum from a superposition of Bessel pump beams . . . . .                      | 68 |

---

## ACRONYMS

---

|      |  |
|------|--|
| SPDC | spontaneous parametric down-conversion |
| DOF  | degree of freedom                      |
| DOFs | degrees of freedom                     |
| LG   | Laguerre-Gaussian                      |
| HG   | Hermite-Gaussian                       |
| IG   | Ince-Gaussian                          |
| OAM  | orbital angular momentum               |
| GBS  | Gaussian boson sampling                |
| SMF  | single-mode fiber                      |
| FWM  | four-wave mixing                       |
| TAM  | total angular momentum                 |
| CW   | continuous wave                        |
| KTP  | potassium titanyl phosphate            |

---

## TOOLS AND METHODS

---

This document was typeset using the typographical look-and-feel `classicthesis` developed by André Miede and Ivo Pletikosić.

The content of this thesis primarily encompasses analytical work. Wherever results are shown for specific physical parameters, computational tools have been employed to evaluate the respective analytical expressions for numerical values. In particular, Wolfram Mathematica v. 12.3 [1] was used for the results shown in Sec. 3.6, in Sec. 4.1, in Sec. 4.2, in Sec. 5.1, and Cuba library for multidimensional numerical integration [2] in Sec. 6.2 and in Sec. 6.3. In Sec. 6.3.2, we have utilized the code provided by Dosseva *et al.* [3], to determine the customized poling of a crystal. Moreover, all figures shown in this thesis have been created with Wolfram Mathematica v. 12 and Inkscape v. 0.92 [4].



---

## INTRODUCTION

---

Our understanding and perception of the world around us are deeply tied to the interaction of light with matter. The origins of experiments on the light-matter interaction can be traced back to the 17th century when the bright-minded scientist Isaac Newton demonstrated that color is a property of light. He showed through his experiments on the interaction of light with prisms that white light can be separated into a color comb, such as a rainbow. Since then, the study of light-matter interaction has remained at the forefront of the scientific inquiry.

Surprisingly, despite earlier observations of light diffraction by Francesco Grimaldi, Newton proposed that light is composed of small corpuscles. However, this hypothesis was eventually challenged by Thomas Young in 1802, who presented a compelling evidence for the wave nature of light in his renowned double-slit experiment. Another prominent figure, Augustin Jean Fresnel, further supported the wave nature of light through his extensive research on light diffraction.

It was left to James Clerk Maxwell to complete the classical picture of light. Maxwell built upon Michael Faraday's earlier findings that a changing magnetic field creates an electric field. He proposed a reciprocal relationship, suggesting that a changing electric field should also create a magnetic field. This postulate immediately led to the formulation of electromagnetic wave equations [5]. One truly remarkable aspect of Maxwell's theory was the prediction that the electromagnetic field propagates at a constant speed, which turns out to be the speed of light. It was then concluded that light is, in fact, a transverse electromagnetic wave. This idea aligned with the theories of Fresnel, who also deduced that light must be a transverse wave, in order to explain its polarization. This description of light as an electromagnetic wave was experimentally demonstrated by Heinrich Hertz in 1888.

Nevertheless, a few observations were difficult to understand with the existing wave theory of light. One of the most prominent experiments was the photoelectric effect, namely the emission of electrons when light hits a material. In 1905, Albert Einstein provided a successful explanation for the photoelectric effect by proposing that light consists of discrete bundles, or quanta, of energy [6]. This reintroduction of the particle nature of light differed from Newton's corpuscles, which were understood

as particles localized in space. Instead, the concept of Einstein emphasizes the discrete nature of energy. This idea of energy quantization was not entirely new. A few years earlier, Max Planck had addressed the issue of black body radiation by proposing that thermal radiation is emitted and absorbed in discrete energy packets [7].

On one hand, light showed a wave character in the experiments of Young and Fresnel, on the other hand, the black body radiation and the photoelectric effect demonstrated the particle nature of light. In 1924, Louis de Broglie introduced the concept of wave-particle duality to explain these observations. He highlighted that particles can exhibit both, wave-like and particle-like characteristics. The capstone of these developments was the arising of quantum mechanics, which took place in the summer and winter of 1925 mainly through the works of Werner Heisenberg, Max Born, Pascual Jordan, Paul Dirac, and Erwin Schrödinger.

A significant milestone in the experimental study of light-matter interaction was the development of the laser by Maiman in 1960 [8]. A laser is a bright, coherent light with a fixed and stable wavelength. Prior to the development of lasers, experiments relied on incoherent light sources like sunlight, candlelight, sodium lamps, or light bulbs. The development of lasers revolutionized numerous fields of science and technology, spanning biotechnology, precision measurements, communication, and remote sensing. Another important consequence of the laser invention was the establishment of a new research field of light-matter interaction, referred to as nonlinear optics [9].

Nonlinear optics encompasses the study of how the optical properties of a material system can be altered by the presence of light. These processes are called *nonlinear* since they occur when the response of a material system to an applied optical field does not depend linearly on the field strength. There are various nonlinear processes, and some fundamental examples include sum-frequency generation, where two input frequencies  $\omega_1$  and  $\omega_2$  are mixed to generate a third photon at frequency  $\omega_3 = \omega_1 + \omega_2$ , difference-frequency generation, where two input frequencies  $\omega_1$  and  $\omega_2$  are mixed to generate a third photon at frequency  $\omega_3 = \omega_1 - \omega_2$ , SPDC, where a single input frequency  $\omega_1$  is spontaneously converted into two new frequencies  $\omega_1 = \omega_2 + \omega_3$ . Among these nonlinear processes, SPDC holds a special place, as the classical theory of light cannot adequately explain the spontaneous appearance of two new frequencies. Instead, a quantum description is required to fully understand the SPDC process. Perhaps, SPDC represents the two main breakthroughs of research on light-matter interaction, (i) the quantum interpretation of light and (ii) the development of nonlinear optics through the invention of lasers.

In SPDC, a nonlinear crystal converts high-energy photons from a laser field into photon pairs, commonly referred to as *signal* and *idler* [10] [see Fig. 1.1 (a) and (b)].

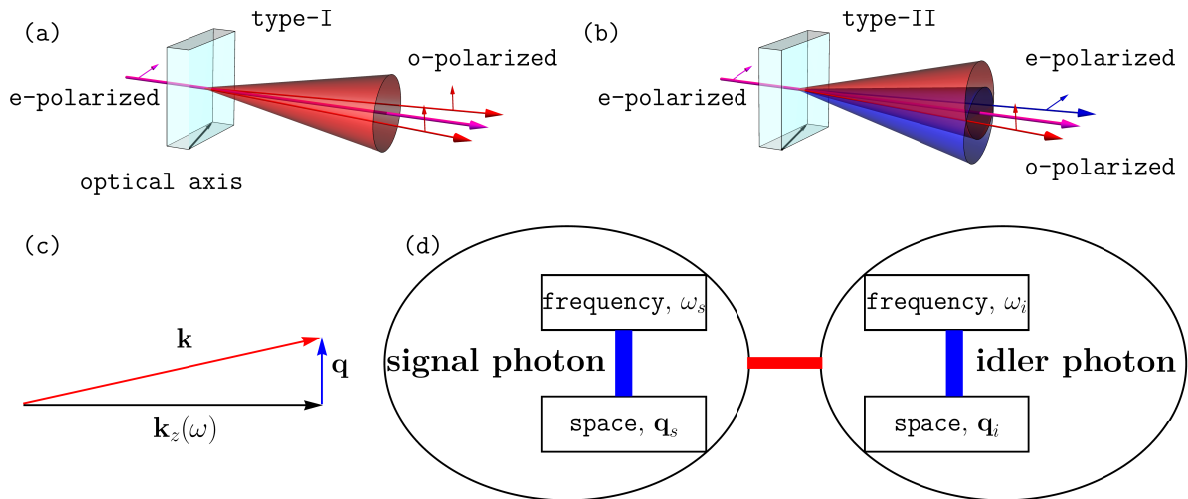


Figure 1.1: Consider the plane formed by the optical axis of the crystal and the propagation direction of the incident beam. The light is classified as *ordinary* polarized (o-polarized) when its polarization is perpendicular to that plane, and *extraordinary* polarized (e-polarized) when its polarization is parallel to the plane. In type-I phase matching [subfigure (a)], both the signal and idler beams are o-polarized and form a single cone, while the pump beam is e-polarized. In type-II phase matching [subfigure (b)], the pump beam is e-polarized, and the signal and idler beams have different polarization, forming two cones. A third possible combination, called type-0, is not shown in the provided figures. In type-0, all beams are o-polarized. (c) The representation of the momentum vector as the sum of transverse and longitudinal components. The paraxial regime is valid, if the transverse momentum of the beam is much smaller than the longitudinal component,  $|\mathbf{q}| \ll k_z$ . (d) Schematic correlations in SPDC. The blue lines represent the spatio-spectral correlations of an individual photon, while the red line indicates the entanglement between signal and idler photons. Decoupling of spatio-spectral correlation implies that the blue lines should disappear. The additional requirement for a pure single-mode photon state is the elimination of the red line.

The quantum nature of SPDC stems from its spontaneous occurrence, similar to the radioactive decay. The splitting of a photon into a photon pair and the exact timing of this event are inherently unpredictable. One of the notable experiments in the field of SPDC was performed in 1995 when Kwiat *et al.* introduced and demonstrated the first efficient source of polarization entanglement [11] in type-II phase matching, [see Fig. 1.1 (b)]. This development marked a milestone in the exploration of entangled photons.

Since then, photon pairs generated via SPDC have become an invaluable experimental platform for fundamental quantum science [12, 13]. They have played a prominent role in various applications within quantum teleportation [14], quantum information processing [15], including recent experiments in photonic quantum computing [16]. Photon pairs from SPDC have been demonstrated to exhibit entanglement not only in the polarization degree of freedom (DOF) [11, 17–19], but also in time bins [20–23], path [24], or in the transverse spatial DOF [25–29] depending on the interplay between

the pump beam and the interaction geometry. In 2022, Anton Zeilinger received a Nobel Prize for his groundbreaking experiments using entangled quantum states from SPDC [30–32].

Theoretical and experimental studies of SPDC have mostly focused on the paraxial regime, which assigns a well-defined direction to the pump, signal, and idler beams. Assuming that the propagation is in the  $z$  direction, the momentum vector can be presented as  $\mathbf{k} = \mathbf{q} + \mathbf{z} k_z(\mathbf{q}, \omega)$ , where the magnitude of the longitudinal component is given by  $k_z = \sqrt{(n\omega/c)^2 - |\mathbf{q}|^2}$  [see Fig. 1.1 (c)]. In the paraxial regime, the three-dimensional momentum vector is then fully described by the two-dimensional transverse momentum vector  $\mathbf{q}$  and scalar frequency  $\omega$ ,  $\mathbf{k} = (\mathbf{q}, \omega)$ . Within the context of paraxial SPDC, the transverse momentum  $\mathbf{q}$  of photons is usually referred to as the *spatial DOF*, and the frequency  $\omega$  as the *spectral DOF* of photons.

Quantum optics applications often focus on either the spatial or spectral DOF, where each DOF is usually addressed independently by employing filtering techniques [33]. In the spatial DOF, much of the research has been motivated by improving fiber coupling efficiency [34, 35] as well as exploring high-dimensional spatial entanglement [26, 36, 37]. Unlike two-dimensional polarization entanglement, high-dimensional entangled states are not limited to two levels but can possess an arbitrary number of discrete levels. These states offer an increased information capacity and exhibit enhanced robustness against background noise and potential hacking attacks in quantum key distribution [38].

In the spectral DOF, the main objective has been to engineer single-mode photon states, as they play a crucial role for protocols based on multiphoton interference [39], measurement-based quantum computing [40, 41], photonic Gaussian boson sampling (GBS) [33, 42] or photonic quantum repeaters [43]. Indistinguishable and pure single-photon states have been generated either by tailoring the nonlinearity of the crystal [3, 44–50] or by using counter-propagating photon pair generation in periodically poled waveguides [51]. Here, the indistinguishability refers to the identical quantum properties of photons, while the purity quantifies the degree to which a single photon is isolated from the environment. A highly pure single photon exhibits minimal correlation with its surroundings, which ensures its integrity as an independent quantum entity.

Nevertheless, the spatial and spectral degrees of freedom (DOFs) of a single photon generated in SPDC have been known to be coupled [see Fig. 1.1 (d)] due to the X-shaped spatiotemporal correlations [52–54]. This coupling poses a fundamental challenge in protocols involving entangled photon sources or pure single photons. It introduces a vulnerability to entanglement and makes it more susceptible to environmental influences. One such example is the generation of high-dimensional

entangled states in the spatial DOF. Any presence of decoherence or noise in the spectral DOF can spread to the spatial DOF and can cause a loss of entanglement or a reduction in its quality.

Except for the spatio-spectral correlation of a single photon, the correlation between photon pairs themselves is disadvantageous in protocols that require pure single-photon states. To see this, suppose a measurement is performed only on the signal photon, without considering the entire composite signal-idler system. In that case, the measured signal photon will be in a mixed state due to its correlation with the idler photon. It is worth noting that the generation of indistinguishable single-mode photons has mostly been limited to the spectral DOF alone, while the impact of engineering the nonlinearity of the crystal on spatial DOF remains largely unexplored.

A number of existing theoretical methods suffer from similar limitations, as they also only consider either the spatial or spectral DOF of photons. For example, the narrowband approximation assumes the generation of a single frequency for both signal and idler photons [55, 56], which can not be achieved with any realistic filter. Furthermore, the plane wave approximation assumes loosely focused pump and collection beams for the signal and idler [52, 57], which results in only a single spatial mode for both photons. Others assume the use of very thin nonlinear crystals [58–63], which eliminates the spatio-spectral coupling. The work presented in [64] utilizes a more realistic theory, but it is based on numerical calculations. Therefore, it is of utmost importance to develop a general analytical theory that does not rely on a specific pump beam or nonlinear crystal and goes beyond the common narrowband, plane wave, and thin crystal approximations. Such a theory will ensure its practical applicability in experimental settings, providing a more accurate and versatile description of entanglement in SPDC. Challenges in developing such a theory include a quantitative description of the spatio-spectral coupling, the consideration of large Hilbert spaces, the use of complex structured pump beams etc.

This dissertation aims to bridge the gap between the fundamental theory of SPDC and its practical applications. In Chap. 3, we develop a comprehensive theory that encompasses the spatio-spectral characteristics of the quantum mechanical state of photon pairs, also known as the biphoton state. This theory accurately describes the inseparability of the spatial and spectral DOFs, and it applies to a wide range of experimental setups. Furthermore, our approach is not limited to a single dispersion relation in the crystal and captures all types of nonlinear crystals, which produce SPDC photons in the quasicollinear regime (pump, signal, and idler photons propagating in the same direction). Moreover, the developed theory is applicable to arbitrary paraxial pump beams and effective nonlinearities of a crystal.

In Chap. 3.5, the biphoton state is decomposed into an LG basis to simplify the state construction. This decomposition allows for a mode-by-mode construction of the state, which proves particularly beneficial when the experiment can only access a part of the full state, referred to as the subspace state. The LG decomposition of the biphoton state will also help us to understand a key aspect of the fundamental nature of spatio-spectral coupling and demonstrate its close relationship with the Gouy phase of the pump, signal, and idler beams [see Chap. 4].

As an application, we employ the developed theory and the understanding of the spatio-spectral coupling to control the entanglement of photon pairs from SPDC. The efficient control of the entanglement is achieved by modifying the effective nonlinearity of a crystal and the spatial distribution of the pump. The primary focus is on the creation of high-dimensional entangled states in the spatial DOF [see Chap. 5] and the generation of pure single-mode photons [see Chap. 6]. Interestingly, these applications require contrasting approaches: Maximizing the correlation between photons is essential for high-dimensional entangled state generation, whereas minimizing the correlation between them is crucial for an efficient single-photon source.

---

## MATHEMATICAL FRAMEWORK AND NOTATIONS

---

In this chapter, we introduce the mathematical tools and notations that will be utilized in this dissertation. Our coverage will not be exhaustive, as it will be more convenient to introduce and discuss some mathematical concepts in the respective chapters.

### 2.1 BASIC CONCEPTS

We adopt the *bra* and *ket* notation introduced by P. A. M. Dirac throughout this thesis [65]. The state of a physical quantum system is represented by a ket vector denoted by  $|\mathbf{a}\rangle$ . This state vector is postulated to contain complete information about the physical system. Mathematically, it represents a vector in an abstract (complex) Hilbert space  $\mathcal{H}$ . In a  $n$ -dimensional vector space  $\mathbb{C}^n$ , a ket vector can be identified with a column vector

$$|\mathbf{a}\rangle = \begin{pmatrix} a_1 \\ \vdots \\ a_n \end{pmatrix},$$

where  $a_n$  are in general complex numbers. Various operations can be carried out on kets. For instance, the addition of two kets results in a new ket  $|c\rangle = |a\rangle + |b\rangle$ . We can also multiply a ket state  $|\mathbf{a}\rangle$  by a complex number  $\alpha$ , which yields another ket,  $\alpha|\mathbf{a}\rangle$ .

Similarly, the concept of the *bra* space can be introduced, which is the *dual* vector space to the ket space. It is postulated that for every ket, there exists a corresponding bra in the dual bra space. This relationship is denoted by  $|\mathbf{a}\rangle^\dagger = \langle \mathbf{a}|$ , where the bra vector is obtained from the ket vector by taking the conjugate transpose. Consequently, the bra vector  $\langle \mathbf{a}|$  can be represented in a  $n$ -dimensional vector space  $\mathbb{C}^n$  as a row vector

$$\langle \mathbf{a}| = (a_1^* \ \dots \ a_n^*).$$

Within the bra and ket notations, an important mathematical operation known as the inner product is defined. The inner product of a bra  $\langle a|$  and a ket  $|b\rangle$  is denoted as  $\langle a, b\rangle$ . Two fundamental properties of the inner product should be mentioned. First, the relation  $|a\rangle^\dagger = \langle a|$  implies that

$$\langle a, b\rangle = \langle b, a\rangle^*.$$

Second, the inner product is a positive definite metric

$$\langle a, a\rangle \geq 0,$$

where the equality sign holds only if  $|a\rangle$  is a null ket,  $|a\rangle = \mathbf{0}$ . The inner product of two vectors can be zero, even if none of them is a null ket

$$\langle a, b\rangle = 0.$$

In this situation,  $|a\rangle$  and  $|b\rangle$  are called orthogonal kets.

The properties of the inner product are essential for the probabilistic interpretation of quantum mechanics. In that interpretation, it is also necessary for ket vectors to be normalized. The normalization of the ket  $|\tilde{a}\rangle$  can be achieved as follows

$$|a\rangle = \frac{1}{\langle \tilde{a}, \tilde{a}\rangle} |\tilde{a}\rangle.$$

Here, the normalized ket  $|a\rangle$  satisfies  $\langle a, a\rangle = 1$ , where  $|\tilde{a}\rangle$  is assumed to be a non-null ket.

## 2.2 SEPARABILITY AND ENTANGLEMENT OF BIPARTITE STATES

The quantum systems are usually not isolated from each other, instead, they interact. The simplest scenario is the interaction of two systems A and B, with respective Hilbert spaces  $\mathcal{H}_A$  and  $\mathcal{H}_B$ . The Hilbert space of the composite bipartite system is the *tensor* product of the two Hilbert spaces  $\mathcal{H}_A \otimes \mathcal{H}_B$ . We introduce a complex orthonormal basis set for each Hilbert space, denoted as  $|a_i\rangle$  for  $\mathcal{H}_A$  and  $|b_j\rangle$  for  $\mathcal{H}_B$ . The most general state in the composite space  $\mathcal{H}_A \otimes \mathcal{H}_B$  is then given by

$$|\psi\rangle = \sum_{i,j} \psi_{ij} |a_i\rangle |b_j\rangle, \quad (2.1)$$

where  $\psi$  can be understood as the coefficient matrix of the composite state with matrix elements  $\psi_{ij}$ . The state Eq. (2.1) is called separable if it is possible to express the



composite state as a product state from individual Hilbert spaces  $|\psi\rangle = |\psi\rangle_A \otimes |\psi\rangle_B$ . The individual states of a separable state are treated independently, i.e., measurements on one system do not affect the outcomes of measurements on the second system. However, this state cannot always be written as a product state,  $|\psi\rangle \neq |\psi\rangle_A \otimes |\psi\rangle_B$ .

We observe correlations between the two systems from  $\mathcal{H}_A$  and  $\mathcal{H}_B$ , when the composite state is not separable. The composite state needs to be treated as a whole, and the individual systems cannot be considered independently anymore. A state that is not separable is called an *entangled state*. Entangled quantum states are not separable, regardless of the spatial separation of their components. This is a manifestation of an aspect of quantum mechanics known as quantum nonlocality.

In order to clarify the concept of entanglement, we consider a system of a photon pair with defined polarization. We assume that each photon can have two polarization states, horizontal (H) and vertical (V), denoted by the states  $|H\rangle$  and  $|V\rangle$ . We define two composite states in the following way

$$|\Phi\rangle = \frac{1}{\sqrt{2}}(|H\rangle_A |V\rangle_B + |V\rangle_A |V\rangle_B), \quad |\Psi\rangle = \frac{1}{\sqrt{2}}(|H\rangle_A |V\rangle_B + |V\rangle_A |H\rangle_B).$$

Although they may initially appear similar, there is a crucial distinction between these two states. The state  $|\Phi\rangle$  is a separable state, while the state  $|\Psi\rangle$  is an entangled state. In fact, the first state can be written as

$$|\Phi\rangle = \frac{1}{\sqrt{2}}(|H\rangle_A + |V\rangle_A) \otimes |V\rangle_B, \tag{2.2}$$

which is a separable state. The polarization measurement outcome of the second photon is always vertical,  $|V\rangle_B$ , regardless of whether the first photon is measured in the horizontal  $|H\rangle_A$  or the vertical state  $|V\rangle_A$ .

The state  $|\Psi\rangle$  is however, not separable. The polarization measurement of the second photon is correlated with the measurement of the first photon. If the first photon is measured in the horizontal state  $|H\rangle_A$ , the second photon would be measured in the vertical state  $|V\rangle_B$ . Conversely, if the first photon is measured in the vertical state  $|V\rangle_A$ , the second photon would be measured in the horizontal state  $|H\rangle_B$ . The polarization measurement of one photon defines the polarization of the second photon instantaneously, whereas neither of the photons possesses its well-defined polarization prior to the measurement.

## 2.3 SCHMIDT NUMBER AND PURITY

It is straightforward to identify that the state given in Eq. (2.2) is separable. However, determining the separability of a state becomes increasingly challenging when the state is more complex. The Schmidt decomposition of a bipartite state is a valuable tool for identifying whether a state is separable or not [66–69]. In order to construct the Schmidt decomposition of the bipartite state (2.1), we first have to diagonalize the matrix  $\psi$ .

The diagonalization of  $\psi$  is possible when systems A and B have state spaces of the same dimension. Consequently, the singular value decomposition theorem [70] implies that the coefficient matrix  $\psi$  of the state (2.1) can be expressed in the following form

$$\psi = U \Lambda V^\dagger, \quad (2.3)$$

where the matrices  $U$  and  $V$  have orthogonal columns,  $U^\dagger U = 1$  and  $V^\dagger V = 1$ , and the matrix  $\Lambda$  is diagonal with entries  $\Lambda_{kk} = \lambda_k$  and property  $\lambda_k \geq \lambda_{k+1}$ . These diagonal matrix elements are also known as the singular values of the matrix  $\psi$ . The number of nonzero singular values is called the *Schmidt rank* of the matrix.

It follows from Eq. (2.3) that the coefficients  $\psi_{ij}$  can be represented as [66]

$$\psi_{ij} = \sum_{k=1}^r \lambda_k U_{ik} V_{jk}^*,$$

where  $r$  is the Schmidt rank. We can now insert the coefficients  $\psi_{ij}$  back into Eq. (2.1),

$$\begin{aligned} |\psi\rangle &= \sum_{i,j,k} \lambda_k U_{ik} V_{jk}^* |a_i\rangle \otimes |b_j\rangle \\ &= \sum_{k=1}^r \lambda_k \left[ \sum_i U_{ik} |a_i\rangle \right] \otimes \left[ \sum_j V_{jk}^* |b_j\rangle \right], \end{aligned}$$

and introduce two new bases,  $|u_k\rangle = \sum_i U_{ik} |a_i\rangle$  in the Hilbert space  $\mathcal{H}_A$  and  $|v_k\rangle = \sum_j V_{jk}^* |b_j\rangle$  in  $\mathcal{H}_B$ . We finally obtain for the composite state

$$|\psi\rangle = \sum_{k=1}^r \lambda_k |u_k\rangle \otimes |v_k\rangle. \quad (2.4)$$

Expression (2.4) is known as the Schmidt decomposition of the initial state (2.1) with  $|u_k\rangle$  and  $|v_k\rangle$  being the Schmidt modes and  $\lambda_k$  the corresponding singular values. The state (2.4) is the diagonal form of the state (2.1) and consists of a single summation.

Consider now the quantity  $K = 1/\sum_k \lambda_k^4$ , known as the Schmidt number. We have  $\sum_k \lambda_k^2 = 1$ , since the state  $|\psi\rangle$  must be normalized. Consequently, the quantity  $\sum_k \lambda_k^4$  is always smaller than one,  $\sum_k \lambda_k^4 \leq 1$ , or equivalently,  $K \geq 1$ . This implies that the  $K$  can be equal to one if and only if the first singular value is non-zero, namely  $\lambda_1 = 1$ , while  $\lambda_k = 0$  for  $k = 2, 3, \dots$ . In this case, the state (2.4) becomes a separable state

$$|\psi\rangle = |u_1\rangle |v_1\rangle.$$

Therefore, we can conclude that the condition  $K > 1$  serves as a criterion for determining whether a state is entangled or separable.

In general, the Schmidt number is a transparent and experimentally direct measure of entanglement. It can be interpreted as the *average* number of composite states  $|u_n\rangle |v_n\rangle$  involved in the composite state. The larger the value of  $K$ , the higher the entanglement. Besides Schmidt number, various approaches have been developed to experimentally detect and certify high-dimensional entangled states. For more details, we refer to a review article [71].

## 2.4 REDUCED DENSITY OPERATOR AND PURITY

### 2.4.1 Density operator of a pure state

As discussed earlier, the ket vector  $|a\rangle$  can be identified with a column vector in a  $n$ -dimensional vector space  $\mathbb{C}^n$ . We can equivalently describe the same state using the density operator given by

$$\rho = |a\rangle \langle a|. \quad (2.5)$$

The operator  $\rho$  can be identified with a matrix acting on a  $n$ -dimensional vector space  $\mathbb{C}^n$  if the row and column vector representation of bra and ket are considered. Therefore, the density operator is also referred to as a density matrix. The density matrix of the form (2.5) possesses two important features. First, the trace of  $\rho$  is equal to one,  $\text{Tr}(\rho) = 1$ , which follows from the normalization of the state  $|a\rangle$ . Second, the square of the density matrix (2.5) yields the same matrix

$$\rho^2 = |a\rangle \langle a| |a\rangle \langle a| = |a\rangle \langle a| = \rho. \quad (2.6)$$

The so-called *purity* of the state (2.5) is given by

$$\text{Tr}(\rho^2) = \text{Tr}(\rho) = 1, \quad (2.7)$$

where we used the relation (2.6) and the normalization of the state.

The density operator formulation is mathematically equivalent to the state vector approach if the state of the physical system is well known. However, it provides a much more convenient language for thinking about physical systems whose state is not completely known. A quantum system whose state  $|\alpha\rangle$  is known exactly is said to be in a *pure* state with the corresponding density operator (2.5). Otherwise,  $\rho$  describes a *mixed* state.

#### 2.4.2 Density operator of a mixed state

A quantum mechanical experiment is usually performed on an ensemble, which consists of collections of identically prepared physical systems. A collection of physical systems is called a pure ensemble if every member of the ensemble is characterized by the same ket vector. However, ensembles can also include mixtures of different pure ensembles, each assigned with certain probabilities. For instance, we have not yet discussed how to describe quantum-mechanically an ensemble of physical systems for which some, say 70% are characterized by  $|\alpha\rangle$ , and the remaining 30% are characterized by some other  $|\beta\rangle$ . This example is referred to as a mixed state, also known as a statistical mixture. Mathematically, a mixed state is described with the density operator as follows

$$\rho = \sum_i p_i |\alpha_i\rangle \langle \alpha_i|, \quad (2.8)$$

where  $p_i$  represents the probabilities associated with each pure state  $|\alpha_i\rangle$ . The density operator (2.8) contains all the physically significant information we can possibly obtain about the ensemble in question.

Similar to pure states, a mixed state must satisfy the normalization condition  $\text{Tr}(\rho) = \sum_i p_i = 1$ . However, we have a different situation for the purity (2.7). The trace of  $\rho^2$  gives

$$\text{Tr}(\rho^2) = \sum_i p_i^2 \leq \left( \sum_i p_i \right)^2 = 1,$$

where equality holds if and only if the state is pure. Therefore, the purity  $\text{Tr}(\rho^2)$  serves as a criterion for determining how mixed the state is.

### 2.4.3 Reduced density operator

An important utility of the density operator formalism is its applicability to describe subsystems of a composite quantum system individually. Such a description is provided by the reduced density operator. We again consider the bipartite state (2.4), but this time in the density operator formalism

$$\rho_{AB} = |\psi\rangle\langle\psi| = \sum_{k=1}^r \sum_{k'=1}^r \lambda_k \lambda_{k'} |\mathbf{u}_k\rangle |\mathbf{v}_k\rangle \langle\mathbf{u}_{k'}| \langle\mathbf{v}_{k'}|. \quad (2.9)$$

Assume we are only interested in the properties and behavior of the subsystem  $A$ , meaning that all measurements are performed on the subsystem  $A$  without considering the entire composite system. Consequently, we need to calculate the *average* outcome for each measurement on  $A$  by summing over all possible states of the subsystem  $B$ . Mathematically, the averaging over  $B$  is obtained by tracing out the subsystem  $B$  from the joint density matrix. The trace is independent of representation, hence, we can use any basis  $|\mathbf{v}_n\rangle$  from the Hilbert space  $\mathcal{H}_b$  in order to calculate it,

$$\rho_A = \text{Tr}_B(\rho_{AB}) = \sum_n \langle\mathbf{v}_n| \rho_{AB} |\mathbf{v}_n\rangle = \sum_{k=1}^r \lambda_k^2 |\mathbf{u}_k\rangle \langle\mathbf{u}_k|.$$

The state of the subsystem  $A$  is now described by the reduced density matrix  $\rho_A$ . The identification of  $\rho_A$  as a description for the state of the system  $A$  is not immediately apparent. However, its physical justification lies in the fact that the reduced density operator accurately predicts the measurement statistics obtained for the system  $A$ . Similarly, The reduced density matrix of the subsystem  $B$  is derived as follows

$$\rho_B = \text{Tr}_A(\rho_{AB}) = \sum_n \langle\mathbf{u}_n| \rho_{AB} |\mathbf{u}_n\rangle = \sum_{k=1}^r \lambda_k^2 |\mathbf{v}_k\rangle \langle\mathbf{v}_k|.$$

The reduced matrices  $\rho_A$  and  $\rho_B$  exhibit a similar structure to the density matrix of a mixed state given by Eq. (2.8). They describe a statistical mixture of pure Schmidt modes. To ascertain whether the reduced density matrix is genuinely mixed, we need to evaluate its purity

$$\text{Tr}(\rho_A^2) = \text{Tr}(\rho_B^2) = \sum_{k=1}^r \lambda_k^4 = 1/K. \quad (2.10)$$

The relation (2.10) reveals the close connection between the purity of the reduced matrix and the Schmidt number  $K$ . Especially, if the composite state is entangled ( $K > 1$ ), the reduced state of a subsystem will always be in a mixed state. In other

words, when two subsystems are entangled, tracing over one system will result in the second subsystem being in a mixed state, leading to a loss of information.

---

## THEORY OF SPONTANEOUS PARAMETRIC DOWN-CONVERSION

---

We will develop a cohesive quantum description of photon pairs from [SPDC](#) within the paraxial regime in this chapter. A simple-to-use closed expression will be presented for the biphoton state, which encompasses the full spectral and spatial properties of the signal and idler photons.

We will begin with an introduction to the theory of nonlinear optics, to lay the groundwork for our analysis. This will provide the necessary knowledge for understanding the underlying principles of [SPDC](#). Subsequently, we will adopt the quantization of the electromagnetic field, in order to describe the quantum nature of [SPDC](#). Additionally, an experiment will be presented to support and validate the theoretical framework.

Parts of the material presented in this chapter were published or submitted previously in the following references:

*Generalized description of the spatio-temporal biphoton state in spontaneous parametric down-conversion*

B. Baghdasaryan, C. Sevilla-Gutiérrez, F. Steinlechner, and S. Fritzsche  
*PHYSICAL REVIEW A* **106**, 063711 (2022)

*Spectral properties of transverse Laguerre-Gauss modes in parametric down-conversion*

C. Sevilla-Gutiérrez, Varun Raj Kaipalath, B. Baghdasaryan, Markus Gräfe, S. Fritzsche, and F. Steinlechner

*submitted to PHYSICAL REVIEW A*, arxiv: doi: 10.48550/ARXIV.2209.01913

### 3.1 NONLINEAR OPTICS

Light, as an electromagnetic field, is described in free space by the time and position-dependent electric  $\mathbf{E}(\mathbf{r}, t)$  and magnetic  $\mathbf{H}(\mathbf{r}, t)$  fields, satisfying the Maxwell equations. When an electromagnetic wave propagates inside a medium, the electric field acts on each charged particle. The field displaces the positive charges in the direction of the

field and the negative charges in the opposite direction. Consequently, the electric field in the medium consists of the initial electric field  $\mathbf{E}(\mathbf{r}, t)$  and the induced field arising from the electric dipoles. The electric and magnetic fields in the medium are called the electric displacement  $\mathbf{D}(\mathbf{r}, t)$  and the magnetic flux density  $\mathbf{B}(\mathbf{r}, t)$ . Here, we are only interested in the electric field, since the contribution of the magnetic component to the nonlinear processes is relatively weak.

The relationship between the initial electric field and the field in the medium is given by

$$\mathbf{D}(\mathbf{r}, t) = \epsilon_0 \mathbf{E}(\mathbf{r}, t) + \mathbf{P}(\mathbf{r}, t),$$

where  $\epsilon_0$  is the vacuum permittivity, and  $\mathbf{P}$  is called dielectric polarization density. The dielectric polarization density describes the macroscopic sum of electric dipole moments induced by the electric field. It depends on the medium and the applied electric field. In the vacuum, the electric displacement  $\mathbf{D}$  and the electric field  $\mathbf{E}$  are up to a constant identical, since the dielectric polarization density vanishes,  $\mathbf{P} = 0$ . The relationship between the dielectric polarization density  $\mathbf{P}$  and the electric field  $\mathbf{E}$  is approximately linear if the electric field is weak. However, high-order contributions to the dielectric polarization become significant, when the electric field strength increases. If the energy of the electric field is conserved in the process, the dielectric polarization density  $\mathbf{P}$  in terms of the electric field  $\mathbf{E}$  can be represented as a power series in the field strength [9]

$$P_i = \epsilon_0 (\chi_{ij}^{(1)} E_j + \chi_{ijk}^{(2)} E_j E_k + \chi_{ijkl}^{(3)} E_j E_k E_l + \dots), \quad (3.1)$$

where  $\chi^{(n)}$  are tensors of rank  $n$ , also known as the  $n$ -th-order susceptibilities of the medium. The linear term in Eq. (3.1) with susceptibility  $\chi^{(1)}$  accounts for the linear response of the medium to the applied optical field. It describes, for instance, the refraction or dispersion characteristics of the pump field (laser beam) in the medium. The higher-order terms in the expansion describe optical processes in which the dielectric polarization density depends on the strength of the applied optical field in a nonlinear manner.

The medium is referred to as linear if all coefficients  $\chi^{(n)}$  except  $\chi^{(1)}$  are equal to zero. A medium is called nonlinear when it possesses non-zero higher-order susceptibility coefficients. Typically, the higher-order susceptibility coefficients  $\chi^{(2)}$  and  $\chi^{(3)}$  are several orders of magnitude smaller than  $\chi^{(1)}$ , making nonlinear processes observable only at very high field strengths.



## 3.2 HAMILTONIAN OF PARAMETRIC DOWN-CONVERSION

In order to fully comprehend SPDC from a quantum-mechanical perspective, the classical Hamiltonian of the electromagnetic field in the crystal should be derived and subsequently quantized. The total energy density of the electromagnetic field in the medium can be described as follows

$$\mathbf{D} \cdot \mathbf{E} = \mathbf{D}_n \cdot \mathbf{E}_n = \epsilon_0[\mathbf{E}_n + \chi_{nj}^{(1)} \mathbf{E}_j] \cdot \mathbf{E}_n + \epsilon_0 \chi_{nj}^{(2)} E_j E_k E_n, \quad (3.2)$$

where we considered the polarization density up to the second-order term. The first term in Eq. (3.2) is the contribution to the electromagnetic energy with the same initial electric field response of the material. The second term describes nonlinear processes, which involve the mixing of three fields. Spontaneous parametric down-conversion is such a process where the mixing occurs between the pump, signal, and idler beams. Therefore, we focus solely on the second-order contribution to the energy.

In general, the SPDC process depends on the polarization of the pump, signal, and idler fields. However, we can simplify the analysis by considering only the scalar fields. This simplification is possible since the polarization of the interacting beams is typically fixed and remains constant in the experimental realizations of SPDC. Usually, the polarization of the fields is fixed in a way that corresponds to the dominating susceptibility in the crystal. There are three possible combinations of linear polarization states for the three beams, which are determined by their orientation with respect to the optical axis of the crystal. Thereby, one distinguishes between type-0 [72], type-I [73], and type-II [74] phase matching conditions [for more details see Fig. 1.1(a) and (b)].

When the directions of the beams are fixed, the susceptibility tensor operator reduces to a scalar effective nonlinear coefficient,  $\chi_{\text{psi}}^{(2)} \mathbf{e}_p \mathbf{e}_s \mathbf{e}_i = \chi_{\text{eff}}^{(2)}$ , where the unit vectors denote the direction of the corresponding electric fields of the pump, signal and idler beams. Hence, we can now express the interaction Hamiltonian as

$$H_I(t) = \epsilon_0 \int_{\mathcal{V}} d^3 \mathbf{r} \chi_{\text{eff}}^{(2)} E_p(\mathbf{r}, t) E_s(\mathbf{r}, t) E_i(\mathbf{r}, t). \quad (3.3)$$

Here, the integration extends over the volume  $\mathcal{V}$  of the nonlinear medium, and  $E_p(\mathbf{r}, t)$ ,  $E_s(\mathbf{r}, t)$ , and  $E_i(\mathbf{r}, t)$  are the scalar electric fields of the pump, signal, and idler beams, respectively. This interaction Hamiltonian captures the general expression for the contribution to the total energy arising from second-order nonlinear optical processes.

It is mathematically convenient for further discussion to consider the electric field in the momentum space, where it can be expressed as a superposition of plane waves,

$$\mathbf{E}(\mathbf{r}, t) = i \int d^3\mathbf{k} \epsilon_{\mathbf{k}} [\alpha_{\mathbf{k}} e^{i(\mathbf{k}\cdot\mathbf{r} - \omega_{\mathbf{k}}t)} - \alpha_{\mathbf{k}}^* e^{-i(\mathbf{k}\cdot\mathbf{r} - \omega_{\mathbf{k}}t)}].$$

Here we distinguish between the *positive* and *negative* frequency parts of the field

$$\mathbf{E}^+(\mathbf{r}, t) = i \int d^3\mathbf{k} \epsilon_{\mathbf{k}} \alpha_{\mathbf{k}} e^{i(\mathbf{k}\cdot\mathbf{r} - \omega_{\mathbf{k}}t)} = [\mathbf{E}^-(\mathbf{r}, t)]^*,$$

where the factor  $\epsilon_{\mathbf{k}}$  ensures the appropriate unit of the electric field. We adopt the method of the canonical quantization, in order to quantize the free electromagnetic field. In this approach, the amplitude of the field is replaced with the photon annihilation operator, denoted as  $\alpha_{\mathbf{k}} \rightarrow \hat{a}(\mathbf{k})$ ,

$$\hat{\mathbf{E}}^+(\mathbf{r}, t) = \frac{i}{(2\pi)^{3/2}} \int d^3\mathbf{k} \sqrt{\frac{\hbar\omega_{\mathbf{k}}}{2\epsilon_0}} \hat{a}(\mathbf{k}) e^{i(\mathbf{k}\cdot\mathbf{r} - \omega_{\mathbf{k}}t)} = [\mathbf{E}^-(\mathbf{r}, t)]^*.$$

The creation operator  $\hat{a}^\dagger(\mathbf{k})$  creates a photon in the mode characterized by the wavevector  $\mathbf{k}$ , while the annihilation operator  $\hat{a}(\mathbf{k})$  destroys a photon in that mode. The creation and annihilation operators fulfill the common commutator relations for continuous variables

$$[\hat{a}(\mathbf{k}), \hat{a}^\dagger(\mathbf{k}')] = \delta(\mathbf{k} - \mathbf{k}'). \quad (3.4)$$

Alternatively, we can achieve the same quantized form of the electric field by expressing the classical field amplitudes as functions of the conjugate canonical variables  $q$  and  $p$ . The canonical variables need to be then rewritten as operators with the corresponding commutation relation. Finally, we need to express the field operator in terms of creation and annihilation operators, leading us to an equivalent result like in Eq. (3.4).

We can now insert the quantized electric fields into Eq. (3.3)

$$\hat{H}_I(t) = \epsilon_0 \int_{\mathcal{V}} d^3\mathbf{r} \chi_{\text{eff}}^{(2)} [\hat{\mathbf{E}}_p^+(\mathbf{r}, t) + \hat{\mathbf{E}}_p^-(\mathbf{r}, t)] [\hat{\mathbf{E}}_s^+(\mathbf{r}, t) + \hat{\mathbf{E}}_s^-(\mathbf{r}, t)] [\hat{\mathbf{E}}_i^+(\mathbf{r}, t) + \hat{\mathbf{E}}_i^-(\mathbf{r}, t)]. \quad (3.5)$$

The resulting expression for the interaction Hamiltonian is a sum of eight different terms. However, only the terms containing  $\hat{\mathbf{E}}_p^+ \hat{\mathbf{E}}_s^- \hat{\mathbf{E}}_i^-$  and  $\hat{\mathbf{E}}_p^- \hat{\mathbf{E}}_s^+ \hat{\mathbf{E}}_i^+$  lead to energy-conserving processes and thus contribute appreciably to the down-conversion process. The contributions due to the other six terms get averaged out when the interaction Hamiltonian is integrated over time. Therefore, we neglect the contributions due

to these other terms. Neglecting these contributions is equivalent to making the rotating-wave approximation as in the case of treating atomic absorption and emission processes [75]. We note that these approximations hold only for second-order nonlinear optical processes such as SPDC and that certain non-energy-conserving terms may lead to important contributions for the higher-order nonlinear optical processes beyond second-order [76, 77]. Thus, the effective interaction Hamiltonian for the process of parametric down-conversion can be given by the following simplified form

$$\hat{H}_I(t) = \epsilon_0 \int_{\mathcal{V}} d^3\mathbf{r} \chi_{\text{eff}}^{(2)} \hat{E}_p^+(\mathbf{r}, t) \hat{E}_s^-(\mathbf{r}, t) \hat{E}_i^-(\mathbf{r}, t) + \text{H.c.}, \quad (3.6)$$

where H.c. refers to hermitian conjugate.

### 3.3 PARAXIAL APPROXIMATION

Experimentally, the SPDC process has been mostly investigated in the paraxial regime, as most optical elements are designed to support paraxial beams. The theoretical analysis has also predominantly focused on the paraxial regime, not only to align with experimental conditions but also because it enables the derivation of analytical expressions.

In the paraxial regime, beams are characterized by a well-defined direction of propagation, where it is usually assumed to be the  $z$  direction. The momentum vector can be written as  $\mathbf{k} = \mathbf{q} + k_z(\mathbf{q}, \omega)\mathbf{z}$  with the magnitude of the longitudinal component  $k_z = \sqrt{(n\omega/c)^2 - |\mathbf{q}|^2}$ . Here,  $\mathbf{q}$  is the transverse momentum,  $n$  is the refractive index of the medium and  $\omega$  is the frequency. Since the propagation direction is fixed, the three-dimensional momentum vector can be fully described by the two-dimensional transverse momentum vector  $\mathbf{q}$  and scalar frequency  $\omega$ ,  $\mathbf{k} = (\mathbf{q}, \omega)$ .

The electric field operator in the paraxial regime reads

$$\hat{E}^+(\mathbf{r}, t) = \frac{i}{(2\pi)^{3/2}} \int d\mathbf{q} d\omega \sqrt{\frac{\hbar\omega}{2\epsilon_0}} \hat{a}(\mathbf{q}, \omega) e^{i(\mathbf{k}_\perp \cdot \mathbf{r}_\perp + k_z \cdot z - \omega t)},$$

where  $\omega_k$  is replaced with  $\omega$  due to the separate consideration of  $\mathbf{q}$  and  $\omega$  in the paraxial regime. Here, the annihilation (creation) operator destroys (creates) a photon in a plane-wave spatial mode with transverse wave vector  $\mathbf{q}$  and frequency  $\omega$ . The transverse momentum  $\mathbf{q}$  of photons is usually referred to as the spatial DOF and the frequency  $\omega$  to as the spectral DOF of photons.

The full interaction Hamiltonian in the paraxial regime is now given by

$$\begin{aligned} \hat{H}_I(t) = & \epsilon_0 \int_{\mathcal{V}} d\mathbf{r}_\perp dz \chi_{\text{eff}}^{(2)} \iiint d\mathbf{q}_p d\mathbf{q}_s d\mathbf{q}_i d\omega_p d\omega_s d\omega_i A_p(\omega_p) A_s^*(\omega_s) A_i^*(\omega_s) \\ & \times e^{i(\mathbf{q}_p - \mathbf{q}_s - \mathbf{q}_i) \cdot \mathbf{r}_\perp} e^{i(k_{p,z} - k_{s,z} - k_{i,z}) \cdot z} e^{-i(\omega_p - \omega_s - \omega_i)t} \\ & \times \hat{a}(\mathbf{q}_p, \omega_p) \hat{a}^\dagger(\mathbf{q}_s, \omega_s) \hat{a}^\dagger(\mathbf{q}_i, \omega_i) + \text{H.c.}, \end{aligned} \quad (3.7)$$

where the following notation is introduced

$$A_j(\omega_j) = \frac{i}{(2\pi)^{3/2}} \sqrt{\frac{\hbar\omega}{2\epsilon_0}}. \quad (3.8)$$

### 3.4 BIPHOTON STATE

#### 3.4.1 Time evolution of the biphoton state

We have obtained the interaction Hamiltonian (3.7) for parametric down-conversion in the paraxial regime, which can be used to describe the evolution of the biphoton state. In the interaction picture, the time evolution of a state can be expressed using the time-evolution operator

$$|\Psi\rangle = \exp\left(-\frac{i}{\hbar} \int_0^{t'} \hat{H}_I dt\right) |\Psi_{\text{initial}}\rangle, \quad (3.9)$$

where  $t'$  is the interaction time. The state at  $t = 0$ ,  $|\Psi_{\text{initial}}\rangle$ , consists of the initial states of the pump, idler, and signal fields. The pump field is a strong paraxial laser beam, which can be modeled as a multimode coherent state. The signal and idler fields are both initially in the vacuum state. Therefore, the composite initial state is given by

$$|\Psi_{\text{initial}}\rangle = |V(\mathbf{q}, \omega_p)\rangle |\text{vac}\rangle,$$

where  $V(\mathbf{q}, \omega_p)$  is the angular distribution of the pump, and  $|\text{vac}\rangle$  represent the vacuum state.

It is known from experiments that the SPDC interaction is very weak. Hence, we can use a series expansion of the time-ordered exponential in Eq. (3.9). We consider the first order, which corresponds to the generation of a photon pair

$$\exp\left(-\frac{i}{\hbar} \int_0^{t'} \hat{H}_I dt\right) = 1 - \frac{i}{\hbar} \int_0^{t'} \hat{H}_I dt \dots$$

The second and the higher-order terms in the expansion are the states of four- and higher-photon fields. The probability of generation of these fields can be neglected in the low gain regime compared to photon pair generation. In the high gain regime, when the laser intensity increases, higher photon number states become significant. The biphoton state gains a simplified form

$$|\Psi\rangle = |\text{vac}\rangle - \frac{i}{\hbar} \int_0^{t'} \hat{H}_I dt |V(\mathbf{q}_p, \omega_p)\rangle |\text{vac}\rangle, \quad (3.10)$$

where the vacuum term is out of interest. We insert the interaction Hamiltonian from Eq. (3.7) into Eq. (3.10) and arrive at

$$\begin{aligned} |\Psi\rangle = & -\frac{i}{\hbar} \int_0^{t'} dt \epsilon_0 \int_{\mathcal{V}} d\mathbf{r}_\perp dz \chi_{\text{eff}}^{(2)} \int \int d\mathbf{q}_p d\mathbf{q}_s d\mathbf{q}_i d\omega_p d\omega_s d\omega_i \\ & \times A_p(\omega_p) A_s^*(\omega_s) A_i^*(\omega_s) e^{i(\mathbf{q}_p - \mathbf{q}_s - \mathbf{q}_i) \cdot \mathbf{r}_\perp} e^{i(k_{p,z} - k_{s,z} - k_{i,z}) \cdot z} e^{-i(\omega_p - \omega_s - \omega_i)t} \\ & \times \hat{a}(\mathbf{q}_p, \omega_p) \hat{a}^\dagger(\mathbf{q}_s, \omega_s) \hat{a}^\dagger(\mathbf{q}_i, \omega_i) |V(\mathbf{q}_p, \omega_p)\rangle |\text{vac}\rangle + \text{H.c.} \end{aligned} \quad (3.11)$$

We can make a few additional assumptions, to simplify the expression of the biphoton state.

(i) The reduction in pump intensity due to the [SPDC](#) process is much smaller than the average intensity of the pump beam itself. This implies that the quantum state of the pump is effectively constant, i.e., the quantum effects of the pump beam can be neglected in this treatment. Therefore, the annihilation operator of the pump photon can be replaced with the field amplitude of the pump beam. This replacement can also be justified by using the fact that the pump beam is modeled as a multimode coherent state: a coherent state is an eigenstate of the annihilation operator, and the action of  $\hat{a}$  on it,  $\hat{a} |V(\mathbf{q}_p, \omega_p)\rangle$  yields the amplitude of the field.

(ii) If the crystal is pumped by a pulsed laser, the interaction time is essentially determined by the pulse duration. It is assumed that at the time,  $t = 0$  the pump field is zero inside the crystal. We restrict our attention to times  $t$  after the completion of the interaction,  $t > t'$ , i.e., after the pulse has exited the crystal. The interaction Hamiltonian is zero for times before  $t = 0$  or after  $t'$ . Thus, the limits of integration in Eq. (3.10) may be extended to infinity, giving rise to a Dirac delta function

$$\int_{-\infty}^{\infty} dt e^{i(\omega_p - \omega_s - \omega_i)t} \rightarrow \delta(\omega_p - \omega_s - \omega_i).$$

This condition ensures the energy conservation in [SPDC](#). Since we are interested in [SPDC](#) once a steady-state condition has been reached, the integration limits can be extended to infinity for a steady continuous wave ([CW](#)) pump too.

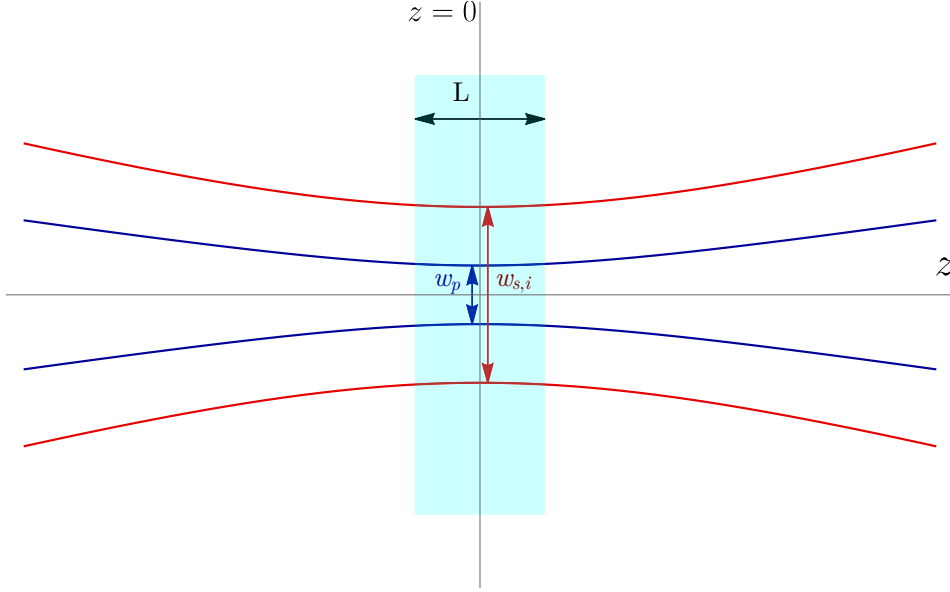


Figure 3.1: Pump (blue line) and collection beams (red line) are all focused in the middle of the crystal at  $z = 0$ .

(iii) The crystal and the pump beam have typical transverse cross-sections in the order of millimeters and micrometers, respectively. Hence, we can assume that the crystal compared to the pump beam is infinitely extended in the transverse direction. This allows us to extend the integration limits in the  $x - y$  plane to infinity, yielding again a Dirac delta function

$$\int d\mathbf{r}_\perp e^{i(\mathbf{q}_p - \mathbf{q}_s - \mathbf{q}_i)\mathbf{r}_\perp} \rightarrow \delta(\mathbf{q}_p - \mathbf{q}_s - \mathbf{q}_i).$$

Assuming the crystal has length  $L$  and it is placed at  $z = 0$ , the remaining spatial integration in the  $z$  direction goes from  $-L/2$  to  $L/2$ .

(iv) The pump and the collection beams propagate in the quasicollinear regime (close to the  $z$  axis), and are assumed to be focused in the middle of the crystal (see Fig. 3.1).

(v) The function  $A_j(\omega_j)$  is slowly varying compared to the pump function and the exponential term in Eq. (3.11). Therefore, we can approximate  $A_j(\omega_j)$  by its value at the central frequency and take it out of the integrals.

These assumptions yield the biphoton state given by

$$\begin{aligned} |\Psi\rangle \propto & -\frac{i}{\hbar} \epsilon_0 \int_{-L/2}^{+L/2} dz \chi_{\text{eff}}^{(2)} \int d\mathbf{q}_s d\mathbf{q}_i d\omega_s d\omega_i e^{i(k_{p,z} - k_{s,z} - k_{i,z}) \cdot z} \\ & \times V(\mathbf{q}_s + \mathbf{q}_i, \omega_s + \omega_i) \hat{a}^\dagger(\mathbf{q}_s, \omega_s) \hat{a}^\dagger(\mathbf{q}_i, \omega_i) |\text{vac}\rangle + \text{H.c.}, \end{aligned}$$

where we omitted the coherent state of the laser since it is in the product state with the biphoton state. This indicates that there is no correlation between the remaining pump field and generated signal, and idler photons.

The final expression for the biphoton state in the paraxial regime in a more compact way reads

$$|\Psi\rangle = \iint d\mathbf{q}_s d\mathbf{q}_i d\omega_s d\omega_i \Phi(\mathbf{q}_s, \mathbf{q}_i, \omega_s, \omega_i) \hat{a}^\dagger(\mathbf{q}_s, \omega_s) \hat{a}^\dagger(\mathbf{q}_i, \omega_i) |\text{vac}\rangle, \quad (3.12)$$

where the so-called biphoton mode function is given by

$$\Phi(\mathbf{q}_s, \mathbf{q}_i, \omega_s, \omega_i) = N_0 V(\mathbf{q}_s + \mathbf{q}_i, \omega_s + \omega_i) \int_{-L/2}^{+L/2} dz \chi_{\text{eff}}^{(2)}(z) e^{i(k_{p,z} - k_{s,z} - k_{i,z}) \cdot z}, \quad (3.13)$$

with  $N_0$  being the normalization constant. The biphoton mode function  $\Phi(\mathbf{q}_s, \mathbf{q}_i, \omega_s, \omega_i)$  contains the rich high-dimensional spatio-spectral structure of SPDC that arises from the coupling between the wave vectors of the pump, signal, and idler beams.

To complete the specification of the biphoton mode function, we need to address the spatial and spectral properties of the pump beam. We will employ an LG beam for the spatial distribution of the pump. The advantage of this choice is that an arbitrary paraxial optical beam can be expressed as a sum of LG beams  $\sum_{p,\ell} a_{p,\ell} \text{LG}_p^\ell$ . The mode numbers  $p$  and  $\ell$  of an LG beam are associated with the radial momentum and the OAM projection of photons, respectively [78]. The theory developed for an LG pump can be easily extended to SPDC with a specific pump configuration. To make this point clear, consider an arbitrary pump beam, where the expansion coefficients  $a_{p,\ell}$  of the decomposition  $\sum_{p,\ell} a_{p,\ell} \text{LG}_p^\ell$  are known. If the known state pumped by an LG beam is denoted by  $|\psi\rangle_{p,\ell}$ , the revised state will be just the linear superposition with the same coefficients,  $\sum_{p,\ell} a_{p,\ell} |\psi\rangle_{p,\ell}$ .

Finally, the temporal distribution of the pump is modeled with a Gaussian envelope of pulse duration  $t_0$ ,  $S(\omega_p) = \exp[-(\omega_p - \omega_{0,p})^2 t_0^2/4] t_0/\sqrt{\pi}$  [79], but which can be extended to any arbitrary pump spectrum. Concluding, the paraxial pump beam used in our derivation of the biphoton state is given by

$$V(\mathbf{q}_s + \mathbf{q}_i, \omega_s + \omega_i) = \text{LG}_p^\ell(\mathbf{q}_s + \mathbf{q}_i) \exp[-(\omega_s + \omega_i - \omega_{0,p})^2 t_0^2/4] t_0/\sqrt{\pi}.$$

### 3.4.2 Phase mismatch in the $z$ direction

The important component of the mode function (3.13) is the phase mismatch in the  $z$  direction  $\Delta k_z = k_{p,z} - k_{s,z} - k_{i,z}$ , which characterizes the differences in the energies

and momenta of the signal and idler photons. Accurate determination of  $\Delta k_z$  is essential for the quantitative description of SPDC, which we will undertake in the following.

Experimentally generated light sources are usually not monochromatic and often exhibit a frequency distribution. Consequently, apart from the central frequencies satisfying the energy conservation  $\omega_{p,0} = \omega_{s,0} + \omega_{i,0}$ , a bandwidth of frequencies is generated around the central frequency  $\omega = \omega_0 + \Omega$ . Here, we assume that the magnitude of the deviation  $\Omega$  from the central frequency is significantly smaller than the central frequency itself, ( $\Omega \ll \omega_0$ ). Furthermore, in the paraxial approximation, the modulus of the transverse momentum is much smaller than the modulus of the momentum  $|\mathbf{q}| \ll k$ . Hence, we can apply the Taylor series on  $k_z$  (Fresnel approximation) to  $|\mathbf{q}|/k$  and also on  $k(\Omega)$  to small  $\Omega$ ,

$$k_z = k(\Omega) \sqrt{1 - \frac{|\mathbf{q}|^2}{k(\Omega)^2}} \approx k + \frac{\Omega}{u_g} + \frac{G\Omega^2}{2} - \frac{|\mathbf{q}|^2}{2k},$$

where  $k$  is the modulus of the momentum vector  $k_j = n_j \omega_j/c$ ,  $n$  is the refractive index,  $c$  is the speed of light in vacuum,  $u_g = 1/(\partial k/\partial \Omega)$  is the group velocity and  $G = \partial/\partial \Omega (1/u_g)$  is the group velocity dispersion, evaluated at the respective central frequency. Here, we also assume that the propagation is along a principal axis of the crystal, so we can ignore the Poynting vector walk-off of extraordinary beams in the crystal. Spatial walk-off occurs only for a light beam with extraordinary polarization, propagating at some angle against the optical axes, so that the refractive index and the phase velocity become dependent on that angle. The walk-off angle can then be calculated from the equation  $\tan \rho = -\partial n_e/\partial \theta/n_e$ . The derivative of the extraordinary index is zero for  $\theta = 0$ .

We can now substitute the corresponding  $k_z$  of the pump, signal, and idler beams into the phase mismatch  $\Delta k_z$  and use the relation  $\rho_p^2 = \rho_s^2 + \rho_i^2 + 2\rho_s\rho_i \cos(\varphi_i - \varphi_s)$  in the cylindrical coordinates  $\mathbf{q} = (\rho, \varphi)$  to arrive at

$$\Delta k_z = \Delta\Omega + \rho_s^2 \frac{k_p - k_s}{2k_p k_s} + \rho_i^2 \frac{k_p - k_i}{2k_p k_i} - \frac{\rho_s \rho_i}{k_p} \cos(\varphi_i - \varphi_s), \quad (3.14)$$

where the frequency part  $\Delta\Omega$  is given by

$$\Delta\Omega = \frac{\Omega_s + \Omega_i}{u_{g,p}} - \frac{\Omega_s}{u_{g,s}} - \frac{\Omega_i}{u_{g,i}} + \frac{G_p(\Omega_s + \Omega_i)^2}{2} - \frac{G_s \Omega_s^2}{2} - \frac{G_i \Omega_i^2}{2}. \quad (3.15)$$

Here, we assumed the momentum conservation at central frequencies,  $\Delta k = k_p - k_s - k_i = 0$ . The condition  $\Delta k = 0$  ensures a constructive interference in the crystal between the pump, signal, and idler beams. The momentum conservation is usually



performed with birefringent crystals [80] or more recently by periodic poling along the crystal axis,  $k_p - k_s - k_i - 2\pi/\Lambda = 0$ , where  $\Lambda$  is the poling period [81].

### 3.5 BIPHOTON STATE DECOMPOSED IN LAGUERRE-GAUSSIAN BASIS

Both the transverse spatial [55, 82] and frequency DOFs [83] have been successfully used in the continuous space for continuous variable information processing (different from quantum information processing associated with quadrature operators). However, the continuous variable space is more often discretized using a set of discrete modes in practical experimental settings. The reason is that discrete modes are easy to manipulate and detect using efficient experimental techniques [84, 85]. The discretization of the biphoton state has been previously done by using Bessel [86], Hermite-Gaussian (HG) [69, 87–89], LG [90–92], or Ince-Gaussian (IG) [93] modes. The discretization of the biphoton state is also useful in those experiments, where the focus is not on the complete biphoton state, but rather on its projection into a finite Hilbert space, also known as a *subspace* state. In this scenario, only a finite number of discrete modes are sufficient to fully describe the experiment.

#### 3.5.1 Laguerre Gaussian decomposition

We discussed in the last subsection that the pump beam will be modeled with an LG beam. The angular distribution of an LG beam in the momentum space is given by

$$LG_p^\ell(\rho, \varphi) = e^{-\frac{\rho^2 w^2}{4}} e^{i\ell \varphi} \sum_{u=0}^p T_u^{p,\ell} \rho^{2k+|\ell|}, \quad (3.16)$$

where  $T_u^{p,\ell}$  reads as

$$T_u^{p,\ell} = \sqrt{\frac{p!(p+|\ell|)!}{\pi}} \left(\frac{w}{\sqrt{2}}\right)^{2u+|\ell|+1} \frac{(-1)^{p+u} (i)^\ell}{(p-u)! (|\ell|+u)! u!}.$$

These LG modes are eigenstates of the OAM operator [94]. In the context of SPDC, the projection of OAM is conserved during down-conversion if the paraxial and quasi-collinear regimes are valid [25, 95, 96]. Therefore, it is convenient to decompose the biphoton state into LG modes. Moreover, in many settings, the biphoton state shows cylindrical symmetry. Hence, it becomes very easy to derive analytical expressions for the LG decomposition of the biphoton state, since the LG modes are cylindrical symmetric too.

The biphoton state in the LG basis  $|p, \ell, \omega\rangle = \int d\mathbf{q} \text{LG}_p^\ell(\mathbf{q}) \hat{a}^\dagger(\mathbf{q}, \omega) |\text{vac}\rangle$  reads

$$|\Psi\rangle = \iint d\omega_s d\omega_i \sum_{p_s, p_i=0}^{\infty} \sum_{\ell_s, \ell_i=-\infty}^{\infty} C_{p, p_s, p_i}^{\ell_s, \ell_i}(\omega_s, \omega_i) |p_s, \ell_s, \omega_s\rangle |p_i, \ell_i, \omega_i\rangle, \quad (3.17)$$

where the coincidence amplitudes are calculated from the overlap integral  $C_{p, p_s, p_i}^{\ell_s, \ell_i} = \langle p_s, \ell_s, \omega_s; p_i, \ell_i, \omega_i | \Psi \rangle$ ,

$$C_{p, p_s, p_i}^{\ell_s, \ell_i}(\omega_s, \omega_i) = \iint d\mathbf{q}_s d\mathbf{q}_i \Phi(\mathbf{q}_s, \mathbf{q}_i, \omega_s, \omega_i) [\text{LG}_{p_s}^{\ell_s}(\mathbf{q}_s)]^* [\text{LG}_{p_i}^{\ell_i}(\mathbf{q}_i)]^*. \quad (3.18)$$

We used the notation  $C_{p, p_s, p_i}^{\ell_s, \ell_i}$  for the coincidence amplitudes, in order to indicate the mode numbers of the pump ( $p, \ell$ ), signal ( $p_s, \ell_s$ ), and idler ( $p_i, \ell_i$ ) photons. The construction of the biphoton state reduces simply to the calculation of  $C_{p, p_s, p_i}^{\ell_s, \ell_i}$ .

The summations in Eq. (3.17) run over all possible mode numbers. As we mentioned, often only a finite number of modes are relevant to the system under consideration. These summations can then be truncated at some reasonable value to get an approximate state to the full biphoton state. This is what we call a subspace state. Truncating the summations in this manner simplifies the mathematical analysis. It allows, for instance, to construct the density matrix or to calculate the Schmidt decomposition of the state very easily. The determination of the Schmidt decomposition is a challenging task to solve for the full biphoton state.

Note, that we discretize here only the transverse spatial DOF, but in principle, it is also possible to discretize the frequency DOF [97].

### 3.5.2 Derivation of coincidence amplitudes

In this subsection, we will present the detailed derivation of the integrals in Eq. (3.18) for the coincidence amplitudes. We will also provide a concise summary at the end of this subsection. An important step of the derivation, which is worth mentioning, is that we will show the conservation of OAM in SPDC.

We first substitute Eqs. (3.13)-(3.16) into Eq. (3.18),

$$C_{p, p_s, p_i}^{\ell_s, \ell_i} = N_0 \sum_{u=0}^p \sum_{s=0}^{p_s} \sum_{i=0}^{p_i} T_u^{p, \ell} (T_s^{p_s, \ell_s})^* (T_i^{p_i, \ell_i})^* \times \int dz d\rho_s d\rho_i d\varphi_s d\varphi_i \Theta(z, \rho_s, \rho_i, \varphi_i - \varphi_s) e^{i\ell\varphi_s} e^{i(-\ell_s\varphi_s - \ell_i\varphi_i)}, \quad (3.19)$$

where the function  $\Theta(z, \rho_s, \rho_i, \varphi_i - \varphi_s)$  is defined as

$$\begin{aligned} \Theta(z, \rho_s, \rho_i, \varphi_i - \varphi_s) = & \chi_{\text{eff}}^{(2)}(z) [\rho_s^2 + \rho_i^2 + 2\rho_s\rho_i \cos(\varphi_i - \varphi_s)]^{\frac{2u+(|\ell|-\ell)}{2}} \rho_s^{|\ell_s|+2s+1} \rho_i^{|\ell_i|+2i+1} \\ & \times \exp \left[ -\frac{[\rho_s^2 + \rho_i^2 + 2\rho_s\rho_i \cos(\varphi_i - \varphi_s)] w^2}{4} - \frac{\rho_s^2 w_s^2}{4} - \frac{\rho_i^2 w_i^2}{4} \right] \\ & \times \exp \left[ iz \left( \Delta_\Omega + \rho_s^2 \frac{k_p - k_s}{2k_p k_s} + \rho_i^2 \frac{k_p - k_i}{2k_p k_i} - \cos(\varphi_i - \varphi_s) \frac{\rho_s \rho_i}{k_p} \right) \right] \\ & \times \frac{t_0}{\sqrt{\pi}} e^{-\frac{t_0^2 (\Omega_s + \Omega_i)^2}{4}} (\rho_s + \rho_i e^{i(\varphi_i - \varphi_s)})^\ell. \end{aligned} \quad (3.20)$$

In Eq. (3.20), the polar angle  $\varphi$  of the pump beam has been expressed as a function of the signal and idler coordinates,

$$e^{i\ell\varphi} = (\cos\varphi + i\sin\varphi)^\ell = \frac{e^{i\ell\varphi_s}}{\rho_p^\ell} (\rho_s + \rho_i e^{i(\varphi_i - \varphi_s)})^\ell,$$

by taking into account the conservation of transverse momentum,

$$\mathbf{q}_p = \mathbf{q}_s + \mathbf{q}_i = \begin{pmatrix} \rho_s \cos\varphi_s + \rho_i \cos\varphi_i \\ \rho_s \sin\varphi_s + \rho_i \sin\varphi_i \end{pmatrix}.$$

The presentation of the coincidence amplitudes  $C_{p,p_s,p_i}^{\ell,\ell_s,\ell_i}$  in Eq. (3.19) with the function  $\Theta(z, \rho_s, \rho_i, \varphi_i - \varphi_s)$  follows the goal to show the OAM conservation in SPDC. To achieve this, we expand the function  $\Theta(z, \rho_s, \rho_i, \varphi_i - \varphi_s)$  as superposition of plane waves with the phases  $\exp[i\ell'(\varphi_i - \varphi_s)]$  (Fourier series with complex coefficients),

$$\Theta(z, \rho_s, \rho_i, \varphi_i - \varphi_s) = \sum_{\ell'=-\infty}^{\infty} f_{\ell'}(z, \rho_s, \rho_i) e^{i\ell'(\varphi_i - \varphi_s)}. \quad (3.21)$$

Subsequently, we substitute Eq. (3.21) into Eq. (3.19) and perform the integrations over the polar angles  $\varphi_s$  and  $\varphi_i$ ,

$$\sum_{\ell'=-\infty}^{\infty} f_{\ell'}(z, \rho_s, \rho_i) \int_0^{2\pi} \int_0^{2\pi} e^{i\ell\varphi_s} e^{i(-\ell_s\varphi_s - \ell_i\varphi_i)} e^{i\ell'(\varphi_i - \varphi_s)} d\varphi_s d\varphi_i \propto \delta_{\ell', \ell - \ell_s} \delta_{\ell', \ell_i}. \quad (3.22)$$

As expected, the Kronecker delta functions appear in Eq. (3.22) which enforce the conservation of OAM  $\ell - \ell_s = \ell_i$ . This conservation holds in the quasicollinear paraxial regime [98], where the spin-orbital angular momentum coupling is not significant [99]. However, in a noncollinear regime, the conservation of total angular momentum (TAM)

becomes crucial, and studying this aspect can be an interesting topic for future investigations.

Going back to the expression (3.19), we now calculate the integrals over polar coordinates  $\varphi_{s,i}$  explicitly. For simplicity, we consider the coincidence amplitudes  $C_{p,p_s,p_i}^{\ell,\ell_s,\ell_i}$  for positive OAM numbers of the pump beam  $\ell \geq 0$ . The coincidence amplitudes for  $\ell < 0$  are then given by  $C_{p,p_s,p_i}^{\ell,\ell_s,\ell_i} = (C_{p,p_s,p_i}^{-\ell,-\ell_s,-\ell_i})^*$ , which follows from Eq. (3.18). Furthermore, the brackets in Eq. (3.20) should be rewritten as finite sums by using the binomial formula. For instance, the first bracket is written as

$$[\rho_s^2 + \rho_i^2 + 2\rho_s\rho_i \cos(\varphi_i - \varphi_s)]^u = \sum_{m=0}^u \binom{u}{m} (\rho_s^2 + \rho_i^2)^{u-m} [2\rho_s\rho_i \cos(\varphi_i - \varphi_s)]^m.$$

The *cosine* function can be expressed as the sum of two exponential functions by using Euler's formula, which should be again expressed as a Binomial sum. After this step, the angular integration takes the form of the integral representation of the Bessel function of the first kind [100]

$$\frac{1}{2\pi} \int_0^{2\pi} e^{in\varphi \pm iz \cos(\varphi - \varphi')} d\varphi = (\pm i)^n e^{in\varphi'} J_n(z).$$

Next, the sum representation of the Bessel function should be used

$$J_n(z) = \sum_{r=0}^{\infty} \frac{(-1)^r}{r! \Gamma(r+n+1)} \left(\frac{z}{2}\right)^{2r+n}, \quad (3.23)$$

which transforms the integration over the radial coordinates into

$$\int_0^{\infty} d\rho \rho^n e^{-a\rho^2} = \frac{\Gamma(\frac{n+1}{2})}{2a^{\frac{n+1}{2}}}.$$

The final result is achieved via summing over  $r$  from Eq. (3.23) by using the definition of the *Regularized* hypergeometric function [101]. The coincidence amplitudes read for  $\ell \geq 0$

$$\begin{aligned} C_{p,p_s,p_i}^{\ell,\ell_s,\ell_i} = & N_0 \pi^{3/2} t_0 e^{-\frac{t_0^2(\Omega_s + \Omega_i)^2}{4}} \delta_{\ell,\ell_s+\ell_i} \sum_{u=0}^{\ell} \sum_{s=0}^{p_s} \sum_{i=0}^{p_i} T_u^{p,\ell} (T_s^{p_s,\ell_s})^* (T_i^{p_i,\ell_i})^* \\ & \sum_{n=0}^{\ell} \sum_{m=0}^u \binom{\ell}{n} \binom{u}{m} \sum_{f=0}^{u-m} \sum_{v=0}^m \binom{u-m}{f} \binom{m}{v} \Gamma[h] \Gamma[b] \\ & \times \int_{-L/2}^{L/2} dz \chi_{\text{eff}}^{(2)}(z) e^{iz\Delta\Omega} \frac{D^d}{H^h B^b} {}_2\tilde{F}_1 \left[ h, b, 1+d, \frac{D^2}{HB} \right], \end{aligned} \quad (3.24)$$

and  $C_{p,p_s,p_i}^{\ell,\ell_s,\ell_i} = (C_{p,p_s,p_i}^{-\ell,-\ell_s,-\ell_i})^*$  for  $\ell < 0$ . The function  ${}_2\tilde{F}_1$  is known as the *regularized hypergeometric* function [101]. The coefficients of Eq. (3.24) are given by

$$\begin{aligned} H &= \frac{w_p^2}{4} + \frac{w_s^2}{4} - iz \frac{k_p - k_s}{2k_p k_s}, & D &= -\frac{w_p^2}{4} - iz \frac{1}{2k_p}, \\ B &= \frac{w_p^2}{4} + \frac{w_i^2}{4} - iz \frac{k_p - k_i}{2k_p k_i}, & d &= \ell_i + m - n - 2\nu, \\ h &= \frac{1}{2}(2 + 2s + \ell + \ell_i + 2(-f + u) - 2n - 2\nu + |\ell_s|), \\ b &= \frac{1}{2}(2 + 2f + 2i + \ell_i + 2m - 2\nu + |\ell_i|), \end{aligned}$$

where  $w_p$ ,  $w_s$ , and  $w_i$  are the beam waists of the pump signal and the idler beams, respectively.

The expression (3.24) for the coincidence amplitudes constitutes the main result of this chapter. It allows the spatial and spectral emission profiles to be reconstructed mode by mode and is applicable in any experimental setting that exhibits cylindrical symmetry. It can be readily used to calculate many characteristics of SPDC: joint spectral density, photon bandwidths, pair-collection probability, heralding ratio, spectral and spatial correlation, and many more. Its novelty in comparison to previous expressions known in the literature is expressed in the correct description of modal spatio-spectral coupling under the non-degeneracy condition. Previously, these could mainly be achieved through numerical calculations or for special cases with a limited scope of applicability.

### 3.6 EXPERIMENTAL VERIFICATION

In this subsection, we present the results of the experimental verification of Eq. (3.24). Two aspects have been tested: the LG mode decomposition of the biphoton state and the joint frequency spectrum of several LG mode. Here, we will not go much into detail about the realization of the experiment, but rather what has been measured and how it compares with the theoretical predictions.

The experiment in Ref. [102] has been restricted to a collimated monochromatic Gaussian pump ( $\lambda_p = 404.8$  nm)

$$V(\mathbf{q}_s + \mathbf{q}_i) = \frac{w_p}{\sqrt{2\pi}} \exp\left(-\frac{w_p^2}{4}|\mathbf{q}_s + \mathbf{q}_i|^2\right),$$

which has been focused by a lens ( $f_1 = 200$  mm) into the center of a 20 mm long type-II periodically poled potassium titanyl phosphate (KTP) crystal producing SPDC around

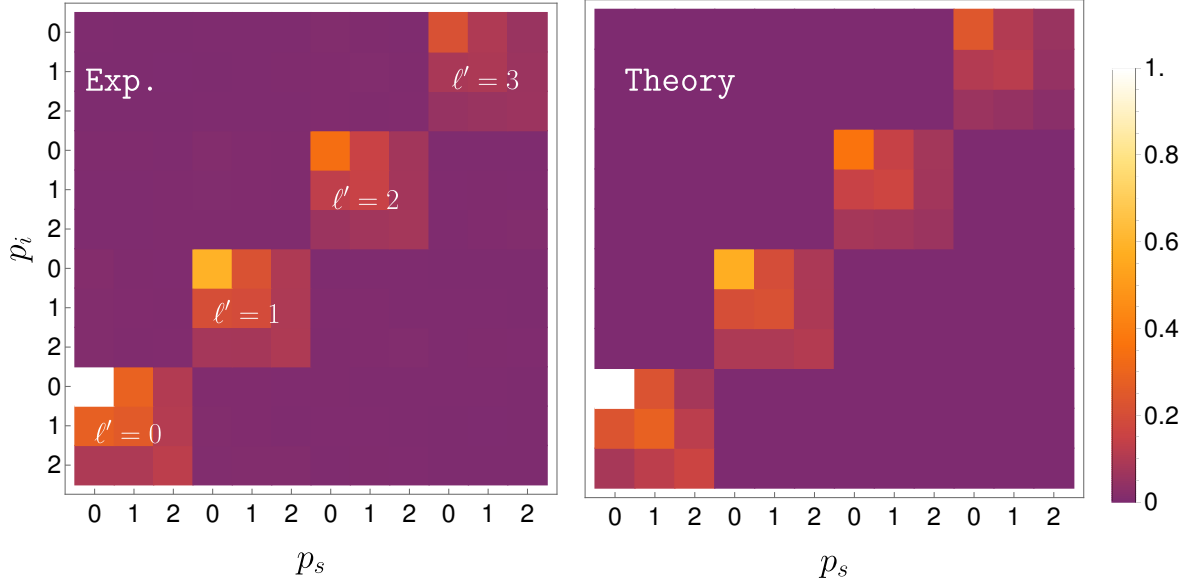


Figure 3.2: Spatial mode decomposition of the spectrally broadband SPDC emission in the subspace of the LG basis  $p_{s,i} = 0, 1, 2$  and  $\ell' = 0, \pm 1, \pm 2, \pm 3$  and for a pump waist  $w_p = 60 \mu\text{m}$  and a collection waist  $w_{s,i} = 30 \mu\text{m}$ .

809.6 nm. The resulting pump waist is  $w_p \approx 60 \mu\text{m}$ . The fact of a CW laser  $S(\omega_p) \propto \delta(\omega_p - \omega_{0,p})$  sets the condition  $\Omega_s = -\Omega_i := \Omega$ . Additionally, OAM conservation ensures  $\ell_s = -\ell_i = 0 := \ell'$ . Therefore, the biphoton state is simplified to

$$|\Psi\rangle = \iint d\Omega \sum_{p_s, p_i=0}^{\infty} \sum_{\ell'=-\infty}^{\infty} C_{p_s, p_i}^{|\ell'|}(\Omega) |p_s, \ell', \Omega\rangle |p_i, -\ell', -\Omega\rangle, \quad (3.25)$$

where the coincidence amplitudes  $C_{p_s, p_i}^{|\ell'|}$  are given by

$$C_{p_s, p_i}^{|\ell'|}(\Omega) \propto \sum_{s=0}^{p_s} \sum_{i=0}^{p_i} \frac{w_p}{\sqrt{2}} (T_s^{p_s, \ell'})^* (T_i^{p_i, -\ell'})^* \int_{-L/2}^{L/2} dz \exp \left[ iz \left( \frac{\Omega}{u_i} - \frac{\Omega}{u_s} - \frac{\Omega^2}{2} (G_i + G_s) \right) \right] \frac{D^{-|\ell'|}}{H^{1+s} B^{1+i}} {}_2\tilde{F}_1 \left[ 1 + s, 1 + i, 1 - |\ell'|, \frac{D^2}{HB} \right]. \quad (3.26)$$

First, we consider the joint mode decomposition of the biphoton state into the LG basis. The spatial mode decomposition has been performed by projecting the biphoton states in different combinations of LG modes  $|l_i, p_i, \ell_s, p_s\rangle \langle l_i, p_i, \ell_s, p_s|$ . Specifically, we focused on the subspace of the LG basis with  $p_{s,i} = 0, 1, 2$  and  $\ell' = 0, \pm 1, \pm 2, \pm 3$ . The collection waists for both the signal and idler photons were fixed at  $w_{s,i} = 30 \mu\text{m}$ . Figure 3.2 displays the experimental and theoretical mode correlation matrix obtained in the broadband regime, without the use of frequency filters. The highest

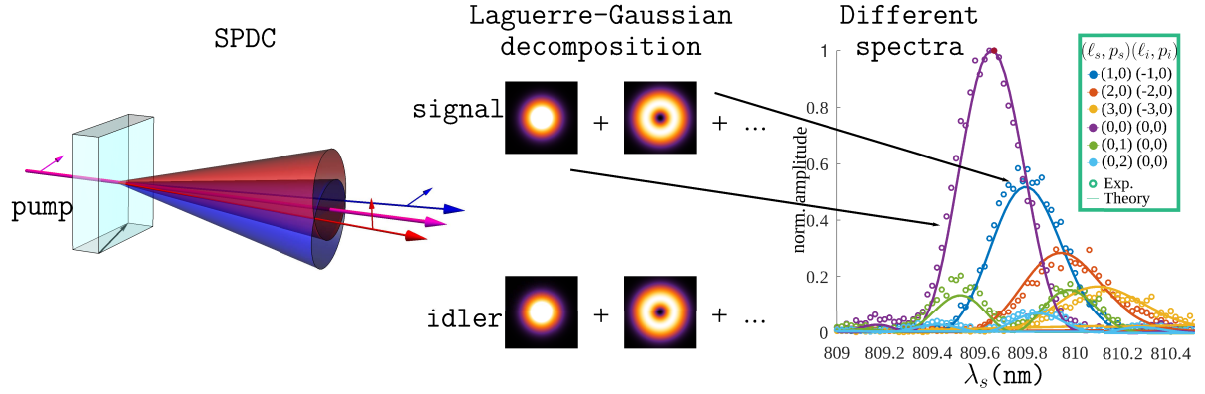


Figure 3.3: Illustration of the biphoton state decomposed into the LG basis. On the right side, the joint spectrum of six modes of the LG decomposition is depicted. Experimental measurements are shown with dotted curves taken from Ref. [102], while the theoretical calculations are presented with solid curves.

amplitude is detected in the fundamental Gaussian mode. The theoretical correlation matrix has been calculated with Eq. (3.26) by summing over the range of frequencies  $\Omega = 4$  nm. As we can see, the mode decomposition of the biphoton state encoded in amplitudes  $C_{p_s, p_i}^{|\ell|}$  agrees remarkably well with the experimental observations.

The spectral dependence of each spatial mode can be analyzed by sending one of the photons to a monochromator. This process automatically projects the idler photon into the spectral state,  $\omega_i = \omega_p - \omega_s$ . Figure 3.3 shows the joint spectrum of different spatial modes. The center wavelength of high-order modes is observed to be shifted from the quasicollinear phase-matched wavelength due to the high transverse momentum contributions. This observation is expected since high-order modes carry a high average transverse momentum magnitude. Consequently, the phase mismatch is compensated at different wavelengths. Here, we again can confirm the agreement between the theory and the experiment. More realizations of the experiment were performed for different crystal lengths, pump, and collection waists. All results show very good agreement with the theoretical predictions.

It is evident from Fig. 3.3 that different spatial LG modes exhibit distinct spectra, i.e., any modification to the spatial properties results in corresponding alterations in the spectrum. This is called spatio-spectral coupling. We can conclude that there are two distinct types of correlation in SPDC. The first is the correlation between signal and idler photons, indicating that the phase matching function cannot be factorized into signal and idler components,  $\Phi(\mathbf{q}_s, \mathbf{q}_i, \omega_s, \omega_i) \neq \Phi_s(\mathbf{q}_s, \omega_s)\Phi_i(\mathbf{q}_i, \omega_i)$ . The second is the correlation between spatial and spectral DOFs of a single photon,  $\Phi(\mathbf{q}_s, \mathbf{q}_i, \omega_s, \omega_i) \neq \Phi_{\mathbf{q}}(\mathbf{q}_s, \mathbf{q}_i)\Phi_{\omega}(\omega_s, \omega_i)$ .

Our theoretical description of the biphoton state in the paraxial regime has been successfully validated through experimental measurements. An advantage of the expression (3.24) is its flexibility, as it does not specify the pump beam or the crystal

nonlinearity in terms of  $\chi^{(2)}$ . This opens up possibilities for exploring how different pump beams and crystal configurations can affect the spatio-spectral coupling and the entanglement between the signal and idler photons.

In more detail, the experimental work [102] aimed to address settings inaccessible with previous theoretical works based on the narrowband and the plane wave approximation.

At the end of this section, I would like to acknowledge Carlos Sevilla-Gutiérrez and Varun Raj Kaipalath for the collection and analysis of the experimental data.



---

## SPATIO-SPECTRAL COUPLING IN SPONTANEOUS PARAMETRIC DOWN-CONVERSION

---

The usual applications in quantum optics utilize either the spatial or spectral **DOFs**, neglecting the correlation between them. However, as already mentioned in the introduction, the spatio-spectral coupling remains a fundamental issue in many protocols based on entangled photon sources. This coupling introduces a vulnerability to entanglement and makes it more susceptible to external influences. Therefore, it is crucial to thoroughly understand how the decoupling between the spatial and spectral **DOFs** of photons can be realized.

The most straightforward approach to achieve this decoupling is to employ filtering techniques [33]. Spatial filtering is based on a single-mode fiber (**SMF**) that collects photons in a Gaussian mode and blocks all photons with higher spatial modes. Spectral filtering is achieved by the application of narrowband filters to select a specific range of wavelengths for the signal and idler photons. Although filtering can eliminate the spatio-spectral coupling, it is associated with high optical losses, which could be problematic, especially considering the low conversion rate of **SPDC**.

The insights drawn from Fig. 3.3 illustrate that the **SPDC** photons can exhibit distinct spectra when they are projected into different spatial **LG** modes. An alternative technique to achieve the spatio-spectral decoupling is to ensure uniform spectra across all modes of the **LG** decomposition (3.17). In that scenario, altering the spatial modes will not result in different spectral responses, which indicates the decoupling of the spatial and spectral **DOFs**. In this chapter, our main focus is to investigate under which conditions different spatial modes exhibit an identical spectrum. Before delving into that task, we will analyze the impact of spectral filters on the spatio-spectral coupling and evaluate their efficiency.

Parts of the material presented in this chapter were published previously in the following reference:

*Generalized description of the spatio-temporal biphoton state in spontaneous parametric down-conversion*

B. Baghdasaryan, C. Sevilla-Gutiérrez, F. Steinlechner, and S. Fritzsche

*PHYSICAL REVIEW A* **106**, 063711 (2022)

#### 4.1 SPECTRAL FILTERING

We have already discussed in Chap. 2.4.3 that tracing over the signal photon will leave the idler in a mixed state if there is entanglement between the two photons. Similarly, we can investigate the correlation between the spatial and spectral DOFs of photons. Instead of tracing over the state of a single photon, we can perform a trace operation over a specific DOF. For instance, the reduced spatial biphoton state is obtained by tracing out the frequency DOF [103]

$$\begin{aligned}\rho_{\mathbf{q}} &= \text{Tr}_{\omega}(\rho) = \int d\omega_s'' d\omega_i'' \langle \omega_s'', \omega_i'' | \rho | \omega_s'', \omega_i'' \rangle \\ &= \int d\mathbf{q}_s d\omega_s d\mathbf{q}_i d\omega_i d\mathbf{q}'_s d\mathbf{q}'_i \Phi(\mathbf{q}_s, \mathbf{q}_i, \omega_s, \omega_i) \Phi^*(\mathbf{q}'_s, \mathbf{q}'_i, \omega_s, \omega_i) |\mathbf{q}_s, \mathbf{q}_i\rangle \langle \mathbf{q}'_s, \mathbf{q}'_i|. \end{aligned} \quad (4.1)$$

The correlation between the spatial and spectral DOFs can be determined by calculating the purity of the reduced spatial biphoton state

$$\begin{aligned}\text{Tr}(\rho_{\mathbf{q}}^2) &= \int d\mathbf{q}_s d\omega_s d\mathbf{q}_i d\omega_i d\mathbf{q}'_s d\omega'_s d\mathbf{q}'_i d\omega'_i \\ &\quad \times \Phi(\mathbf{q}_s, \mathbf{q}_i, \omega_s, \omega_i) \Phi^*(\mathbf{q}'_s, \mathbf{q}'_i, \omega_s, \omega_i) \Phi(\mathbf{q}'_s, \mathbf{q}'_i, \omega'_s, \omega'_i) \Phi^*(\mathbf{q}_s, \mathbf{q}_i, \omega'_s, \omega'_i). \end{aligned} \quad (4.2)$$

The spatio-spectral correlation is absent, if and only if the condition  $\text{Tr}(\rho_{\mathbf{q}}^2) = 1$  is ensured. Similarly, we can compute the purity of the reduced spectral biphoton state by tracing out the transverse momentum  $\rho_{\omega} = \text{Tr}_{\mathbf{q}}(\rho)$ . However, the purity of the reduced spectral biphoton state does not yield any new insights beyond what can be obtained from the purity of the reduced spatial biphoton state, since we have  $\text{Tr}(\rho_{\mathbf{q}}^2) = \text{Tr}(\rho_{\omega}^2)$ .

The expression in Eq. (4.2) can be enormously simplified for the degenerate scenario  $k_s = k_i = k_p/2$

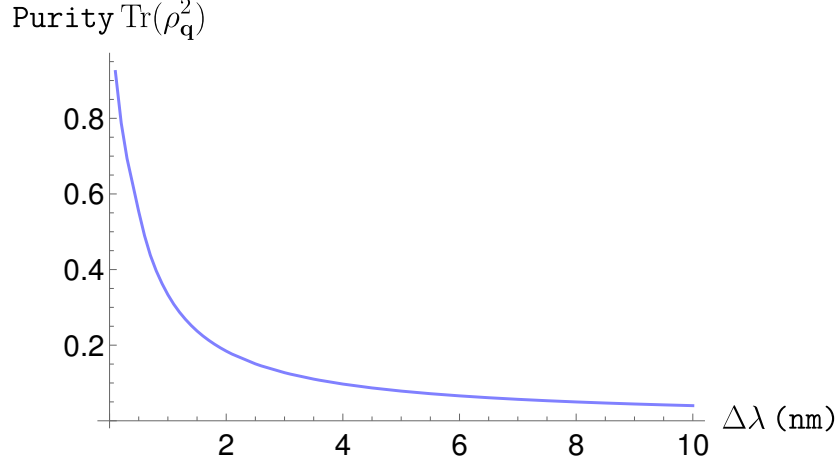


Figure 4.1: Purity of the reduced spatial biphoton state as a function of the bandwidth of spectral filters.

$$\begin{aligned} \text{Tr}(\rho_{\mathbf{q}}^2) &\propto \int d\omega_s d\omega_i d\omega'_s d\omega'_i S_p(\omega_s + \omega_i)^2 S_p(\omega'_s + \omega'_i)^2 \\ &\times \left| \int d\mathbf{q}_- \phi(\mathbf{q}_-, \omega_s, \omega_i) \phi(\mathbf{q}_-, \omega'_s, \omega'_i) \right|^2, \end{aligned} \quad (4.3)$$

where  $\mathbf{q}_- = \mathbf{q}_s - \mathbf{q}_i$ ,  $S_p(\omega_s + \omega_i)$  is the temporal distribution of the pump, and the phase matching function from Eq. (3.13) reads now

$$\phi(\mathbf{q}_-, \omega_s, \omega_i) = \int_{-L/2}^{L/2} dz \chi_{\text{eff}}^{(2)}(z) \exp \left[ iz \left( \Delta_{\Omega}(\omega_s, \omega_i) + \frac{|\mathbf{q}_-|^2}{2k_p} \right) \right].$$

The most remarkable aspect of the expression (4.3) is the absence of the spatial distribution of the pump beam. This implies that the purity  $\text{Tr}(\rho_{\mathbf{q}}^2)$  is independent of the spatial pump beam. In other words, the spatio-spectral coupling cannot be reduced by just changing the spatial distribution of the pump beam, when the full biphoton state is considered. However, the pump shaping can be used to reduce the spatio-spectral correlations in a given subspace, which is discussed in Sec. 5.2.

In general, the integrals in Eq. (4.3) have to go over all possible frequencies. The use of spectral filters in front of signal and idler photons truncates the integration over the frequency according to the bandwidth of the filter. Figure 4.1 illustrates the relationship between the purity and the filter bandwidth expressed in terms of wavelength. The calculations are performed with the same parameters, which have been used in the experiment described in Sec. 3.6. Achieving a nearly pure state necessitates the use of extremely narrow filters. In particular, a standard spectral filter with a bandwidth of 1 nm would leave the state in a mixed state with a purity

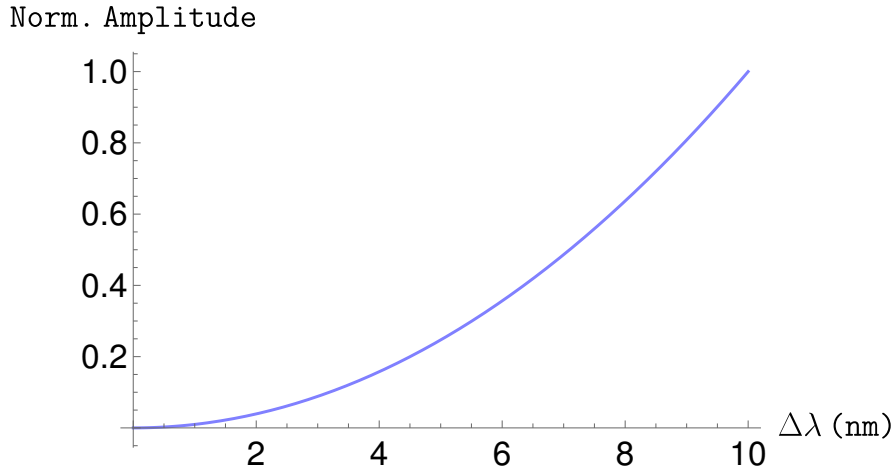


Figure 4.2: Brightness of the SPDC source as a function of the bandwidth of the spectral filter. The curve is normalized in the range of  $\Delta\lambda = 10$  nm.

of 0.33. In order to achieve a purity of 0.99, a narrowband filter with a bandwidth of  $\Delta\lambda = 0.001$  nm is required, which is practically impossible.

We can conclude that narrowband filters are not effective in completely eliminating the mixed nature of the state. Moreover, the filtering process significantly compromises the brightness of the source. Figure 4.2 shows the normalized brightness as a function of the filter bandwidth. The normalization has been done for  $\Delta\lambda = 10$  nm. As we can see, the total brightness is reduced up to 0.5 already for a very broad filter of bandwidth  $\Delta\lambda \approx 8$  nm. These findings illustrate that an alternative and more robust technique is necessary to eliminate spatio-spectral correlations without mainly relying on filtering.

Results in Fig. 4.2 are applicable only for this particular experiment. It is possible to generalize the results by normalizing the filter bandwidth to the full width at half maximum of plane wave collinear SPDC. However, the results displayed in Fig. 4.2 remain qualitatively the same.

#### 4.2 SPATIO-SPECTRAL COUPLING AND THE GOUY PHASE

We explore the possibility of achieving uniform spectra across different spatial modes of the LG decomposition (3.17). This will ensure the decoupling of the spatial and spectral DOFs for selected modes since the joint spectrum of photons will remain constant when switching between these LG modes. To facilitate future discussion, it is advantageous to emphasize that the shape of the spectrum of photons is intricately linked to the Gouy phase of interacting beams.

The role of the Gouy phase in nonlinear processes has been investigated before. For instance, in SPDC, the variation of the Gouy phase  $\psi_G(z) = (N + 1) \arctan(z/z_R)$

within the propagation distance has been used to control the relative phase of two different LG modes of the measurement basis [104, 105]. Here,  $N$  is the combined LG mode number  $N = 2p + |\ell|$ , and  $z_R$  is the Rayleigh length. Similarly, in the context of four-wave mixing (FWM), the conversion dynamics between LG modes are profoundly influenced by the Gouy phase [106]. The authors have observed that the presence of a relative Gouy phase between modes with different mode numbers  $N$  leads to a reduction in FWM efficiency.

We have a similar situation in SPDC. Assume pump, signal, and idler beams have been projected into LG modes with different mode numbers  $N$ . This results in different Gouy phases for the three beams while they propagate, inducing a phase mismatch between them. The presence of a phase mismatch, in turn, leads to a reduced efficiency of mode down-conversion. How large the reduction of the efficiency is, depends on the phase mismatch. In other words, different relative Gouy phases (phase mismatches),

$$\psi_{G,R} = \psi_{G,p} - \psi_{G,s} - \psi_{G,i},$$

result in distinct efficiencies of spatial mode down-conversion. Since the spatial and spectral DOFs are coupled, the spectrum of spatial modes will also be impacted by  $\psi_{G,R}$ . In summary, the relative Gouy phases influence the spatial mode down-conversion, and thus also the spectrum of the spatial modes due to the spatio-spectral coupling. This statement can be proved analytically for the degenerate scenario  $k_p = 2k_s$  and fixed  $z_{R,p} = z_{R,i} = z_{R,s}$ , which we show next.

The condition  $z_{R,p} = z_{R,i} = z_{R,s}$  matches the Gouy angle  $\arctan(z/z_R)$  for all beams. Hence, the relative Gouy phase can be written as

$$\psi_{G,p} - \psi_{G,s} - \psi_{G,i} = (N_p - N_s - N_i - 1) \arctan(z/z_R).$$

This equation demonstrates that  $\psi_{G,R}$  is now fully determined by the relative mode number  $N_R = N_p - N_s - N_i$ . Hence, the relative Gouy phase should remain unchanged, if  $N_R$  is fixed.

If the Gouy phase is the only reason for the existence of different spectral dependencies among spatial modes, the shape of the spectrum should remain the same for a fixed  $\psi_{G,R}$ , or equivalently for a fixed  $N_R$ . Indeed, after simplifying the expression of the coincidence amplitudes from Eq. (3.24) under the degeneracy condition  $k_p = 2k_s$ , we obtain

$$C_{p,p_s,p_i}^{\ell_s,\ell_i}(\Omega_s, \Omega_i) \propto \int_{-L/2}^{L/2} dz e^{iz\Delta\Omega} \frac{(i2z + k_p w_p^2)^{N_R}}{(-i2z + k_p w_p^2)^{N_R+1}}. \quad (4.4)$$

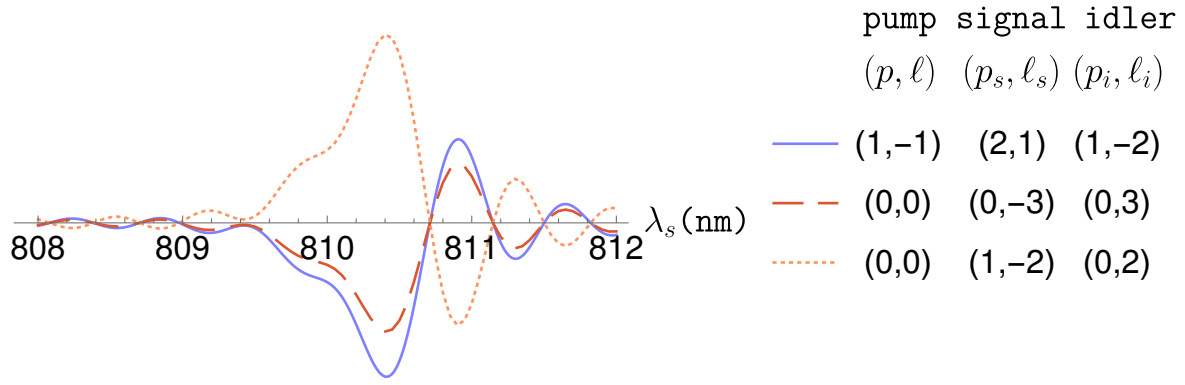


Figure 4.3: Interplay of the Gouy phase with the spectral **DOF**. Consider a pump beam that consists of a superposition of the **LG** modes  $\text{LG}_1^{-2} + \text{LG}_0^0$ . We explore three distinct mode combinations for the signal and idler, which could be generated in the down-conversion process, each having the same relative mode number  $N_R = -6$ . The spectra corresponding to these three modes are all identical, differing only by a constant factor.

We see from Eq. (4.4) that the spectral response of coincidence amplitudes  $C_{p,p_s,p_i}^{\ell_s,\ell_i}(\Omega_s, \Omega_i)$  encoded only in the term  $e^{iz\Delta\Omega}$  remains unaffected up to a constant if  $N_R$  is fixed. On the other hand,  $N_R$  can be rewritten as

$$N_R = \frac{\psi_{G,R}}{\arctan(z/z_R)} + 1. \quad (4.5)$$

Therefore, it follows from Eqs. (4.4) and (4.5) that the spectral response of spatial modes is determined by the relative Gouy phase  $\psi_{G,R}$ . This confirms our initial assertion. We would like to remind that the simplified form of Eq. (4.4) is a result of the assumptions  $k_p = 2k_s$  and  $z_{R,p} = z_{R,i} = z_{R,s}$ . The analytical proof for the general case can require more effort, which we omit here.

The interplay of the Gouy phase with the spectral **DOF** can be illustrated in a numerical example. Consider a pump beam, which is a superposition of the **LG** modes  $\text{LG}_1^{-2} + \text{LG}_0^0$ . Within this framework, we examine three possible mode combinations for signal and idler, all having the same relative mode number  $N_R = -6$ . The spectra corresponding to these three modes are presented in Fig. 4.3. Remarkably, despite utilizing distinct **LG** pump modes, a careful selection of signal and idler modes leads to an identical shape of the spectrum for all three mode combinations, up to a constant factor.

---

## HIGH-DIMENSIONAL ENTANGLED STATES IN THE SPATIAL DEGREE OF FREEDOM

---

The pioneer quantum-entanglement-based protocols, such as quantum cryptography or quantum teleportation, relied on two-dimensional quantum systems called qubits. In Sec. 2.2, we have already introduced the Bell state

$$|\Psi\rangle = \frac{1}{\sqrt{2}}(|H\rangle_A |V\rangle_B + |V\rangle_A |H\rangle_B),$$

which is a two-dimensional entangled state. Each system (qubit) in this state has two levels, corresponding to vertical and horizontal polarization. Apart from two-dimensional systems, we can also think of discrete high-dimensional quantum systems, also known as qudits. A qudit is a quantum system that is not constrained to two dimensions but can have any number of discrete levels.

Qudits offer several advantages over qubits. First, they provide an increased information capacity compared to qubits. Any additional orthogonal state used in the encoding scheme increases the encoded information. In addition, qudit states demonstrate an increased resilience against background noise and potential hacking attacks. Therefore, the utilization of qudits in quantum cryptographic protocols can enhance the security and resilience of quantum communication systems [38].

Orbital angular momentum states of photons are a promising candidate to implement qudits. Unlike polarization, OAM can take on an infinite number of values, ranging from minus infinity to plus infinity. Theoretical investigations have explored entangled OAM state generation in SPDC in the context of the thin crystal approximation [107, 108]. Experimental advancements have gone beyond the thin crystal regime and successfully generated high-dimensional entangled states in the OAM DOF [37, 109]. The state generation in Ref. [109] has been achieved by employing a superposition of LG modes as the pump source. The correct superposition for the pump has been determined with a simultaneous perturbation stochastic approximation algorithm [110].

In this section, we also employ a superposition of **LG** modes for the pump, to generate entangled states in the **OAM** basis. This includes the states generated in Ref. [109]. Our method is very straightforward and requires no optimization algorithm. In comparison to Refs. [107, 108], our approach addresses the impact of the spatio-spectral coupling on high-dimensional entangled states and goes beyond the thin crystal regime. In particular, in order to generate high-dimensional entangled states in the spatial **DOF**, it is necessary to carefully select those modes that maintain the same relative Gouy phase, as in the example of Fig. 4.3. Note that state engineering in the thin crystal regime can be inefficient due to an infinite amount of spatial modes generated in the down-conversion.

Parts of the material presented in this chapter were published previously in the following reference:

*Generalized description of the spatio-temporal biphoton state in spontaneous parametric down-conversion*

B. Baghdasaryan, C. Sevilla-Gutiérrez, F. Steinlechner, and S. Fritzsche  
*PHYSICAL REVIEW A* **106**, 063711 (2022)

## 5.1 PUMP BEAM ENGINEERING

### 5.1.1 Narrowband regime

As an illustrative example, we consider the subspace of the first four positive **OAM** numbers  $\ell_s, \ell_i = 0, 1, 2, 3$ , referred to as  $S_4$ . For simplicity, the radial modes are set to  $p_s = p_i = 0$ . We first apply the narrowband regime  $\Omega_s = \Omega_i = 0$ , and later generalize the approach to the broadband regime. Here we use the simplified notation,

$$|p_s = 0, \ell_s, \Omega_s = 0\rangle |p_i = 0, \ell_i, \Omega_i = 0\rangle := |\ell_s, \ell_i\rangle. \quad (5.1)$$

Our goal is to engineer a four-dimensional maximally entangled state in this subspace.

We start with the discussion of a possible decoupling of spatial and spectral **DOFs**. We have demonstrated that decoupling within a specific subspace becomes feasible when all modes from that subspace possess the same relative Gouy phase. In  $S_4$ , all modes consist of only positive **OAM** numbers, which leads to the same relative mode number  $N_R = |\ell| - |\ell_s| - |\ell_i| = 0$ , where  $\ell = \ell_s + \ell_i$ . Consequently, all modes exhibit the same relative Gouy phase or, i.e., the same spectrum when the condition  $z_{R,p} = z_{R,i} = z_{R,s}$  is satisfied. This ensures that any state in this subspace is separable in terms of the spatial and spectral **DOFs**. Our attention can now be directed toward the engineering process itself.



The pump beam is modeled as a superposition of LG modes in the following way,

$$V = \sum_{\ell=0}^6 a_{\ell} \text{LG}_0^{\ell},$$

where the range of the summation is determined by the minimum and maximum values of OAM in the subspace,  $\ell = [\min(\ell_s + \ell_i), \max(\ell_s + \ell_i)]$ . The expansion coefficients  $a_{\ell}$  are initially unknown and need to be determined. Since the pump function appears in Eq. (3.17) linearly, the corresponding state in the subspace  $S_4$  can be expressed as

$$|\Psi_4\rangle = \sum_{\ell_s, \ell_i=0}^3 \left( \sum_{\ell=0}^6 a_{\ell} C_{0,0,0}^{\ell, \ell_s, \ell_i} \right) |\ell_s, \ell_i\rangle.$$

We can examine the matrix representation of the state  $|\Psi_4\rangle$ , to find the appropriate coefficients  $a_{\ell}$ . The matrix consists of  $4 \times 4$  elements and is given by the left-hand side of the following expression

$$\begin{pmatrix} a_0 C_{0,0} & a_1 C_{1,0} & a_2 C_{2,0} & a_3 C_{3,0} \\ a_1 C_{0,1} & a_2 C_{1,1} & a_3 C_{2,1} & a_4 C_{3,1} \\ a_2 C_{0,2} & a_3 C_{1,2} & a_4 C_{2,2} & a_5 C_{3,2} \\ a_3 C_{0,3} & a_4 C_{1,3} & a_5 C_{2,3} & a_6 C_{3,3} \end{pmatrix} \rightarrow \begin{pmatrix} 0 & 1 & 0 & 0 \\ 1 & 0 & 0 & 0 \\ 0 & 0 & 0 & 1 \\ 0 & 0 & 1 & 0 \end{pmatrix}, \quad (5.2)$$

where we used the notation  $C_{0,0,0}^{\ell_s + \ell_i, \ell_s, \ell_i} = C_{\ell_s, \ell_i}$ . The state becomes maximally entangled in this subspace when the matrix takes the form of a permutation matrix (under consideration of the normalization of the state): each row and each column contain exactly one entry of 1 and the rest are 0. The permutation matrix ensures the linear independence of the selected modes.

The right-hand side of the expression (5.2) is such a state that can be engineered if we select  $a_1 = 1/C_{0,1} \approx 1/C_{1,0}$ ,  $a_5 = 1/C_{2,3} \approx 1/C_{3,2}$  and  $a_0 = a_2 = a_3 = a_4 = a_6 = 0$ , where we assumed degenerate SPDC,  $k_p \approx 2k_s \approx 2k_i$ . This choice leads to the (normalized) state

$$|\Psi_4\rangle = \frac{1}{2}(|0, 1\rangle + |1, 0\rangle + |2, 3\rangle + |3, 2\rangle).$$

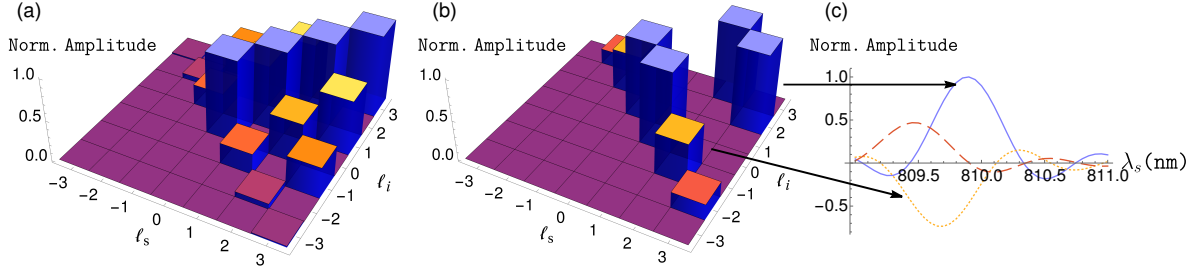


Figure 5.1: Normalized high-dimensional entangled states (a)  $|\Psi_4^d\rangle = \frac{1}{2}(|0,0\rangle + |1,1\rangle + |2,2\rangle + |3,3\rangle)$  and (b)  $|\Psi_4\rangle = \frac{1}{2}(|0,1\rangle + |1,0\rangle + |2,3\rangle + |3,2\rangle)$ . The state  $|\Psi_4\rangle$  is maximally entangled in the subspace  $l_s, l_i = 0, 1, 2, 3$ , but not  $|\Psi_4^d\rangle$  because of the additional modes in the subspace. The state  $|\Psi_4^d\rangle$  is maximally entangled in a smaller subspace, namely in the subspace consisting of only the four modes  $\{|0,0\rangle, |1,1\rangle, |2,2\rangle, |3,3\rangle\}$ . (c) The modes of the signal (idler) involved in the state  $|\Psi_4\rangle$  have the same spectrum (blue solid curve) compared to the modes out of the subspace shown in the same color as corresponding bars (dotted curve for  $|2,-1\rangle$  and dashed curve for  $|3,-2\rangle$ ). These curves correspond only to the spatial modes from (b).

Thus, the state engineering is finished, where the coefficients of the pump superposition  $\{a_1, a_5\}$  should be calculated with the expression (3.24). In the same way, the *diagonal* four-dimensional state from Ref. [109],

$$|\Psi_4^d\rangle = \frac{1}{2}(|0,0\rangle + |1,1\rangle + |2,2\rangle + |3,3\rangle),$$

can be engineered if we select  $\{a_0, a_2, a_4, a_6\}$  to be equal to  $\{1/C_{0,0}, 1/C_{1,1}, 1/C_{2,2}, 1/C_{3,3}\}$  and  $a_1 = a_3 = a_5 = 0$ .

The states  $|\Psi_4^d\rangle$  and  $|\Psi_4\rangle$  are presented in Figs. 5.1 (a) and (b) with the highest bars, blue-colored on top. As we can see, the modes contributing to the states  $|\Psi_4^d\rangle$  and  $|\Psi_4\rangle$  represent just a part of the full OAM emission (spiral spectrum). Therefore, the postselection should be the final step in the engineering process, where the undesirable modes are sorted out. The generation of the state  $|\Psi_4^d\rangle$  gives rise to undesired modes even in the subspace  $S_4$ , which will reduce the entanglement in this subspace, as will be explained better later.

### 5.1.2 Broadband regime

In the broadband regime, we should account for the spectral dependence of the coincidence amplitudes when calculating the coefficients  $a_\ell$  of the pump beam. For instance, the first coefficient in the narrowband regime from the preceding section is

$$a_1 = \frac{1}{C_{0,0,0}^{1,0,1}(\Omega = 0)}.$$

In order to generate the same state in the broadband regime, we need to calculate the magnitude of the coincidence amplitudes over the measured frequency band

$$a_1 = \frac{1}{\left( \int d\Omega |C_{0,0,0}^{1,0,1}(\Omega)|^2 \right)^{0.5}},$$

where the integration is limited to the bandwidth of the spectral filter.

## 5.2 SCHMIDT NUMBER AND THE PURITY OF THE SUBSPACE STATE

In order to evaluate the efficiency of the state preparation in the subspace  $S_4$ , we can calculate the Schmidt number and the purity of the presented states  $|\Psi_4^d\rangle$  and  $|\Psi_4\rangle$ . The calculations employ the same experimental parameters as in Ref. [109]: 15-mm-thick periodically poled **KTP** crystal designed for a collinear degenerate type-II phase matching, **CW** laser of wavelength 405 nm with beam waist  $w_p = 25 \mu\text{m}$  and detection beams of radius  $w_{s,i} = 33 \mu\text{m}$ .

The modes  $\{|0, 2\rangle, |2, 0\rangle, |1, 3\rangle, |3, 1\rangle\}$  in Fig. 5.1 (a) are non-desirable and lead to a decrease of entanglement in  $S_4$ . As a result, the state  $|\Psi_4^d\rangle$  exhibits an azimuthal Schmidt number of  $K = 2.04$ , which is less than the Schmidt number of 4 calculated for the state  $|\Psi_4\rangle$ . Hence, the preparation of  $|\Psi_4\rangle$  is more efficient within  $S_4$  compared to  $|\Psi_4^d\rangle$ . Here the term azimuthal refers to the fact that only **OAM** modes are considered and the radial modes are set to  $p_s = p_i = 0$ .

It should be noted that a Schmidt number of 4 is necessary but not sufficient for a four-dimensional state to be classified as maximally entangled. To achieve maximal entanglement in  $S_4$ , the state  $|\Psi_4\rangle$  must also be spatially pure, indicating the absence of the spatio-spectral coupling.

As previously mentioned, all states generated in the subspace  $S_4$  are decoupled in the spatial and spectral **DOFs**, as all modes in  $S_4$  possess the same relative Gouy phase. In order to calculate the spatial purity of  $|\Psi_4\rangle$  explicitly, we need the reduced density matrix of the state. Since we consider only **OAM** of photons, the biphoton state transforms into

$$|\Psi\rangle = \iint d\Omega \sum_{\ell_s, \ell_i = -\infty}^{\infty} C_{\ell_s, \ell_i}(\Omega) |\ell_s, \Omega\rangle |\ell_i, -\Omega\rangle. \quad (5.3)$$

The trace over the spectral domain of the density matrix  $\rho = |\Psi\rangle\langle\Psi|$  yields

$$\rho_q = \sum_{\ell_s, \ell_i} \sum_{\tilde{\ell}_s, \tilde{\ell}_i} A_{\ell_s, \ell_i}^{\tilde{\ell}_s, \tilde{\ell}_i} |\ell_s, \ell_i\rangle \langle \tilde{\ell}_s, \tilde{\ell}_i|. \quad (5.4)$$

where  $A_{\ell_s, \ell_i}^{\tilde{\ell}_s, \tilde{\ell}_i} = \int d\Omega C_{\ell_s, \ell_i}(\Omega) [C_{\tilde{\ell}_s, \tilde{\ell}_i}(\Omega)]^*$  is the overlap integral of the spectra of the OAM modes. The equation (5.4) is very useful to calculate the purity of the reduced spatial biphoton state in small subspaces in comparison to Eq. (4.1), where we have integrals instead of summations.

We run the summations in Eq. (5.4) over  $\ell_s, \ell_i, \tilde{\ell}_s, \tilde{\ell}_i = 0, 1, 2, 3$ , renormalize the state, construct the density matrix of the subspace  $\rho_{\mathbf{q},s}$ , and calculate the corresponding purity  $\text{Tr}(\rho_{\mathbf{q},s}^2)$ . Here the subscript  $s$  indicates the consideration of the subspace  $S_4$ . In fact, the states  $|\Psi_4\rangle$  and  $|\Psi_4^d\rangle$  are both pure,  $\text{Tr}(\rho_{\mathbf{q},s}^2) = 1$ , which aligns with our previous argument. The spectra of the modes contributing to the state  $|\Psi_4\rangle$ , namely  $|0, 1\rangle, |1, 0\rangle, |2, 3\rangle, |3, 2\rangle$ , are identical and depicted by the blue curve in Fig. 5.1 (c).

### 5.3 SCHMIDT NUMBER AND THE PURITY OF THE FULL STATE

The subspace  $S_4$  is a part of the full SPDC emission. In Fig. 5.1 (b), the first four OAM modes out of the subspace,  $|2, -1\rangle, |-1, 2\rangle, |-2, 3\rangle$  and  $|3, -2\rangle$ , possess different spectra in contrast to the modes in  $S_4$ , shown in Fig. 5.1 (c). The appearance of modes with distinguishable spectra indicates the inseparability of the spatial and spectral DOFs out of  $S_4$ . The more distinguishable modes contribute to the state, the stronger the spatio-spectral coupling. This, in turn, leads to a decreased purity for the reduced spatial biphoton state.

In a small subspace such  $\ell_s, \ell_i = -3, -2, \dots, 2, 3$ , the purity of the state from Fig. 5.1 (a) equals 0.81 and for the state from Fig. 5.1 (b) 0.72. For a comparison, a fundamental Gaussian pump beam leads to a purity of 0.6. However, these differences are valid only for a finite size of subspaces. As we have already shown in Sec. 4.1 [see Eq. (4.3)], the purity of the reduced spatial biphoton state is independent of the spatial distribution of the pump beam. The only difference in the state preparation of the states  $|\Psi_4\rangle$  and  $|\Psi_4^d\rangle$  is the pump beam. Therefore, the states  $|\Psi_4\rangle$  and  $|\Psi_4^d\rangle$  possess overall the same purity when the whole Hilbert space is considered.

The Schmidt number of the full spatio-spectral biphoton state is also different in comparison to the subspace state. The total Schmidt number can be calculated from the reduced density matrix in space and frequency for the signal by tracing over the idler  $\rho_{\text{signal}} = \text{Tr}_{\text{idler}}(\rho)$  [103]

$$\begin{aligned} \text{Tr}(\rho_{\text{signal}}^2) &= \int d\mathbf{q}_s d\Omega_s d\mathbf{q}_i d\Omega_i d\mathbf{q}'_s d\Omega'_s d\mathbf{q}'_i d\Omega'_i \\ &\times \Phi(\mathbf{q}_s, \mathbf{q}_i, \Omega_s, \Omega_i) \Phi^*(\mathbf{q}'_s, \mathbf{q}_i, \Omega'_s, \Omega_i) \\ &\times \Phi(\mathbf{q}'_s, \mathbf{q}'_i, \Omega'_s, \Omega'_i) \Phi^*(\mathbf{q}_s, \mathbf{q}'_i, \Omega_s, \Omega'_i). \end{aligned} \quad (5.5)$$

The Schmidt number is then given by  $K = 1/\text{Tr}(\rho_{\text{signal}}^2)$  [see Eq. (2.10)]. The number of both spatial and spectral Schmidt modes in the range of frequencies  $810 \pm 10 \text{ nm}$  equals 140, where  $810 \text{ nm}$  is the central frequency for the signal and idler photons. This high Schmidt number comes from the spectral entanglement since we consider a CW pump. In contrast, if we consider only photons generated at the central frequency  $810 \text{ nm}$  (narrowband regime), the number of Schmidt modes is small and equals 5.8. This is the average number of the spatial modes generated only at the frequency  $810 \text{ nm}$ .

Finally, a small remark about the thin crystal regime, which is achieved for  $L \ll z_{R,p}$  [59]. In that regime, the signal and idler beams have a very broad frequency bandwidth, which can be considered as a constant. Therefore, the biphoton state effectively possesses only the spatial DOF leading to spatio-spectral decoupling. The problem with this regime is that it gives rise to a huge amount of spatial modes. Assume we keep all parameters the same as in Ref. [109], but change the crystal length to  $L = 1 \mu\text{m}$ . The thin crystal regime is then well achieved according to Ref. [59]. The state becomes spatially pure but possesses a large amount of Schmidt modes,  $10^7$ . This implies that if we are interested in only a few modes from the whole Hilbert space, most of the modes should be sorted out, which makes the state engineering in the thin crystal regime inefficient.

#### 5.4 N-DIMENSIONAL STATE IN THE OAM BASIS

In the preceding sections, we have shown how to engineer and characterize four-dimensional entangled states. A natural next step is the generalization of state engineering to an N-dimensional Hilbert space. There are several ways, how an N-dimensional state can be engineered. The main aspects that should be taken into account are again the decoupling of the spatial and spectral DOFs and the efficiency of the state preparation.

The simplest is to generate an N-dimensional state on the *diagonal* subspace, where  $\ell_s = \ell_i$ . In this case, all modes on the diagonal share the same relative mode number, as indicated by the relation

$$N_R = |\ell_s + \ell_i| - |\ell_s| - |\ell_i| = |2\ell_s| - 2|\ell_s| = 0.$$

Therefore, the modes in this subspace have the same relative Gouy phase (assuming  $z_{R,p} = z_{R,i} = z_{R,s}$ ), which in turn leads to the decoupling of spatial and spectral DOFs. In order to engineer an N-dimensional entangled state in a diagonal subspace  $S_d$ ,

$$|\Psi_N\rangle = \frac{1}{\sqrt{N}} \sum_{\ell \in S_d} |\ell, \ell\rangle,$$

the pump beam needs to have the following form

$$V = \sum_{\ell \in S_d} \frac{1}{C_{\ell,\ell}} \text{LG}_0^{2\ell}, \quad (5.6)$$

where the sum goes over the joint OAM modes included in  $S_d$ . The resulting state is maximally entangled only within the subspace  $S_d$ . The coincidence amplitudes are calculated according to our notation  $C_{\ell,\ell} = C_{0,0,0}^{2\ell,\ell,\ell}$  with Eq. (3.24). For instance, to construct the arbitrarily three-dimensional state,

$$|\Psi_3\rangle = \frac{1}{\sqrt{3}}(|-2, -2\rangle + |1, 1\rangle + |3, 3\rangle),$$

the corresponding pump beam has to be a superposition of three LG modes in the following way

$$V \propto \frac{1}{C_{-2,-2}} \text{LG}_0^{-4} + \frac{1}{C_{1,1}} \text{LG}_0^2 + \frac{1}{C_{3,3}} \text{LG}_0^6. \quad (5.7)$$

Figure 5.2 displays the mode distribution of the biphoton state in the LG basis for the pump given by Eq. (5.7). As expected, the three modes  $|-2, -2\rangle$ ,  $|1, 1\rangle$  and  $|3, 3\rangle$  have the same amplitude. However, many undesirable modes are generated outside the considered subspace, which need to be filtered out in the postselection process. The state  $|\Psi_3\rangle$  is maximally entangled in the subspace consisting of only the same modes contributing to the state,  $\{|-2, -2\rangle, |1, 1\rangle, |3, 3\rangle\}$ .

The relative phase between modes is also straightforward to control. Assume that the modes  $|-2, 2\rangle$  and  $|1, 1\rangle$  should have phase differences  $\theta_1$  and  $\theta_2$  compared to the mode  $|3, 3\rangle$

$$|\Psi_3\rangle = \frac{1}{\sqrt{3}}(e^{i\theta_1} |-2, -2\rangle + e^{i\theta_2} |1, 1\rangle + |3, 3\rangle).$$

It is then easy to show that the pump beam should undergo a small adjustment

$$V \propto \frac{e^{i\theta_1}}{C_{-2,-2}} \text{LG}_0^{-4} + \frac{e^{i\theta_2}}{C_{1,1}} \text{LG}_0^2 + \frac{1}{C_{3,3}} \text{LG}_0^6.$$

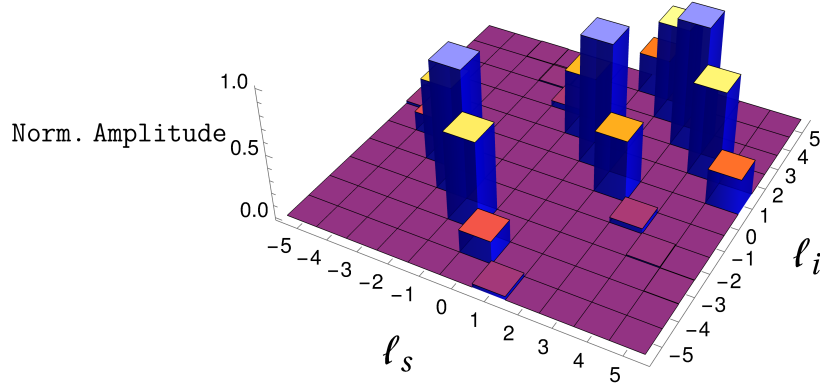


Figure 5.2: Normalized three-dimensional entangled state  $|\Psi_3\rangle = \frac{1}{\sqrt{3}}(|-2, -2\rangle + |1, 1\rangle + |3, 3\rangle)$ . The state  $|\Psi_3\rangle$  is maximally entangled in the subspace consisting of only three modes  $\{|-2, -2\rangle, |1, 1\rangle, |3, 3\rangle\}$ .

This just implies that the phase of the pump mode is transferred to the corresponding generated mode.

The high-dimensional state generation in the diagonal subspace is one of the possibilities. As we have already seen, it is possible to generate a four-dimensional entangled state with off-diagonal modes [see the state  $|\Psi_4\rangle = \frac{1}{2}(|0, 1\rangle + |1, 0\rangle + |2, 3\rangle + |3, 2\rangle)$  in Fig. 5.1 (b)]. We have also shown that the state preparation for  $|\Psi_4\rangle$  is more efficient than the preparation of the diagonal state  $|\Psi_4^d\rangle = \frac{1}{2}(|0, 0\rangle + |1, 1\rangle + |2, 2\rangle + |3, 3\rangle)$ . The reason is the appearance of modes outside the considered subspace, which are more in the diagonal state engineering approach than in the off-diagonal case. The appearance of more modes is the result of mixing four LG modes for the pump beam in the case of  $|\Psi_4^d\rangle$ , while for the state  $|\Psi_4\rangle$  only two pump modes are required.

It is also possible to generate off-diagonal entangled states in a five-dimensional Hilbert space by keeping the condition of the same relative Gouy phase. The general form of the five-dimensional state can be presented as follows

$$|\Psi_5^G\rangle = \frac{1}{\sqrt{5}} \left( \left| \frac{r-1}{2}, \frac{r+1}{2} \right\rangle + \left| \frac{r+1}{2}, \frac{r-1}{2} \right\rangle + \left| \frac{r+3}{2}, \frac{r+3}{2} \right\rangle + \left| \frac{r+5}{2}, \frac{r+7}{2} \right\rangle + \left| \frac{r+7}{2}, \frac{r+5}{2} \right\rangle \right),$$

where  $r$  is an odd integer number  $r = \pm 1, \pm 3, \dots$ , and the superscript  $G$  refers to the term *general*. The degeneracy of the signal and idler photons is again assumed  $k_s = k_i$ . The pump, which generates this state, reads

$$V \propto \frac{1}{C_{\frac{r-1}{2}, \frac{r+1}{2}}} \text{LG}_0^r + \frac{1}{C_{\frac{r+3}{2}, \frac{r+3}{2}}} \text{LG}_0^{r+3} + \frac{1}{C_{\frac{r+5}{2}, \frac{r+7}{2}}} \text{LG}_0^{r+6}.$$

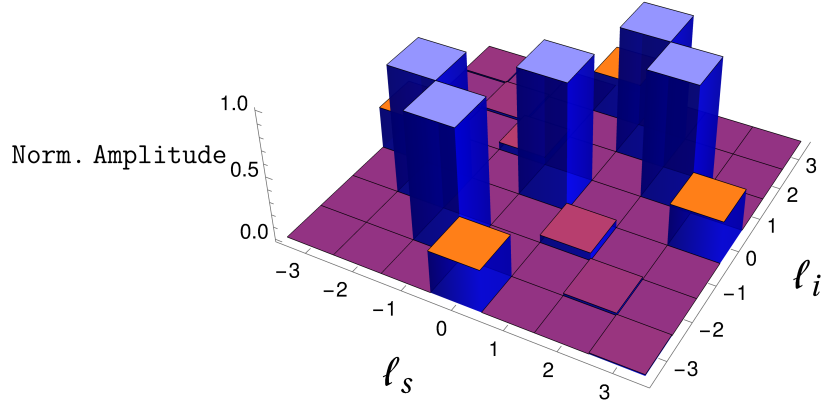


Figure 5.3: Normalized five-dimensional entangled state  $|\Psi_5\rangle = \frac{1}{\sqrt{5}}(|-1, -2\rangle + |-2, -1\rangle + |0, 0\rangle + |1, 2\rangle + |2, 1\rangle)$ .

For example, setting  $r = -3$ , we get for the pump

$$V \propto \frac{1}{C_{-2,-1}} \text{LG}_0^{-3} + \frac{1}{C_{0,0}} \text{LG}_0^0 + \frac{1}{C_{1,2}} \text{LG}_0^3,$$

which generates the state

$$|\Psi_5\rangle = \frac{1}{\sqrt{5}}(|-1, -2\rangle + |-2, -1\rangle + |0, 0\rangle + |1, 2\rangle + |2, 1\rangle). \quad (5.8)$$

This state is displayed in Fig. 5.3. Note that we ignored in Eq. (5.8) the contribution of the states  $|1, -1\rangle$ ,  $|-1, 1\rangle$ ,  $|2, -2\rangle$ , and  $|-2, 2\rangle$ , which are negligible compared to  $|0, 0\rangle$ .

The generation of off-diagonal entangled states of dimensions higher than five becomes challenging. There is no combination of modes that we can select to have the same amplitude and fulfill the selection rule of the same relative Gouy phase simultaneously.



---

## SPATIALLY INDISTINGUISHABLE SINGLE MODE PHOTONS FROM DOMAIN-ENGINEERED CRYSTAL

---

Quantum applications, such as measurement-based quantum computing [40, 41], photonic Boson sampling [33, 42] and photonic quantum repeaters [43] share a common requirement: the availability of a sufficient number of perfectly indistinguishable and pure single photons. Indistinguishability in this context refers to the identical quantum properties exhibited by photons. Purity quantifies the degree to which a single photon remains isolated from its environment. A highly pure single photon displays minimal correlation with its surroundings, thereby ensuring its integrity as an independent quantum entity.

Although single photons can be reliably sourced through SPDC, the process has limitations in common bulk crystals due to its probabilistic nature. Not all photon pairs are identical, they may be distinguishable. Moreover, we know from Sec. 5 that the photons exhibit high-dimensional entanglement in terms of both the spatial and the spectral DOFs, which is not ideal for single-photon sources. Suppose a measurement is performed only on a single photon, without consideration of the entire composite system. In that scenario, the measured photon will be in a mixed state as a result of the correlation with the second photon (see Sec. 2.4.3). Here, we refer to the reduced mixed state of a single photon as a single-photon state. We also distinguish between the spatial and spectral purity of the single-photon state, which are associated with spatial and spectral correlations between signal and idler photons. The single photon is denoted as *pure*, if no correlation exists with its partner photon.

As discussed earlier in Sec. 4.1, the simplest approach to eliminate the correlation between signal and idler photons is the utilization of spatial and spectral filtering techniques [33]. Spatial filtering is usually very easy to implement by just projecting photons into a SMF, allowing only photons in a Gaussian mode to pass through. Spectral filtering is a more complex task, especially when one needs to isolate a specific spectral state rather than just a range of frequencies. When considering both the spatial and the spectral DOFs simultaneously, the use of filters to select a particular single-mode state becomes less desirable due to the inherent spatio-spectral coupling

in SPDC. The filtering process also introduces high optical losses, as mentioned in Sec. 4.1.

Recent studies have explored that domain-engineered crystals with a modified effective nonlinearity  $\chi_{\text{eff}}^{(2)}$  can minimize the spectral correlations between signal and idler photons [3, 44–50]. Unlike traditional bulk crystals with a constant nonlinearity  $\chi_{\text{eff}}^{(2)} = \text{const.}$ , domain-engineered crystals can offer a tailored Gaussian nonlinear response, resulting in a spectral purity of approximately 99%. However, the studies using the Gaussian nonlinearity have only considered the spectral properties of photons. The photons have still been spatially filtered by employing a SMF.

Here, we show that crystals with a Gaussian nonlinear response partially reduce the spatial correlations between photons. In order to fully eliminate the spatial correlation, we employ a simultaneous engineering of the pump beam and crystal effective nonlinearity. In particular, we will show that another nonlinear response exists rather than the Gaussian, which improves the spatial purity of the single-photon state. Subsequently, we will modify the spatial distribution of the pump beam, in order to further enhance the spatial purity. The knowledge gained in this chapter will take us a step closer to generating spatio-spectral pure photons from SPDC without any filtering.

Parts of the material presented in this chapter were published previously in the following reference:

*Enhancing the purity of single photons in parametric down-conversion through simultaneous pump-beam and crystal-domain engineering*

B. Baghdasaryan, F. Steinlechner, and S. Fritzsche

PHYSICAL REVIEW A **108**,023718 (2023)

## 6.1 SPATIAL BIPHOTON STATE

Since we are interested only in the spatial properties of the biphoton state, we apply the narrowband regime ( $\Omega_s = \Omega_i = 0$ ) to the state from Eq. (3.12). Correspondingly, the monochromatic biphoton state (see also [111, 112]) also referred to as the spatial biphoton state reads

$$|\Psi\rangle = \iint d\mathbf{q}_s d\mathbf{q}_i \Phi(\mathbf{q}_s, \mathbf{q}_i) \hat{a}_s^\dagger(\mathbf{q}_s) \hat{a}_i^\dagger(\mathbf{q}_i) |\text{vac}\rangle. \quad (6.1)$$

The biphoton mode function from Eq. (3.13) is simplified to

$$\Phi(\mathbf{q}_s, \mathbf{q}_i) = N_0 V(\mathbf{q}_s + \mathbf{q}_i) \int_{-L/2}^{L/2} dz \chi_{\text{eff}}^{(2)}(z) \exp(i\Delta k_z z), \quad (6.2)$$

which now contains only the spatial structure of [SPDC](#). The phase mismatch in the  $z$  direction also gets a simplified form

$$\Delta k_z = \rho_s^2 \frac{k_p - k_s}{2k_p k_s} + \rho_i^2 \frac{k_p - k_i}{2k_p k_i} - \frac{\rho_s \rho_i}{k_p} \cos(\varphi_i - \varphi_s). \quad (6.3)$$

The pump is again modeled by a common Gaussian beam profile

$$V(\mathbf{q}_s + \mathbf{q}_i) = \frac{w_p}{\sqrt{2\pi}} \exp\left(-\frac{w_p^2}{4} |\mathbf{q}_s + \mathbf{q}_i|^2\right),$$

with a beam waist  $w_p$ , unless stated otherwise.

The purity of the signal-photon state is obtained by tracing out the signal photon state from the joint state. We need only the spatial purity, therefore, Eq. (5.5) is transformed to

$$P = \int d\mathbf{q}_s d\mathbf{q}_i d\mathbf{q}'_s d\mathbf{q}'_i \Phi(\mathbf{q}_s, \mathbf{q}_i) \Phi^*(\mathbf{q}'_s, \mathbf{q}_i) \Phi(\mathbf{q}'_s, \mathbf{q}'_i) \Phi^*(\mathbf{q}_s, \mathbf{q}'_i), \quad (6.4)$$

where we utilized Eqs. (6.1). Purity from Eq. (6.4) remains the same, if we interchange the idler and signal photons, since  $\text{Tr}(\rho_{\text{idler}}^2) = \text{Tr}(\rho_{\text{signal}}^2)$ . Generally, the purity of the single-photon state is always equal to or less than one. A purity value of  $P = 1$  indicates that there is no entanglement between the signal and idler photons, implying that the biphoton state can be represented as a product state  $|\Psi\rangle = |\Psi\rangle_s |\Psi\rangle_i$ .

## 6.2 OPTIMAL PARAMETERS FOR HIGH PURITY

The attainment of a high purity for the single-photon state requires careful selection of the crystal and pump parameters. In our analysis, we will mainly analyze the dependence of the purity on two parameters, the crystal length  $L$  and the pump beam waist  $w_p$ . Our calculations were based on a [KTP](#) crystal phase matched for type-II [SPDC](#). The pump operates at wavelengths  $\lambda_p = 775$  nm. This process yields two orthogonally polarized photons with a central wavelength of 1550 nm. Note that the results presented in this chapter exhibit minimal variations across all phase matching conditions. This is primarily due to the fact that the dispersion relations of different phase matching conditions have a relatively weaker impact on the spatial [DOF](#) compared to their influence on the spectral [DOF](#).

Initially, we will analyze the spatial purity of the single-photon state in a standard periodically poled [KTP](#) crystal. The presented results are also applicable for bulk crystals, producing quasicollinear [SPDC](#). Subsequently, we assess the performance of

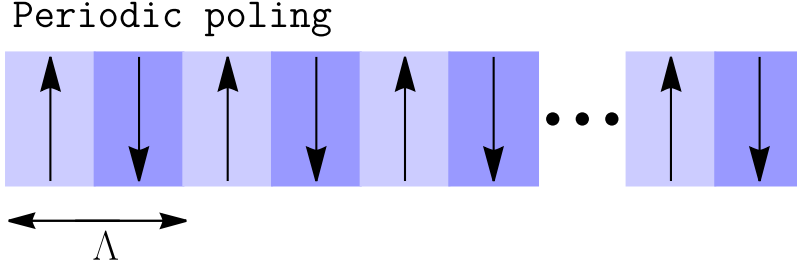


Figure 6.1: Periodically poled crystals consist of thin layers of a birefringent material. The sign of the nonlinear coefficient  $\chi_{\text{eff}}^{(2)}$  of each domain is flipped periodically with the poling period  $\Lambda$ . The flip is achieved by applying a strong electric field to a ferroelectric crystal via patterned electrodes on the crystal surface. This technique enables to achieve the momentum conservation at the desired frequencies without significant changes in the shape of the phase matching function.

KTP and bulk crystals in terms of purity relative to domain-engineered crystals with a Gaussian and also with a more general nonlinear response.

### 6.2.1 Bulk and periodically poled crystals

Usual bulk crystals possess a uniform nonlinear coefficient  $\chi_{\text{eff}}^{(2)} = \text{const.}$ , which leads to a sinc-shaped phase matching function

$$\Phi(\mathbf{q}_s, \mathbf{q}_i) = N_0 V(\mathbf{q}_s + \mathbf{q}_i) L \text{sinc}(L\Delta k_z/2). \quad (6.5)$$

In contrast, periodically poled crystals are composed of thin layers of a birefringent material, wherein the sign of the nonlinear coefficient  $\chi_{\text{eff}}^{(2)}$  is periodically flipped in each domain. This flipping occurs periodically with the poling period  $\Lambda$ , which is a characteristic length scale defining the spatial periodicity of the crystal structure [see Fig. 6.1]. Interestingly, periodically poling also gives rise to an approximate sinc-shaped phase matching function, however with a reduced effective nonlinearity with a factor of  $2/\pi$ .

We can calculate the purity of the single-photon state by inserting the expression (6.5) into Eq. (6.4). Figure 6.2 shows the spatial purity as a function of the beam waist  $w_p$  and the crystal length  $L$ . Notably, the purity remains approximately constant along the curves  $L \propto w_p^2$ . This is not surprising, since under the degeneracy condition  $k_s \approx k_i \approx k_p/2$ , the spatial biphoton state should depend only on the dimensionless focusing parameter  $\bar{w}_p = w_p/\sqrt{\lambda_p L}$  [59, 92] or, equivalently, the beam parameter  $\xi_p = L/(k_p w_p^2)$  discussed in Ref. [113]. The highest achievable purity, which is  $P = 0.73$ , remains constant along the white dashed curve, corresponding to the beam parameter  $\xi_p \approx 1.42$ . This implies that we have the freedom to choose any pair  $(w_p, L)$

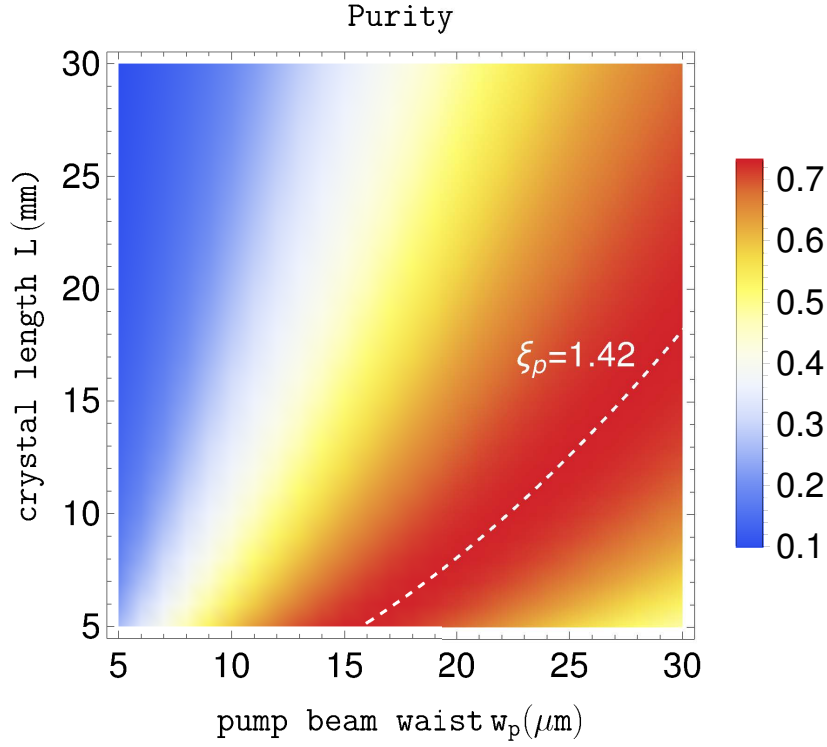


Figure 6.2: Spatial purity as a function of the pump beam waist  $w_p$  and the crystal length  $L$  for standard periodically poled or bulk crystals. The maximum purity of  $P = 0.73$  occurs along the white dashed curve, corresponding to the beam parameter  $\xi = 1.42$ .

lying on this curve, without compromising the spatial purity of the single-photon state.

Most SPDC experiments utilize a SMF, to collect single photons. It is essential to achieve a high pair collection probability to ensure the efficiency of the setup. Therefore, the choice of the proper pair  $(w_p, L)$  along the curve in Fig. 6.2 can be based on the optimization of the pair collection probability into the SMF. The projection modes of the SMF are known to be approximately Gaussian [114]

$$U(\mathbf{q}, w) = \frac{w}{\sqrt{2\pi}} \exp\left(-\frac{w^2}{4}|\mathbf{q}|^2\right).$$

Therefore, the pair collection probability into the SMF is given by the expression

$$R^{(2)} = \left| \iint d\mathbf{q}_s d\mathbf{q}_i \Phi(\mathbf{q}_s, \mathbf{q}_i) [U(\mathbf{q}_s, w_s)]^* [U(\mathbf{q}_i, w_i)]^* \right|^2, \quad (6.6)$$

where  $w_s$  and  $w_i$  are the collection waists of the signal and idler beams, respectively.

The integrals in Eq. (6.6) can be solved analytically for the degenerate scenario  $k_s = k_i = k_p/2$  [113]. The authors of Ref. [113] demonstrated that the highest coupling efficiency is achieved for the beam parameter  $\xi_s = \xi_i = \xi_p = 1.39$ , resulting in a pair

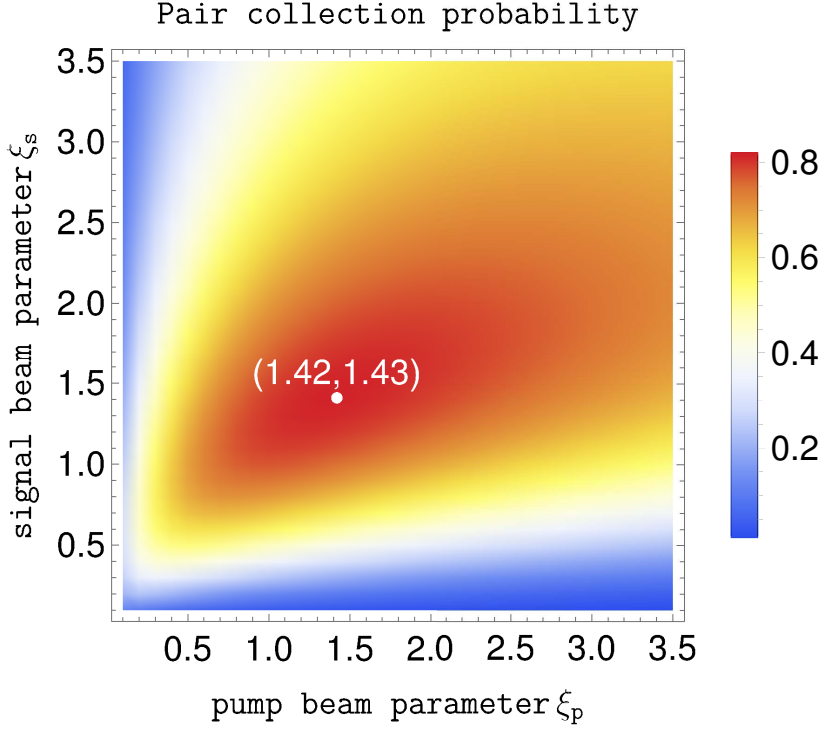


Figure 6.3: Pair collection probability as a function of the pump  $\xi_p$  and signal  $\xi_s$  beam parameters, where the condition  $\xi_s = \xi_i$  is assumed. The highest pair collection probability is achieved at the same beam parameter  $\xi = 1.42$ , which also maximizes the spatial purity.

collection probability into the SMF of approximately  $R^{(2)} \approx 82\%$ . Figure 6.3 illustrates  $R^{(2)}$  as a function of the pump and signal (idler) beam parameters. In our numerical calculations, we obtained similar values of  $\xi_p \approx 1.42$  and  $\xi_s = \xi_i \approx 1.43$ , which lead to  $R^{(2)} \approx 82.2\%$ . The slight deviation from the results of Ref. [113] is due to birefringence in the type-II quasi phase matching configuration considered in our work, where the degeneracy condition  $k_s = k_i = k_p/2$  is not perfectly satisfied.

Remarkably, the optimal values of  $\xi_p$  required to achieve maximum purity and pair collection probability into the SMF are identical. In other words, the optimization of the purity is equivalent to the optimization of the pair collection probability into the SMF. This observation can be explained as follows: When we optimize the purity, we effectively force the signal and idler photons to be more *concentrated* in a specific mode. Consequently, this reduces the spread of the state across different modes. In an ideal scenario with  $P = 1$ , each photon occupies a single-mode state, denoted as  $|\Psi\rangle = |\Psi\rangle_s |\Psi\rangle_i$ . It turns out that this single-mode state  $|\Psi\rangle_{s,i}$  corresponds to a Gaussian state, when the pump beam is Gaussian too. Therefore, the pair collection probability into the SMF, which accepts only photons in a Gaussian mode, increases. However, we will see in Sec. 6.4, that the single mode, where the state is mostly *concentrated*, is the Gaussian state if the pump is also described by a Gaussian.

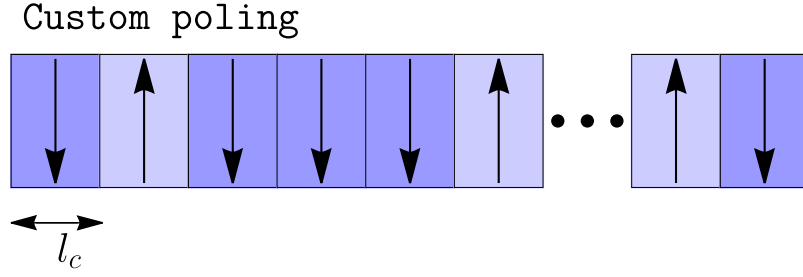


Figure 6.4: The sign of the nonlinear coefficient  $\chi_{eff}^{(2)}$  in each domain is intentionally flipped, in order to achieve the desired effective nonlinearity. The width of each domain equals  $l_c$ , also known as the coherence length. It represents the distance over which the phase between the pump and down-converted photons changes by  $\pi$ .

### 6.2.2 Gaussian nonlinear response

Except for periodically poled crystals, it is also possible to apply custom poling (domain-engineering) of layers in the crystal, as shown in Fig. 6.4. This technique can be used to shape the effective nonlinearity along the crystal. The custom poling has been mostly used to engineer crystal with an approximate Gaussian nonlinear response, modeled as  $\chi_{eff}^{(2)} \propto \exp[-z^2/(\sigma)^2]$  (see Fig. 6.5). In this subsection, we employ a Gaussian nonlinear response and investigate its impact on the purity of the single-photon state. Subsequently, in the next section, we will employ an optimized susceptibility function  $\chi_{eff}^{(2)}(z)$  and compare its performance with the Gaussian nonlinear response.

We can calculate the purity of the single-photon state for a crystal with a Gaussian nonlinear response by inserting  $\chi_{eff}^{(2)} \propto \exp[-z^2/(\sigma)^2]$  into Eq. (6.4). The eight integrals over the transverse momentum can be solved analytically, while the four integrals over  $z$  need to be performed numerically.

Here, we vary the width  $\sigma$  of the Gaussian response and the beam parameter  $\xi_p$ , to optimize the purity. We can increase the maximum spatial purity to  $P = 0.95$  for the parameters  $\xi_p \approx 3$  and  $\sigma \approx L/4$ . The pair collection probability into the SMF is enhanced up to  $R^{(2)} \approx 97\%$ . As we see, domain engineering proves to have a profound impact on the spatial DOF of photons, much like its impact on the spectral DOF: Domain-engineered crystals with a Gaussian nonlinear response reduce the spatial correlations enormously, resulting in high spatial purity. However, the achieved spatial purity of  $P = 0.95$  is still not at the level of the spectral purity  $P = 0.99$  achieved in the previous works.

We might expect that using a narrower Gaussian function for the susceptibility ( $\sigma < L/4$ ) would lead to a higher spatial purity than 0.95. This expectation is based on the idea that a narrower Gaussian function generates fewer spatial modes, potentially

resulting in a higher spatial purity of the single-photon state. However, reducing  $\sigma$  does not lead to an improvement in purity. While a Gaussian function with a narrower width  $\sigma$  can further enhance the spectral purity, a more general function is needed to improve the spatial purity of the single-photon state. The reason behind this is that the phase-mismatch (6.3) in the  $z$  direction of the spatial biphoton state is more complicated because of the quadratic terms than the phase-mismatch of spectral biphoton state from Eq. (3.15), which includes mostly linear terms.

### 6.3 CRYSTAL ENGINEERING

#### 6.3.1 Optimal susceptibility function

In this section, our goal is to explore a more general nonlinear response that can deliver higher purity than the Gaussian nonlinearity. We expect the optimal susceptibility function  $\chi_{\text{eff}}^{(2)}(z)$  to exhibit symmetry with respect to the axis  $z = 0$ , since the well-working Gaussian function is symmetric to that axis too. Therefore, we expand  $\chi_{\text{eff}}^{(2)}(z)$  into cosine series, similar to the Fourier series for even functions

$$\chi_{\text{eff}}^{(2)}(z) = \sum_{n=0}^N c_n \cos(nz/\sigma), \quad (6.7)$$

where the expansion coefficients  $c_n$  are initially unknown and  $\sigma = L/4$ . The purity as a function of  $c_n$ ,  $P = P(c_0, c_1, \dots, c_N)$ , can be constructed by inserting Eq. (6.7) into Eq. (6.4). We truncate the sum at  $N = 7$  in our analysis. The following steps are performed in order to find the optimal expansion coefficients  $c_n$ . (i) Construct the function  $P = P(c_0, c_1, \dots, c_7)$  and calculate its local maximum for the fixed beam parameter  $\xi_p = 1.42$  (as determined in the preceding section). The function FindMaximum from Wolfram Mathematica v. 12.3 [1] is used to calculate this local maximum. (ii) Based on the calculated coefficients  $c_0, c_1, \dots, c_7$ , construct the susceptibility function  $\chi_{\text{eff}}^{(2)}(z)$ . (iii) Optimize the purity as a function of the beam parameter, where the reconstructed susceptibility function  $\chi_{\text{eff}}^{(2)}(z)$  is used. (iv) Repeat the first three steps for the replaced optimal beam parameter until the purity converges. The obtained results are independent of  $\sigma$ , which only affects how rapidly the cosine series converges.

The final optimal value for the beam parameter is  $\xi_p = 3.67$  and the corresponding  $c_n$  coefficients are  $-0.2904, 0.6799, -0.4851, 0.3903, -0.2195, 0.1242, -0.0440, 0.01487$  for  $n = 0, 1, 2, 3, 4, 5, 6$  and  $n = 7$ , respectively. The calculated cosine series and the Gaussian susceptibility functions are displayed in Fig. 6.5 for comparison. The optimized susceptibility function indeed enhances the purity up to 0.98 and the pair collection probability into the SMF up to  $R^{(2)} \approx 99\%$ . This indicates that the Gaussian



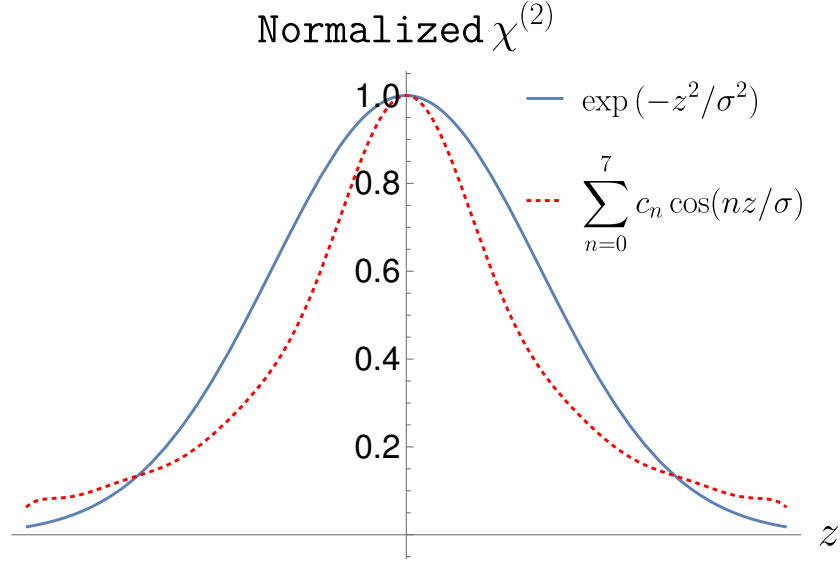


Figure 6.5: Comparison of a normalized Gaussian nonlinear response (blue solid line) with the cosine series nonlinear response (red dashed line). The optimized nonlinear response ensures higher purity of the single-photon state compared to the Gaussian response.

| Parameter                   | Sinc  | Gaussian | Cosine |
|-----------------------------|-------|----------|--------|
| purity of the reduced state | 0.73  | 0.95     | 0.98   |
| coupling into the SMF       | 82%   | 97%      | 99%    |
| heralding efficiency        | 99.4% | 99.86%   | 99.98% |

Table 6.1: Comparison of performances of different nonlinear responses in terms of purity, pair collection probability into a single-mode fiber, and heralding efficiency. The considered nonlinear responses are the common sinlike phase matching from periodically poled or bulk crystals, and Gaussian and optimized cosine series from domain-engineered crystals.

nonlinear response is not the most suitable choice to achieve high spatial purity for the single-photon state. To demonstrate the convergence of the *cosine*-series, we calculate the pair collection probability as a function of the number of terms  $N$  in the series, as shown in Fig. 6.6.

Table 6.1 provides a summary of the crystal performances with different nonlinear responses regarding the spatial purity, pair collection probability into the SMF, and heralding efficiency. The heralding efficiency of the single photon is obtained by tracing out the possible wave vectors of the partner photon (here idler)

$$\eta = \int d\mathbf{q}_i \left| \int d\mathbf{q}_s \Phi(\mathbf{q}_s, \mathbf{q}_i) \mathcal{U}(\mathbf{q}_s, \mathbf{w}_s) \right|^2. \quad (6.8)$$

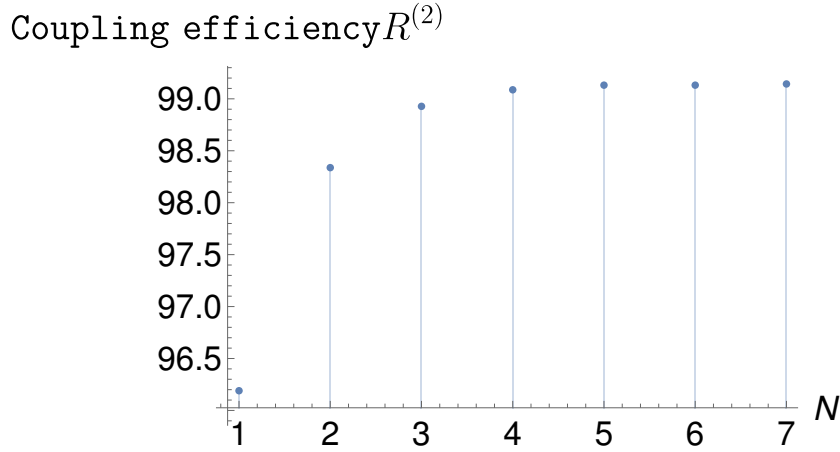


Figure 6.6: Pair collection probability into the SMF as a function of the number of terms in the cosine series for  $\chi_{\text{eff}}^{(2)}(z)$ . Surprisingly, we can achieve a high collection probability of 99% even with a small number of terms, such as  $N = 5$ .

### 6.3.2 Custom poling

The effective nonlinearity of the crystal accessible in the experiment is encoded in the phase matching function. The phase matching function of a crystal with susceptibility given by Eq. 6.7 takes the form

$$\begin{aligned} \phi_{\text{target}}(\Delta k_z) &= \int_{-L/2}^{L/2} dz \sum_{n=0}^7 c_n \cos(nz/\sigma) \exp\left[i\Delta k_z z\right] \\ &= \frac{L}{2} \sum_{n=0}^7 c_n [\text{sinc}(2n - \Delta k_z L/2) + \text{sinc}(2n + \Delta k_z L/2)]. \end{aligned} \quad (6.9)$$

The susceptibility  $\chi_{\text{eff}}^{(2)}$  is modeled as a continuous function of  $z$  in this theoretical treatment. However, we should account for the discontinuous manner of the susceptibility in a crystal in the practical implementation of crystal engineering. Specifically, the poling function can take only on values of  $\pm\chi_{\text{eff},0}^{(2)}$ , where  $\chi_{\text{eff},0}^{(2)}$  is the modulus of the susceptibility  $\chi_{\text{eff}}^{(2)}$ . We employ a domain-engineering process, wherein the nonlinear medium consists of  $M$  domains of birefringent material, each with a length of  $l_c$ , as shown in Fig. 6.4. These domains can be oriented in either the *up* or the *down* direction. Consequently, the phase matching function for the entire crystal becomes a linear superposition of individual phase matching functions for each crystal domain [3]

$$\chi_{\text{eff}}^{(2)}(z) = \chi_{\text{eff},0}^{(2)} \sum_{m=1}^M s_m \text{rect}\left(\frac{z - z_m}{l_c}\right),$$

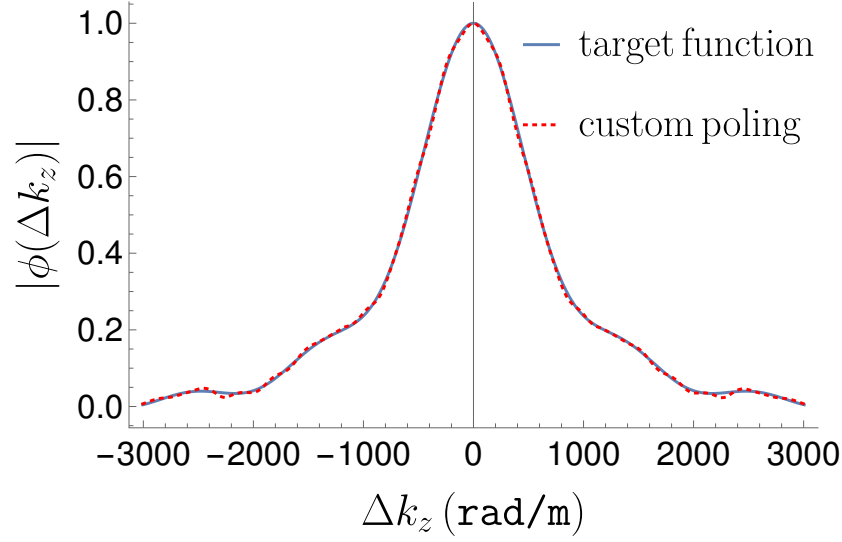


Figure 6.7: Comparison of the normalized target phase matching function calculated by Eq. (6.9) (blue solid line) with the phase matching function of a custom poled crystal (red dashed line). Indeed, custom-poled crystals are capable of producing highly intricate and well-designed target phase matching functions.

where  $s_m$  takes on a value of either 1 or  $-1$  depending on the orientation of the domain and  $z_m = (m - 1/2)l_c - L/2$  specifies the positions of the  $m$ th domain. The corresponding phase matching function is given by

$$\begin{aligned} \phi_s(\Delta k_z) &= \chi_{\text{eff},0}^{(2)} \sum_{m=1}^M s_m \int_{-\infty}^{\infty} dz \text{rect}\left(\frac{z - z_m}{l_c}\right) \exp\left[i\Delta k_z z\right] \\ &\propto \chi_{\text{eff},0}^{(2)} l_c \text{sinc}\left(\frac{\Delta k_z l_c}{2}\right) \sum_{m=1}^M s_m \exp\left[i\Delta k_z z_m\right]. \end{aligned} \quad (6.10)$$

The task is to find the crystal alignment  $s_m$  which yields a phase matching function  $\phi_s$  closest to the target function  $\phi_{\text{target}}$  [the susceptibility function  $\chi_{\text{eff}}^{(2)}$  shown in Fig. 6.5]. Here, we utilize the code provided by Dosseva *et al.* [3], to determine the customized poling of the crystal. The blue solid line in Fig. 6.7 represents the target phase matching function given by Eq. (6.9), and the red dashed line corresponds to the phase matching function of the custom poled crystal (6.10) obtained through the code from Ref. [3]. Our calculations involve 1300 domains, each with a length of 23  $\mu\text{m}$ , resulting in a total crystal length of  $L = 29.9$  mm. As demonstrated in Fig. 6.7, the complex phase matching function described by Eq. (6.9) is excellently reproduced, thereby confirming its suitability and applicability in real experimental setups.

Overall, an engineered crystal typically exhibits a lower effective nonlinearity compared to a periodically poled crystal of the same length. Despite this drawback, in many experimental settings, the benefits of enhanced purity in the generated signal

and idler photons outweigh the cost of reduced efficiency. Furthermore, practical solutions exist to address this limitation. For instance, the reduced nonlinearity can be compensated by increasing the power of the laser source or employing a longer crystal, thereby maintaining a sufficient pair generation rate.

A logical progression for further research would be to incorporate both spectral and spatial DOFs of photons into the optimization scheme. This approach aims to design a source of pure spatio-spectral photon pairs from SPDC that requires no spectral or spatial filtering. The achieved purity of  $P = 0.98$  using the optimized nonlinear response is a significant improvement but it is still quite far from unity. Considering the additional impact of the spectral DOF, this value would decrease vastly. Therefore, achieving a spatio-spectral purity close to unity solely with domain-engineered crystals poses a challenging task.

#### 6.4 PUMP ENGINEERING

In this section, we explore the possibility of enhancing the spatial purity of the single-photon state through pump engineering. Pump engineering has previously been utilized to control spatial correlations in SPDC [36, 109, 115–117]. In our approach, we consider an ansatz involving a superposition of LG modes for the pump

$$V = \sum_{p,\ell} a_{p,\ell} \text{LG}_p^\ell. \quad (6.11)$$

The fundamental approach remains unchanged: We aim to determine the optimal set of coefficients  $a_{p,\ell}$  that maximizes the spatial purity. However, This is a more difficult task than crystal engineering, since the eight-dimensional integral in Eq. (6.4) should be solved fully numerically because of the complex function for the pump from Eq. (6.11). This calculation requires high numerical accuracy, which makes it computationally expensive. Therefore, we need to simplify the task to some extent.

For simplicity, we can employ the biphoton state decomposed into the LG modes from Eq. (3.17) in the narrowband regime

$$|\Psi\rangle = \sum_{p_s, p_i=0}^{\infty} \sum_{\ell_s, \ell_i=-\infty}^{\infty} C_{p, p_s, p_i}^{\ell_s, \ell_i} |p_s, \ell_s\rangle |p_i, \ell_i\rangle, \quad (6.12)$$

and truncate the infinite summations in Eq. (6.12) at reasonable mode number values to consider a subspace state. If the pump beam is given by Eq. (6.11), the coincidence

amplitudes are updated to a similar linear superposition,  $\sum_{p,l} a_{p,l} C_{p,p_s,p_i}^{\ell_s,\ell_i}$ . This truncation enormously simplifies our calculation. The subspace state reads then

$$|\Psi_s\rangle = \sum_{p_s,p_i=0}^H \sum_{\ell_s,\ell_i=-U}^U \left( \sum_{p,l} a_{p,l} C_{p,p_s,p_i}^{\ell_s,\ell_i} \right) |p_s, \ell_s\rangle |p_i, \ell_i\rangle.$$

where  $H$  and  $U$  are the boundaries of the subspace.

We use the optimized phase matching from Sec. 6.3 and construct the purity as a function of the coefficients  $a_{p,l}$ ,  $P = P(a_{p_1,\ell_1}, a_{p_2,\ell_2}, \dots, a_{p_n,\ell_n})$ . The summation over the pump beam modes is performed in the range of  $p = 0, 1, 2$  and  $\ell = -3, -2, \dots, 3$ . We achieve purity of  $P \approx 0.99$  by optimizing the coefficients  $a_{p,l}$  within this restricted range. This is an improvement to the purity  $P = 0.98$  from the preceding section. However, there are trade-offs with respect to the pair collection probability and the heralding efficiency. The pair collection probability drops to 0.64, and the heralding efficiency reduces to 99.3%, mainly due to the fact that the generated single mode is no longer the fundamental Gaussian mode.

Figure 6.8 illustrates the decomposition of signal and idler photons in the LG basis for the Gaussian and engineered pump. The engineered pump symmetrizes the mode distribution but it comes at the cost of the Gaussian mode. While the single mode generated by the Gaussian pump remains close to the fundamental Gaussian mode, the single mode generated by the engineered pump is now a superposition of LG modes. This is the reason, why the pair collection probability into the SMF is decreased in the case of an engineered pump.

Despite the reduction in pair collection probability into the SMF, this type of source could be particularly intriguing for experiments that prioritize the purity of photons in certain interference setups rather than the pair collection efficiency. In such cases, the ability to control and enhance the purity of the photons through pump engineering may outweigh the limitations in collection efficiency, making the engineered pump a valuable tool for specific quantum optics experiments and applications.

## 6.5 EFFICIENCY OF PUMP ENGINEERING

We have demonstrated that a shaped pump beam can enhance the spatial purity of the generated photons. A natural question arises: Does the use of a shaped pump come at the cost of reducing the pair creation probability? In general, the efficiency of pair generation will not be significantly affected when transitioning from a Gaussian

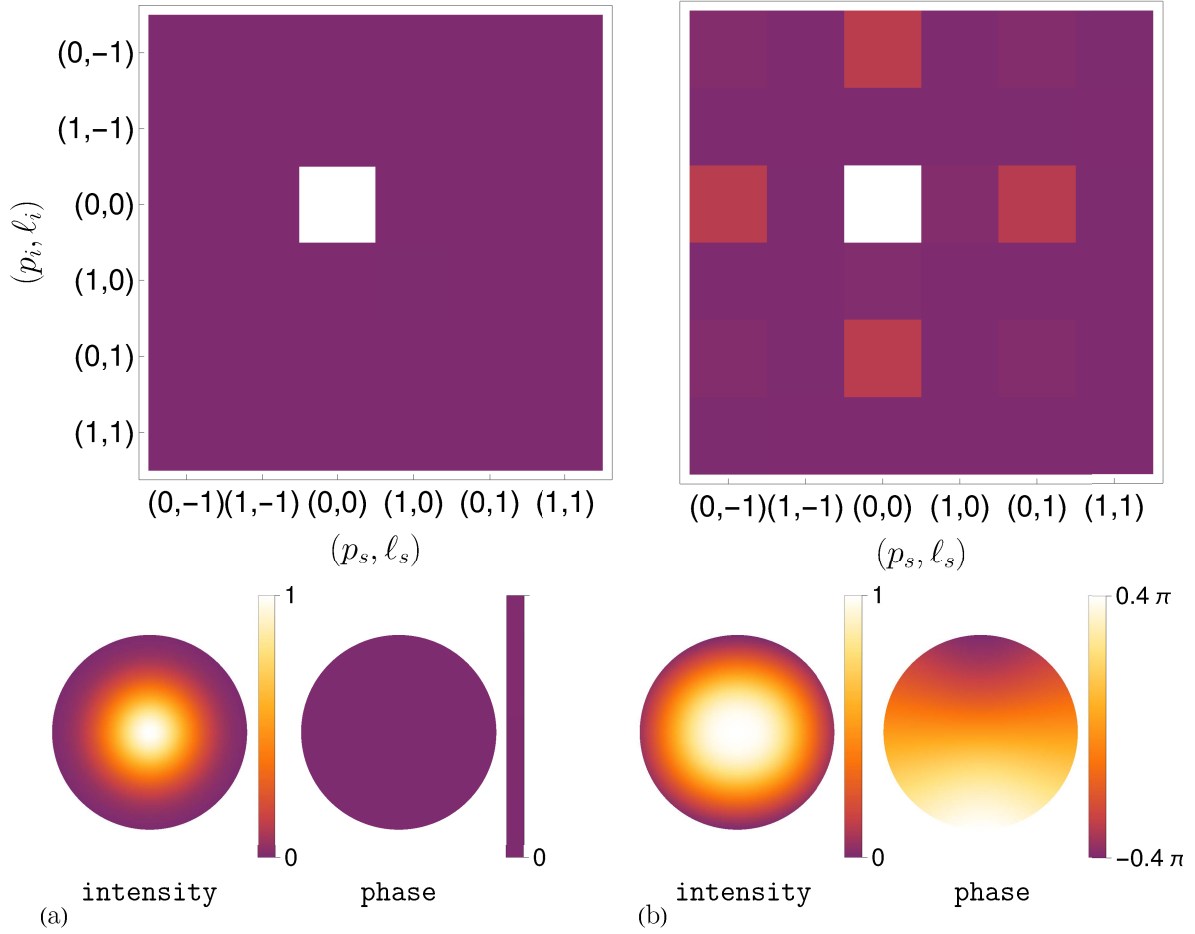


Figure 6.8: Joint mode distribution of the biphoton state in the **LG** basis for (a) a Gaussian beam and (b) for an engineered pump beam. The corresponding beam profiles and phase distributions are presented at the bottom of the figure. The calculations were performed based on the phase matching function derived in Sec. 6.3.

to an engineered pump, as long as the laser intensity remains constant. This statement can be proved by calculating the total pair collection probability

$$R_{\text{total}} = \iint d\mathbf{q}_s d\mathbf{q}_i |\Phi(\mathbf{q}_s, \mathbf{q}_i)|^2. \quad (6.13)$$

These integrals are very easy to solve in the degenerate scenario,  $k_s = k_i = k_p/2$ . If we use the notation  $\mathbf{q}_- = \mathbf{q}_s - \mathbf{q}_i$  and  $\mathbf{q}_+ = \mathbf{q}_s + \mathbf{q}_i$ , the biphoton mode function in the degenerate scenario becomes

$$\Phi(\mathbf{q}_+, \mathbf{q}_-) = N_0 V(\mathbf{q}_+) \phi(\mathbf{q}_-),$$

where the phase matching function  $\phi(\mathbf{q}_-)$  reads

$$\phi(\mathbf{q}_-) = \int_{-L/2}^{L/2} dz \chi_{\text{eff}}^{(2)}(z) \exp \left[ i \frac{|\mathbf{q}_-|^2}{2k_p} z \right].$$

The integrals in Eq. (6.13) can then be simplified to

$$R_{\text{total}} = \frac{1}{4} N_0^2 \int d\mathbf{q}_- |\phi(\mathbf{q}_-)|^2, \quad (6.14)$$

where it is assumed that the pump profile is normalized  $\int d\mathbf{q}_+ |V(\mathbf{q}_+)|^2 = 1$ . It is evident from Eq. (6.14) that the total pair collection probability is independent of the pump beam profile, as long as the intensity of the laser remains constant. The total rate becomes dependent on the pump beam profile only if the crystal produces nondegenerate SPDC. Nonetheless, this dependence is relatively weak based on our calculations.

It is important to acknowledge that in our analysis, we have not accounted for possible losses that may arise from experimentally transforming the Gaussian pump beam into an engineered pump beam profile. These losses can be in principle eliminated by using recent beam shaping approaches, such as multi-plane light conversion techniques using custom computer-generated holograms [118, 119].





---

## CONCLUSIONS AND OUTLOOK

---

In this dissertation, we investigated the process of **SPDC** in bulk and domain-engineered crystals driven by spatially structured laser fields. Our study yielded four prominent accomplishments.

The first achievement is the formulation and subsequent experimental validation of a comprehensive closed-form expression for the spatio-spectral biphoton state decomposed into the **LG** basis [see Chap. 3, Eq. (3.24)]. The expression reveals the dependence of the modal **LG** decomposition of the biphoton state on the frequency and thus correctly describes the spatio-spectral coupling in **SPDC**. The developed theory captures all types of nonlinear crystals, which produce **SPDC** photons in the quasicollinear regime. Moreover, the formalism is applicable to arbitrary paraxial pump beams and effective crystal nonlinearities. Various essential parameters and aspects of **SPDC** can be computed with the expression (3.24), such as the joint spectral density, photon bandwidths, pair-collection probability, heralding ratio, spectral and spatial correlations, Schmidt decomposition, Schmidt number of the state and many more.

The established link in Chap. 4 between the Gouy phase and the spatio-spectral coupling in **SPDC** is the second accomplishment of the thesis. We demonstrated that the spectral characteristics of the down-converted photons are determined by the relative Gouy phase shared among the pump, signal, and idler beams. The decoupling of the spatial and spectral **DOFs** is only feasible when the down-converted photons possess the same relative Gouy phase. Nonetheless, this proves challenging due to the probabilistic nature of **SPDC**. The spatio-spectral coupling can be decreased through strategic employment of pump and crystal engineering for a truncated subspace state. This is especially achieved by constraining the biphoton state into modes that carry the same relative Gouy phase.

Next, in Chapter 5, we constructed high-dimensional entangled states in the **OAM** basis by employing spatially shaped pump beams. The state engineering was based on the interplay between the relative Gouy phase and the spatio-spectral coupling. Specifically, the **OAM** modes that contribute to the high-dimensional state need to

be spectrally indistinguishable, otherwise, the distinguishability arising from the spectral DOF reduces the coherence of the state.

Another challenge of state engineering in the OAM basis involves the appearance of undesired side modes, which do not contribute to the high-dimensional entangled state. The more side modes are generated, the less efficient the source. Within this context, a possible extension of our work will be the employment of domain-engineered crystals to suppress these undesired side modes.

Finally, in the preceding Chap. 6, we studied the impact of crystal domain engineering on the spatial properties of SPDC. In particular, we demonstrated in Sec. 6.2 that the spatial purity of the single-photon state can be increased by using domain-engineered crystals. Moreover, we found that a general nonlinear response rather than the Gaussian one exists [see Fig. 6.5] that improves the spatial purity of the single-photon state, the pair collection probability into the SMF, and the heralding efficiency. We also showed in Sec. 6.4 that the spatial purity can be further enhanced by spatially shaping the pump beam but at the cost of the pair collection probability into the SMF.

Overall, it is not clear whether generating spatially pure single photons from domain-engineered crystals is more efficient than the spatially filtered photons produced in bulk crystals. It is known that engineered crystals are preferred for generating spectrally pure photons due to the significant challenges associated with spectral filtering. Therefore, the use of filters is not preferable in SPDC setups, where both spatial and spectral DOFs are considered simultaneously. As such, engineered crystals offer a more practical solution.

The ultimate future goal is the generation of spatio-spectral pure photons without any spatial and spectral filtering. This task is very challenging compared to the generation of pure single-photon states only in one DOF due to the spatio-spectral coupling. The task of spatio-spectral pure photons can be solved by employing non-paraxial pump beams, where the spatial and spectral DOF cannot be treated separately. Till now, we employed only paraxial beams, which do not possess spatio-spectral coupling.

The presented results in this thesis improve our understanding about the correlations in SPDC. However, there are still many interesting topics and open questions that can be addressed in future works. A few of them are presented in the following:

(i) We demonstrated in Sec. 3.5.2 that only photons satisfying the OAM conservation can be created. This is not the only selection rule for the spatial modes, in which photon pairs can be produced. In particular, when the ratios of the collection modes to the pump mode are set as  $w_s/w_p = w_i/w_p = \sqrt{2}$ , only modes satisfying the condition  $N_s + N_i \geq N_p$  can be produced through SPDC. Here  $N$  is the combined mode number,  $N = 2p + |\ell|$  of an LG mode. To demonstrate the validity of the

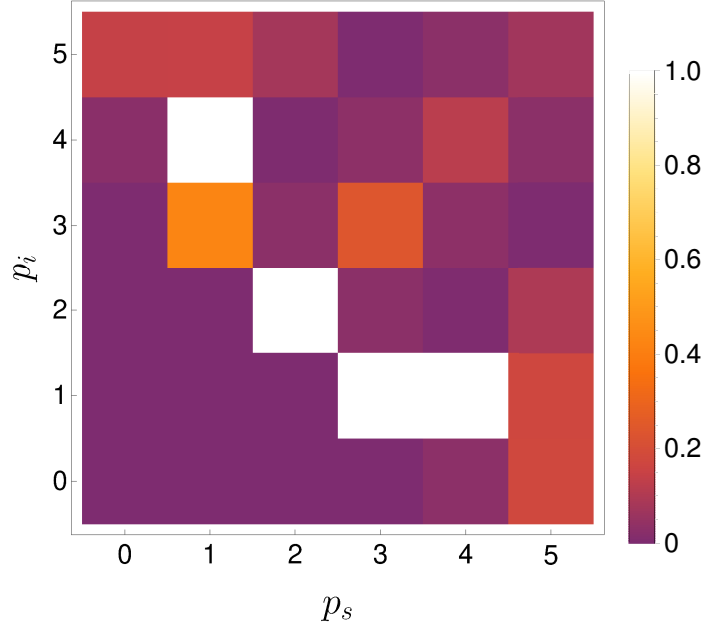


Figure 7.1: Correlation between radial mode numbers of signal  $p_s$  and idler  $p_i$  photons for  $\ell_s = \ell_i = 0$ . Since the pump is an LG beam with  $p = 4$  and  $w_s/w_p = w_i/w_p = \sqrt{2}$ , no radial modes are generated with  $p_s + p_i < 4$ .

condition  $N_s + N_i \geq N_p$ , we examine an LG pump beam with  $p = 4$  and  $\ell = 0$ . Furthermore, we presume the signal and idler photons have zero OAM,  $\ell_s = \ell_i = 0$ , simplifying the condition  $N_s + N_i \geq N_p$  to  $p_s + p_i \geq p$ .

Figure 7.1 displays the correlations between the radial modes of the signal and idler photons. As we can see, no modes are generated that do not satisfy the condition  $p_s + p_i \geq p$ . The further investigation of this observation will improve our understanding of spatial correlations in SPDC. Moreover, it is interesting to examine if the condition  $N_s + N_i \geq N_p$  is linked to the spatio-spectral coupling in SPDC and to the Gouy phase.

(ii) The results presented in this dissertation are confined within the boundaries of the paraxial and quasicollinear regimes. The existing framework for nonparaxial and noncollinear geometries primarily relies on numerical computations. However, the prospect of transforming these approaches into an analytical framework holds the potential to unveil novel dimensions of SPDC. This analytical extension could shed light on aspects that might otherwise remain obscured by the intricacies of numerical approaches.

(iii) The violation of OAM conservation in SPDC is a prominent consequence of the nonparaxial and noncollinear regimes. If the conditions for paraxial propagation are not met, then the spin and orbital angular momentum components of light will become coupled and cannot be measured separately [120]. Thus, the conservation of a distinct physical quantity comes to the forefront, namely TAM of light.

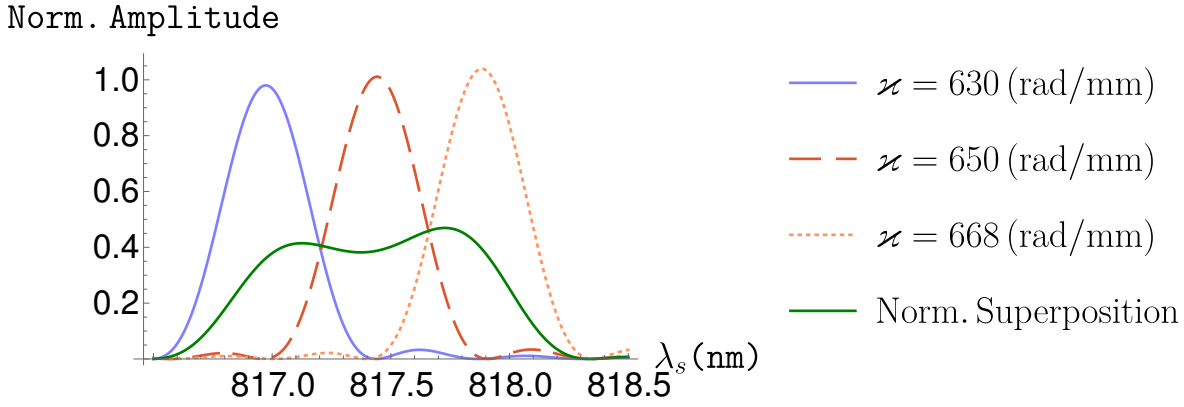


Figure 7.2: Normalized spectra of the signal photon for three CW pump beams with different  $\varkappa$  and their normalized superposition.

An effective way to study the conservation of TAM is by using nonparaxial Bessel beams as the pump source for the crystal. These beams are eigenstates of the TAM operator, and their utilization in experiments can serve to assess TAM. In situations where the paraxial regime is not guaranteed, TAM can be a reliable alternative for encoding and transmitting information through free space.

(iv) Bessel beams can also be used to generate very broadband SPDC, which is highly relevant for frequency multiplexing [121]. The Bessel beam in the momentum space under the paraxial regime reads

$$a_{\varkappa\ell}(\mathbf{q}) = \sqrt{\frac{2\pi}{\varkappa}} (-i)^\ell e^{i\ell\varphi_{\mathbf{q}}} \delta(\mathbf{q} - \varkappa), \quad (7.1)$$

where  $\varkappa = |\mathbf{q}|$  is the modulus of the transverse momentum. When applying the SPDC process with a Bessel pump beam, the delta function in Eq. (7.1) transforms the expression (3.14) of the phase mismatch in the  $z$  direction into

$$\Delta k_z = \Delta\Omega + \frac{\rho_s^2}{k_s} + \frac{\rho_i^2}{2k_i} - \frac{\varkappa^2}{k_p}. \quad (7.2)$$

The term  $\varkappa^2/k_p$  in Eq. (7.2) induces a constant shift in the spectrum of down-converted photons. Therefore, Bessel beams with different  $\varkappa$  induce different shifts of the spectrum. If we use a superposition of pump beams with various  $\varkappa$ , a broad, flat spectrum of SPDC photons can be generated. Figure 7.2 depicts the spectra generated by three separate pump beams, each with varying  $\varkappa$  values, as well as the spectrum produced by their normalized combination.

(v) Another physical quantity that can be studied for the conservation in a non-collinear SPDC is the mode number  $p_{\text{IG}}$  of IG beams. IG beams represent the exact, complete, and orthogonal solutions of the paraxial wave equation in elliptical coordi-

nates. Along with  $p_{\text{IG}}$ , a photon in a **IG** mode is described by the ellipticity parameter  $\epsilon$ , and the quantum number  $m$ . **IG** beams encompass a broader class of paraxial beams, as they converge to the **LG** modes when  $\epsilon \rightarrow 0$  or **HG** modes when  $\epsilon \rightarrow \infty$ . In particular, the following relations hold between the quantum numbers of the **IG** and **LG** modes for  $\epsilon \rightarrow 0$

$$m = \ell, \text{ and } p_{\text{IG}} = 2p + \ell. \quad (7.3)$$

The quantum number  $p_{\text{IG}}$  may function as a more fundamental quantum observable, encoding information about both the radial mode and **OAM** numbers. To comprehend the physical significance of  $p_{\text{IG}}$ , it is crucial to derive the corresponding operator, as it has been performed for the radial mode number of **LG** beams [122]. Subsequently, the observable associated with that operator need to be examined for the conservation in **SPDC**.

(vi) In Chapter 6, we introduced a **SPDC** setup designed to yield spatially pure and indistinguishable photon pairs. The investigations were performed for the low gain regime, where the dominance lies with the two-photon field. If the intensity of the laser is increased (high gain regime), the contribution of higher photon number states becomes significant. In that context, it is unclear whether the purity and indistinguishability of photons are preserved when the laser intensity increases. This question underscores the need for further investigation.

In the high gain regime, the signal and idler beams appear as squeezed light states, which have been ingeniously employed in experiments based on **GBS** [42]. The squeezed light states utilized in **GBS** must also exhibit high photon indistinguishability and purity. These applications aim to demonstrate the quantum computational advantage, often referred to as quantum supremacy.

Summarizing, significant effort is still required to develop reliable and high-performance sources to generate single-photon or maximally entangled states. Nevertheless, the groundwork for these advancements has already been established. Parametric down-conversion has the potential to fulfill this role as an efficient source of distinct quantum states, provided that its inherent probabilistic nature, photon number purity, and challenges related to spatio-spectral coupling are effectively tackled.



---

## BIBLIOGRAPHY

---

- [1] Wolfram Research, Inc. *Mathematica, Version 12.3*. Champaign, IL, 2021.
- [2] T. Hahn. “Cuba—a library for multidimensional numerical integration.” In: *Computer Physics Communications* 168.2 (2005), pp. 78–95. ISSN: 0010-4655. DOI: <https://doi.org/10.1016/j.cpc.2005.01.010>. URL: <https://www.sciencedirect.com/science/article/pii/S0010465505000792>.
- [3] Annamaria Dosseva, Łukasz Cincio, and Agata M. Brańczyk. “Shaping the joint spectrum of down-converted photons through optimized custom poling.” In: *Phys. Rev. A* 93 (1 2016), p. 013801. DOI: [10.1103/PhysRevA.93.013801](https://doi.org/10.1103/PhysRevA.93.013801). URL: <https://link.aps.org/doi/10.1103/PhysRevA.93.013801>.
- [4] Inkscape Project. *Inkscape*. Version 0.92.5. Apr. 16, 2020. URL: <https://inkscape.org>.
- [5] James Clerk Maxwell. “VIII. A dynamical theory of the electromagnetic field.” In: *Philosophical Transactions of the Royal Society of London* 155 (1865), pp. 459–512. DOI: [10.1098/rstl.1865.0008](https://doi.org/10.1098/rstl.1865.0008). eprint: <https://royalsocietypublishing.org/doi/pdf/10.1098/rstl.1865.0008>. URL: <https://royalsocietypublishing.org/doi/abs/10.1098/rstl.1865.0008>.
- [6] A. Einstein. “Über einen die Erzeugung und Verwandlung des Lichtes betreffenden heuristischen Gesichtspunkt.” In: *Annalen der Physik* 322.6 (1905), pp. 132–148. DOI: <https://doi.org/10.1002/andp.19053220607>. eprint: <https://onlinelibrary.wiley.com/doi/pdf/10.1002/andp.19053220607>. URL: <https://onlinelibrary.wiley.com/doi/abs/10.1002/andp.19053220607>.
- [7] Max Planck. “Ueber das Gesetz der Energieverteilung im Normalspectrum.” In: *Annalen der Physik* 309.3 (1901), pp. 553–563. DOI: <https://doi.org/10.1002/andp.19013090310>. eprint: <https://onlinelibrary.wiley.com/doi/pdf/10.1002/andp.19013090310>. URL: <https://onlinelibrary.wiley.com/doi/abs/10.1002/andp.19013090310>.
- [8] T. H. MAIMAN. “Stimulated Optical Radiation in Ruby.” In: *Nature* 187.4736 (1960), pp. 493–494. ISSN: 1476-4687. DOI: [10.1038/187493a0](https://doi.org/10.1038/187493a0). URL: <https://doi.org/10.1038/187493a0>.
- [9] Robert W. Boyd. *Nonlinear Optics, Third Edition*. 3rd. USA: Academic Press, Inc., 2008. ISBN: 0123694701.

- [10] C. K. Hong and L. Mandel. “Theory of parametric frequency down conversion of light.” In: *Phys. Rev. A* 31 (4 1985), pp. 2409–2418. DOI: [10.1103/PhysRevA.31.2409](https://doi.org/10.1103/PhysRevA.31.2409). URL: <https://link.aps.org/doi/10.1103/PhysRevA.31.2409>.
- [11] Paul G. Kwiat, Klaus Mattle, Harald Weinfurter, Anton Zeilinger, Alexander V. Sergienko, and Yanhua Shih. “New High-Intensity Source of Polarization-Entangled Photon Pairs.” In: *Phys. Rev. Lett.* 75 (24 1995), pp. 4337–4341. DOI: [10.1103/PhysRevLett.75.4337](https://doi.org/10.1103/PhysRevLett.75.4337). URL: <https://link.aps.org/doi/10.1103/PhysRevLett.75.4337>.
- [12] Manuel Erhard, Mario Krenn, and Anton Zeilinger. “Advances in high-dimensional quantum entanglement.” In: *Nature Reviews Physics* 2.7 (2020), pp. 365–381. ISSN: 2522-5820. DOI: [10.1038/s42254-020-0193-5](https://doi.org/10.1038/s42254-020-0193-5). URL: <https://doi.org/10.1038/s42254-020-0193-5>.
- [13] Ali Anwar, Chithrabhanu Perumangatt, Fabian Steinlechner, Thomas Jennewein, and Alexander Ling. “Entangled photon-pair sources based on three-wave mixing in bulk crystals.” In: *Review of Scientific Instruments* 92.4 (2021), p. 041101. DOI: [10.1063/5.0023103](https://doi.org/10.1063/5.0023103). URL: <https://doi.org/10.1063/5.0023103>.
- [14] Yi-Han Luo et al. “Quantum Teleportation in High Dimensions.” In: *Phys. Rev. Lett.* 123 (7 2019), p. 070505. DOI: [10.1103/PhysRevLett.123.070505](https://doi.org/10.1103/PhysRevLett.123.070505). URL: <https://link.aps.org/doi/10.1103/PhysRevLett.123.070505>.
- [15] Pieter Kok, W. J. Munro, Kae Nemoto, T. C. Ralph, Jonathan P. Dowling, and G. J. Milburn. “Linear optical quantum computing with photonic qubits.” In: *Rev. Mod. Phys.* 79 (1 2007), pp. 135–174. DOI: [10.1103/RevModPhys.79.135](https://doi.org/10.1103/RevModPhys.79.135). URL: <https://link.aps.org/doi/10.1103/RevModPhys.79.135>.
- [16] Han-Sen Zhong et al. “Quantum computational advantage using photons.” In: *Science* 370.6523 (2020), pp. 1460–1463. DOI: [10.1126/science.abe8770](https://doi.org/10.1126/science.abe8770). URL: <https://www.science.org/doi/pdf/10.1126/science.abe8770>.
- [17] Paul G. Kwiat, Edo Waks, Andrew G. White, Ian Appelbaum, and Philippe H. Eberhard. “Ultrabright source of polarization-entangled photons.” In: *Phys. Rev. A* 60 (2 1999), R773–R776. DOI: [10.1103/PhysRevA.60.R773](https://doi.org/10.1103/PhysRevA.60.R773). URL: <https://link.aps.org/doi/10.1103/PhysRevA.60.R773>.
- [18] Xi-Lin Wang et al. “Experimental Ten-Photon Entanglement.” In: *Phys. Rev. Lett.* 117 (21 2016), p. 210502. DOI: [10.1103/PhysRevLett.117.210502](https://doi.org/10.1103/PhysRevLett.117.210502). URL: <https://link.aps.org/doi/10.1103/PhysRevLett.117.210502>.



- [19] Han-Sen Zhong et al. “12-Photon Entanglement and Scalable Scattershot Boson Sampling with Optimal Entangled-Photon Pairs from Parametric Down-Conversion.” In: *Phys. Rev. Lett.* 121 (25 2018), p. 250505. DOI: [10.1103/PhysRevLett.121.250505](https://doi.org/10.1103/PhysRevLett.121.250505). URL: <https://link.aps.org/doi/10.1103/PhysRevLett.121.250505>.
- [20] P. G. Kwiat, A. M. Steinberg, and R. Y. Chiao. “High-visibility interference in a Bell-inequality experiment for energy and time.” In: *Phys. Rev. A* 47 (4 1993), R2472–R2475. DOI: [10.1103/PhysRevA.47.R2472](https://doi.org/10.1103/PhysRevA.47.R2472). URL: <https://link.aps.org/doi/10.1103/PhysRevA.47.R2472>.
- [21] D. V. Strekalov, T. B. Pittman, A. V. Sergienko, Y. H. Shih, and P. G. Kwiat. “Postselection-free energy-time entanglement.” In: *Phys. Rev. A* 54 (1 1996), R1–R4. DOI: [10.1103/PhysRevA.54.R1](https://doi.org/10.1103/PhysRevA.54.R1). URL: <https://link.aps.org/doi/10.1103/PhysRevA.54.R1>.
- [22] Irfan Ali Khan and John C. Howell. “Experimental demonstration of high two-photon time-energy entanglement.” In: *Phys. Rev. A* 73 (3 2006), 031801(R). DOI: [10.1103/PhysRevA.73.031801](https://doi.org/10.1103/PhysRevA.73.031801). URL: <https://link.aps.org/doi/10.1103/PhysRevA.73.031801>.
- [23] Irfan Ali-Khan, Curtis J. Broadbent, and John C. Howell. “Large-Alphabet Quantum Key Distribution Using Energy-Time Entangled Bipartite States.” In: *Phys. Rev. Lett.* 98 (6 2007), p. 060503. DOI: [10.1103/PhysRevLett.98.060503](https://doi.org/10.1103/PhysRevLett.98.060503). URL: <https://link.aps.org/doi/10.1103/PhysRevLett.98.060503>.
- [24] Alessandro Rossi, Giuseppe Vallone, Andrea Chiuri, Francesco De Martini, and Paolo Mataloni. “Multipath Entanglement of Two Photons.” In: *Phys. Rev. Lett.* 102 (15 2009), p. 153902. DOI: [10.1103/PhysRevLett.102.153902](https://doi.org/10.1103/PhysRevLett.102.153902). URL: <https://link.aps.org/doi/10.1103/PhysRevLett.102.153902>.
- [25] Alois Mair, Alipasha Vaziri, Gregor Weihs, and Anton Zeilinger. “Entanglement of the orbital angular momentum states of photons.” In: *Nature* 412.6844 (2001), pp. 313–316. ISSN: 1476-4687. DOI: [10.1038/35085529](https://doi.org/10.1038/35085529). URL: <https://doi.org/10.1038/35085529>.
- [26] Mario Krenn, Marcus Huber, Robert Fickler, Radek Lapkiewicz, Sven Ramelow, and Anton Zeilinger. “Generation and confirmation of a (100 × 100)-dimensional entangled quantum system.” In: *Proceedings of the National Academy of Sciences* 111.17 (2014), pp. 6243–6247. ISSN: 0027-8424. DOI: [10.1073/pnas.1402365111](https://doi.org/10.1073/pnas.1402365111). URL: <https://www.pnas.org/content/111/17/6243>.

- [27] Jonathan Leach, Barry Jack, Jacqui Romero, Anand K. Jha, Alison M. Yao, Sonja Franke-Arnold, David G. Ireland, Robert W. Boyd, Stephen M. Barnett, and Miles J. Padgett. “Quantum Correlations in Optical Angle–Orbital Angular Momentum Variables.” In: *Science* 329.5992 (2010), pp. 662–665. ISSN: 0036-8075. DOI: [10.1126/science.1190523](https://doi.org/10.1126/science.1190523). eprint: <https://science.sciencemag.org/content/329/5992/662.full.pdf>. URL: <https://science.sciencemag.org/content/329/5992/662>.
- [28] Alipasha Vaziri, Gregor Weihs, and Anton Zeilinger. “Experimental Two-Photon, Three-Dimensional Entanglement for Quantum Communication.” In: *Phys. Rev. Lett.* 89 (24 2002), p. 240401. DOI: [10.1103/PhysRevLett.89.240401](https://doi.org/10.1103/PhysRevLett.89.240401). URL: <https://link.aps.org/doi/10.1103/PhysRevLett.89.240401>.
- [29] J. Romero, D. Giovannini, S. Franke-Arnold, S. M. Barnett, and M. J. Padgett. “Increasing the dimension in high-dimensional two-photon orbital angular momentum entanglement.” In: *Phys. Rev. A* 86 (1 2012), p. 012334. DOI: [10.1103/PhysRevA.86.012334](https://doi.org/10.1103/PhysRevA.86.012334). URL: <https://link.aps.org/doi/10.1103/PhysRevA.86.012334>.
- [30] Dik Bouwmeester, Jian-Wei Pan, Klaus Mattle, Manfred Eibl, Harald Weinfurter, and Anton Zeilinger. “Experimental quantum teleportation.” In: *Nature* 390.6660 (1997), pp. 575–579. ISSN: 1476-4687. DOI: [10.1038/37539](https://doi.org/10.1038/37539). URL: <https://doi.org/10.1038/37539>.
- [31] Jian-Wei Pan, Dik Bouwmeester, Matthew Daniell, Harald Weinfurter, and Anton Zeilinger. “Experimental test of quantum nonlocality in three-photon Greenberger–Horne–Zeilinger entanglement.” In: *Nature* 403.6769 (2000), pp. 515–519. ISSN: 1476-4687. DOI: [10.1038/35000514](https://doi.org/10.1038/35000514). URL: <https://doi.org/10.1038/35000514>.
- [32] R. Ursin et al. “Entanglement-based quantum communication over 144 km.” In: *Nature Physics* 3.7 (2007), pp. 481–486. ISSN: 1745-2481. DOI: [10.1038/nphys629](https://doi.org/10.1038/nphys629). URL: <https://doi.org/10.1038/nphys629>.
- [33] R. van der Meer, J. J. Renema, B. Brecht, C. Silberhorn, and P. W. H. Pinkse. “Optimizing spontaneous parametric down-conversion sources for boson sampling.” In: *Phys. Rev. A* 101 (6 2020), p. 063821. DOI: [10.1103/PhysRevA.101.063821](https://doi.org/10.1103/PhysRevA.101.063821). URL: <https://link.aps.org/doi/10.1103/PhysRevA.101.063821>.
- [34] W. P. Grice, R. S. Bennink, D. S. Goodman, and A. T. Ryan. “Spatial entanglement and optimal single-mode coupling.” In: *Phys. Rev. A* 83 (2 2011), p. 023810. DOI: [10.1103/PhysRevA.83.023810](https://doi.org/10.1103/PhysRevA.83.023810). URL: <https://link.aps.org/doi/10.1103/PhysRevA.83.023810>.

- [35] Vatshal Srivastav, Natalia Herrera Valencia, Saroch Leedumrongwatthanakun, Will McCutcheon, and Mehul Malik. *Characterising and Tailoring Spatial Correlations in Multi-Mode Parametric Downconversion*. 2021. arXiv: [2110.03462](https://arxiv.org/abs/2110.03462) [quant-ph].
- [36] Baghdasar Baghdasaryan and Stephan Fritzsche. “Enhanced entanglement from Ince-Gaussian pump beams in spontaneous parametric down-conversion.” In: *Phys. Rev. A* 102 (5 2020), p. 052412. DOI: [10.1103/PhysRevA.102.052412](https://doi.org/10.1103/PhysRevA.102.052412). URL: <https://link.aps.org/doi/10.1103/PhysRevA.102.052412>.
- [37] Yuanyuan Chen, Wuhong Zhang, Dongkai Zhang, Xiaodong Qiu, and Lixiang Chen. “Coherent Generation of the Complete High-Dimensional Bell Basis by Adaptive Pump Modulation.” In: *Phys. Rev. Applied* 14 (5 2020), p. 054069. DOI: [10.1103/PhysRevApplied.14.054069](https://doi.org/10.1103/PhysRevApplied.14.054069). URL: <https://link.aps.org/doi/10.1103/PhysRevApplied.14.054069>.
- [38] Manuel Erhard, Robert Fickler, Mario Krenn, and Anton Zeilinger. “Twisted photons: new quantum perspectives in high dimensions.” In: *Light: Science & Applications* 7.3 (2018), pp. 17146–17146. ISSN: 2047-7538. DOI: [10.1038/lsa.2017.146](https://doi.org/10.1038/lsa.2017.146). URL: <https://doi.org/10.1038/lsa.2017.146>.
- [39] Lucia Caspani, Chunle Xiong, Benjamin J. Eggleton, Daniele Bajoni, Marco Liscidini, Matteo Galli, Roberto Morandotti, and David J. Moss. “Integrated sources of photon quantum states based on nonlinear optics.” In: *Light: Science & Applications* 6.11 (2017), e17100–e17100. ISSN: 2047-7538. DOI: [10.1038/lsa.2017.100](https://doi.org/10.1038/lsa.2017.100). URL: <https://doi.org/10.1038/lsa.2017.100>.
- [40] Robert Raussendorf, Daniel E. Browne, and Hans J. Briegel. “Measurement-based quantum computation on cluster states.” In: *Phys. Rev. A* 68 (2 2003), p. 022312. DOI: [10.1103/PhysRevA.68.022312](https://doi.org/10.1103/PhysRevA.68.022312). URL: <https://link.aps.org/doi/10.1103/PhysRevA.68.022312>.
- [41] P. Walther, K. J. Resch, T. Rudolph, E. Schenck, H. Weinfurter, V. Vedral, M. Aspelmeyer, and A. Zeilinger. “Experimental one-way quantum computing.” In: *Nature* 434.7030 (2005), pp. 169–176. ISSN: 1476-4687. DOI: [10.1038/nature03347](https://doi.org/10.1038/nature03347). URL: <https://doi.org/10.1038/nature03347>.
- [42] Han-Sen Zhong et al. “Quantum computational advantage using photons.” In: *Science* 370.6523 (2020), pp. 1460–1463. DOI: [10.1126/science.abe8770](https://doi.org/10.1126/science.abe8770). URL: <https://www.science.org/doi/pdf/10.1126/science.abe8770>.
- [43] Koji Azuma, Kiyoshi Tamaki, and Hoi-Kwong Lo. “All-photonic quantum repeaters.” In: *Nature Communications* 6.1 (2015), p. 6787. ISSN: 2041-1723. DOI: [10.1038/ncomms7787](https://doi.org/10.1038/ncomms7787). URL: <https://doi.org/10.1038/ncomms7787>.

- [44] Agata M. Brańczyk, Alessandro Fedrizzi, Thomas M. Stace, Tim C. Ralph, and Andrew G. White. “Engineered optical nonlinearity for quantum light sources.” In: *Opt. Express* 19.1 (2011), pp. 55–65. DOI: [10.1364/OE.19.000055](https://doi.org/10.1364/OE.19.000055). URL: <https://opg.optica.org/oe/abstract.cfm?URI=oe-19-1-55>.
- [45] P. Ben Dixon, Jeffrey H. Shapiro, and Franco N. C. Wong. “Spectral engineering by Gaussian phase-matching for quantum photonics.” In: *Opt. Express* 21.5 (2013), pp. 5879–5890. DOI: [10.1364/OE.21.005879](https://doi.org/10.1364/OE.21.005879). URL: <https://opg.optica.org/oe/abstract.cfm?URI=oe-21-5-5879>.
- [46] J-L. Tambasco, A. Boes, L. G. Helt, M. J. Steel, and A. Mitchell. “Domain engineering algorithm for practical and effective photon sources.” In: *Opt. Express* 24.17 (2016), pp. 19616–19626. DOI: [10.1364/OE.24.019616](https://doi.org/10.1364/OE.24.019616). URL: <https://opg.optica.org/oe/abstract.cfm?URI=oe-24-17-19616>.
- [47] Francesco Graffitti, Dmytro Kundys, Derryck T Reid, Agata M Brańczyk, and Alessandro Fedrizzi. “Pure down-conversion photons through sub-coherence-length domain engineering.” In: *Quantum Science and Technology* 2.3 (2017), p. 035001. DOI: [10.1088/2058-9565/aa78d4](https://doi.org/10.1088/2058-9565/aa78d4). URL: <https://dx.doi.org/10.1088/2058-9565/aa78d4>.
- [48] Francesco Graffitti, Peter Barrow, Massimiliano Proietti, Dmytro Kundys, and Alessandro Fedrizzi. “Independent high-purity photons created in domain-engineered crystals.” In: *Optica* 5.5 (2018), pp. 514–517. DOI: [10.1364/OPTICA.5.000514](https://doi.org/10.1364/OPTICA.5.000514). URL: <https://opg.optica.org/optica/abstract.cfm?URI=optica-5-5-514>.
- [49] Chaohan Cui, Reeshad Arian, Saikat Guha, N. Peyghambarian, Quntao Zhuang, and Zheshen Zhang. “Wave-Function Engineering for Spectrally Uncorrelated Biphotons in the Telecommunication Band Based on a Machine-Learning Framework.” In: *Phys. Rev. Appl.* 12 (3 2019), p. 034059. DOI: [10.1103/PhysRevApplied.12.034059](https://doi.org/10.1103/PhysRevApplied.12.034059). URL: <https://link.aps.org/doi/10.1103/PhysRevApplied.12.034059>.
- [50] Alexander Pickston, Francesco Graffitti, Peter Barrow, Christopher L. Morrison, Joseph Ho, Agata M. Brańczyk, and Alessandro Fedrizzi. “Optimised domain-engineered crystals for pure telecom photon sources.” In: *Opt. Express* 29.5 (2021), pp. 6991–7002. DOI: [10.1364/OE.416843](https://doi.org/10.1364/OE.416843). URL: <https://opg.optica.org/oe/abstract.cfm?URI=oe-29-5-6991>.
- [51] Kai-Hong Luo, Vahid Ansari, Marcello Massaro, Matteo Santandrea, Christof Eigner, Raimund Ricken, Harald Herrmann, and Christine Silberhorn. “Counter-propagating photon pair generation in a nonlinear waveguide.” In: *Opt.*

- Express* 28.3 (2020), pp. 3215–3225. DOI: [10.1364/OE.378789](https://doi.org/10.1364/OE.378789). URL: <http://opg.optica.org/oe/abstract.cfm?URI=oe-28-3-3215>.
- [52] A. Gatti, E. Brambilla, L. Caspani, O. Jedrkiewicz, and L. A. Lugiato. “X Entanglement: The Nonfactorable Spatiotemporal Structure of Biphoton Correlation.” In: *Phys. Rev. Lett.* 102 (22 2009), p. 223601. DOI: [10.1103/PhysRevLett.102.223601](https://doi.org/10.1103/PhysRevLett.102.223601). URL: <https://link.aps.org/doi/10.1103/PhysRevLett.102.223601>.
- [53] O. Jedrkiewicz, A. Gatti, E. Brambilla, and P. Di Trapani. “Experimental Observation of a Skewed X-type Spatiotemporal Correlation of Ultrabroadband Twin Beams.” In: *Phys. Rev. Lett.* 109 (24 2012), p. 243901. DOI: [10.1103/PhysRevLett.109.243901](https://doi.org/10.1103/PhysRevLett.109.243901). URL: <https://link.aps.org/doi/10.1103/PhysRevLett.109.243901>.
- [54] Dasen Zhang and Zhiming Zhang. “The X-like shaped spatiotemporal structure of the biphoton entangled state in a cold two-level atomic ensemble.” In: *Scientific Reports* 7.1 (2017), p. 42373. ISSN: 2045-2322. DOI: [10.1038/srep42373](https://doi.org/10.1038/srep42373). URL: <https://doi.org/10.1038/srep42373>.
- [55] S.P. Walborn, C.H. Monken, S. Pádua, and P.H. Souto Ribeiro. “Spatial correlations in parametric down-conversion.” In: *Physics Reports* 495.4 (2010), pp. 87–139. ISSN: 0370-1573. DOI: <https://doi.org/10.1016/j.physrep.2010.06.003>. URL: <http://www.sciencedirect.com/science/article/pii/S0370157310001602>.
- [56] Silvana Palacios, R. de J. León-Montiel, Martin Hendrych, Alejandra Valencia, and Juan P. Torres. “Flux enhancement of photons entangled in orbital angular momentum.” In: *Opt. Express* 19.15 (July 2011), pp. 14108–14120. DOI: [10.1364/OE.19.014108](https://doi.org/10.1364/OE.19.014108). URL: <http://opg.optica.org/oe/abstract.cfm?URI=oe-19-15-14108>.
- [57] Alejandra Valencia, Alessandro Ceré, Xiaojuan Shi, Gabriel Molina-Terriza, and Juan P. Torres. “Shaping the Waveform of Entangled Photons.” In: *Phys. Rev. Lett.* 99 (24 2007), p. 243601. DOI: [10.1103/PhysRevLett.99.243601](https://doi.org/10.1103/PhysRevLett.99.243601). URL: <https://link.aps.org/doi/10.1103/PhysRevLett.99.243601>.
- [58] Alison M Yao. “Angular momentum decomposition of entangled photons with an arbitrary pump.” In: *New Journal of Physics* 13.5 (2011), p. 053048. DOI: [10.1088/1367-2630/13/5/053048](https://doi.org/10.1088/1367-2630/13/5/053048). URL: <https://doi.org/10.1088%2F1367-2630%2F13%2F5%2F053048>.

- [59] Baghdasar Baghdasaryan, Fabian Steinlechner, and Stephan Fritzsche. “Justifying the thin-crystal approximation in spontaneous parametric down-conversion for collinear phase matching.” In: *Phys. Rev. A* 103 (6 2021), p. 063508. DOI: [10.1103/PhysRevA.103.063508](https://doi.org/10.1103/PhysRevA.103.063508). URL: <https://link.aps.org/doi/10.1103/PhysRevA.103.063508>.
- [60] Yingwen Zhang, Filippus S. Roux, Melanie McLaren, and Andrew Forbes. “Radial modal dependence of the azimuthal spectrum after parametric down-conversion.” In: *Phys. Rev. A* 89 (4 2014), p. 043820. DOI: [10.1103/PhysRevA.89.043820](https://doi.org/10.1103/PhysRevA.89.043820). URL: <https://link.aps.org/doi/10.1103/PhysRevA.89.043820>.
- [61] Yingwen Zhang, Melanie McLaren, Filippus S. Roux, and Andrew Forbes. “Simulating quantum state engineering in spontaneous parametric down-conversion using classical light.” In: *Opt. Express* 22.14 (2014), pp. 17039–17049. DOI: [10.1364/OE.22.017039](https://doi.org/10.1364/OE.22.017039). URL: <http://www.opticsexpress.org/abstract.cfm?URI=oe-22-14-17039>.
- [62] Melanie McLaren, Jacqueline Romero, Miles J. Padgett, Filippus S. Roux, and Andrew Forbes. “Two-photon optics of Bessel-Gaussian modes.” In: *Phys. Rev. A* 88 (3 2013), p. 033818. DOI: [10.1103/PhysRevA.88.033818](https://doi.org/10.1103/PhysRevA.88.033818). URL: <https://link.aps.org/doi/10.1103/PhysRevA.88.033818>.
- [63] R Ramírez-Alarcón, H Cruz-Ramírez, and A B U’Ren. “Effects of crystal length on the angular spectrum of spontaneous parametric downconversion photon pairs.” In: *Laser Physics* 23.5 (2013), p. 055204. DOI: [10.1088/1054-660x/23/5/055204](https://doi.org/10.1088/1054-660x/23/5/055204). URL: <https://doi.org/10.1088/1054-660x/23/5/055204>.
- [64] A. Gatti, T. Corti, E. Brambilla, and D. B. Horoshko. “Dimensionality of the spatiotemporal entanglement of parametric down-conversion photon pairs.” In: *Phys. Rev. A* 86 (5 2012), p. 053803. DOI: [10.1103/PhysRevA.86.053803](https://doi.org/10.1103/PhysRevA.86.053803). URL: <https://link.aps.org/doi/10.1103/PhysRevA.86.053803>.
- [65] P. A. M. Dirac. “A new notation for quantum mechanics.” In: *Mathematical Proceedings of the Cambridge Philosophical Society* 35.3 (1939), 416–418. DOI: [10.1017/S0305004100021162](https://doi.org/10.1017/S0305004100021162).
- [66] Michael A. Nielsen and Isaac L. Chuang. *Quantum Computation and Quantum Information*. Cambridge University Press, 2000. ISBN: 9780521635035. URL: <http://www.cambridge.org/uk/catalogue/catalogue.asp?isbn=9780521635035>.
- [67] F. M. Miatto, H. Di Lorenzo Pires, S. M. Barnett, and M. P. van Exter. “Spatial Schmidt modes generated in parametric down-conversion.” In: *The European Physical Journal D* 66.10 (2012), p. 263. ISSN: 1434-6079. DOI: [10.1140/epjd/e2012-30035-3](https://doi.org/10.1140/epjd/e2012-30035-3). URL: <https://doi.org/10.1140/epjd/e2012-30035-3>.

- [68] F. M. Miatto, T. Brougham, and A. M. Yao. “Cartesian and polar Schmidt bases for down-converted photons.” In: *The European Physical Journal D* 66.7 (2012), p. 183. ISSN: 1434-6079. DOI: [10.1140/epjd/e2012-30063-y](https://doi.org/10.1140/epjd/e2012-30063-y). URL: <https://doi.org/10.1140/epjd/e2012-30063-y>.
- [69] S. S. Straupe, D. P. Ivanov, A. A. Kalinkin, I. B. Bobrov, and S. P. Kulik. “Angular Schmidt modes in spontaneous parametric down-conversion.” In: *Phys. Rev. A* 83 (6 2011), p. 060302. DOI: [10.1103/PhysRevA.83.060302](https://link.aps.org/doi/10.1103/PhysRevA.83.060302). URL: <https://link.aps.org/doi/10.1103/PhysRevA.83.060302>.
- [70] Sudipto Banerjee and Anindya Roy. *Linear Algebra and Matrix Analysis for Statistics*. June 2014, pp. 1–559. ISBN: 9780429174131. DOI: [10.1201/b17040](https://doi.org/10.1201/b17040).
- [71] Nicolai Friis, Giuseppe Vitagliano, Mehul Malik, and Marcus Huber. “Entanglement certification from theory to experiment.” In: *Nature Reviews Physics* 1.1 (2019), pp. 72–87. ISSN: 2522-5820. DOI: [10.1038/s42254-018-0003-5](https://doi.org/10.1038/s42254-018-0003-5). URL: <https://doi.org/10.1038/s42254-018-0003-5>.
- [72] Fabian Steinlechner, Marta Gilaberte, Marc Jofre, Thomas Scheidl, Juan P. Torres, Valerio Pruneri, and Rupert Ursin. “Efficient heralding of polarization-entangled photons from type-o and type-II spontaneous parametric down-conversion in periodically poled KTiOPO<sub>4</sub>.” In: *J. Opt. Soc. Am. B* 31.9 (2014), pp. 2068–2076. DOI: [10.1364/JOSAB.31.002068](http://opg.optica.org/josab/abstract.cfm?URI=josab-31-9-2068). URL: <http://opg.optica.org/josab/abstract.cfm?URI=josab-31-9-2068>.
- [73] Timothy E. Keller and Morton H. Rubin. “Theory of two-photon entanglement for spontaneous parametric down-conversion driven by a narrow pump pulse.” In: *Phys. Rev. A* 56 (2 1997), pp. 1534–1541. DOI: [10.1103/PhysRevA.56.1534](https://link.aps.org/doi/10.1103/PhysRevA.56.1534). URL: <https://link.aps.org/doi/10.1103/PhysRevA.56.1534>.
- [74] Christian Kurtsiefer, Markus Oberparleiter, and Harald Weinfurter. “Generation of correlated photon pairs in type-II parametric down conversion—revisited.” In: *Journal of Modern Optics* 48.13 (2001), pp. 1997–2007. DOI: [10.1080/09500340108240902](https://doi.org/10.1080/09500340108240902). eprint: <https://doi.org/10.1080/09500340108240902>. URL: <https://doi.org/10.1080/09500340108240902>.
- [75] Christopher Gerry and Peter Knight. *Introductory Quantum Optics*. Cambridge University Press, 2004. DOI: [10.1017/CB09780511791239](https://doi.org/10.1017/CB09780511791239).
- [76] Anton Frisk Kockum, Adam Miranowicz, Vincenzo Macrì, Salvatore Savasta, and Franco Nori. “Deterministic quantum nonlinear optics with single atoms and virtual photons.” In: *Phys. Rev. A* 95 (6 2017), p. 063849. DOI: [10.1103/PhysRevA.95.063849](https://link.aps.org/doi/10.1103/PhysRevA.95.063849). URL: <https://link.aps.org/doi/10.1103/PhysRevA.95.063849>.

- [77] Anton Frisk Kockum, Adam Miranowicz, Simone De Liberato, Salvatore Savasta, and Franco Nori. “Ultrastrong coupling between light and matter.” In: *Nature Reviews Physics* 1.1 (2019), pp. 19–40. ISSN: 2522-5820. DOI: [10.1038/s42254-018-0006-2](https://doi.org/10.1038/s42254-018-0006-2). URL: <https://doi.org/10.1038/s42254-018-0006-2>.
- [78] L. Allen, M. W. Beijersbergen, R. J. C. Spreeuw, and J. P. Woerdman. “Orbital angular momentum of light and the transformation of Laguerre-Gaussian laser modes.” In: *Phys. Rev. A* 45 (11 1992), pp. 8185–8189. DOI: [10.1103/PhysRevA.45.8185](https://link.aps.org/doi/10.1103/PhysRevA.45.8185). URL: <https://link.aps.org/doi/10.1103/PhysRevA.45.8185>.
- [79] W. P. Grice and I. A. Walmsley. “Spectral information and distinguishability in type-II down-conversion with a broadband pump.” In: *Phys. Rev. A* 56 (2 1997), pp. 1627–1634. DOI: [10.1103/PhysRevA.56.1627](https://link.aps.org/doi/10.1103/PhysRevA.56.1627). URL: <https://link.aps.org/doi/10.1103/PhysRevA.56.1627>.
- [80] Suman Karan, Shaurya Aarav, Homanga Bharadhwaj, Lavanya Taneja, Arinjoy De, Girish Kulkarni, Nilakantha Meher, and Anand K Jha. “Phase matching in  $\beta$ -barium borate crystals for spontaneous parametric down-conversion.” In: *Journal of Optics* 22.8 (2020), p. 083501. DOI: [10.1088/2040-8986/ab89e4](https://doi.org/10.1088/2040-8986/ab89e4). URL: <https://doi.org/10.1088/2040-8986/ab89e4>.
- [81] K. Fradkin, A. Arie, A. Skliar, and G. Rosenman. “Tunable midinfrared source by difference frequency generation in bulk periodically poled KTiOPO<sub>4</sub>.” In: *Applied Physics Letters* 74.7 (1999), pp. 914–916. DOI: [10.1063/1.123408](https://doi.org/10.1063/1.123408). eprint: <https://doi.org/10.1063/1.123408>. URL: <https://doi.org/10.1063/1.123408>.
- [82] D. S. Tasca, R. M. Gomes, F. Toscano, P. H. Souto Ribeiro, and S. P. Walborn. “Continuous-variable quantum computation with spatial degrees of freedom of photons.” In: *Phys. Rev. A* 83 (5 2011), p. 052325. DOI: [10.1103/PhysRevA.83.052325](https://link.aps.org/doi/10.1103/PhysRevA.83.052325). URL: <https://link.aps.org/doi/10.1103/PhysRevA.83.052325>.
- [83] Nicolas Fabre, Arne Keller, and Pérola Milman. “Time and frequency as quantum continuous variables.” In: *Phys. Rev. A* 105 (5 2022), p. 052429. DOI: [10.1103/PhysRevA.105.052429](https://link.aps.org/doi/10.1103/PhysRevA.105.052429). URL: <https://link.aps.org/doi/10.1103/PhysRevA.105.052429>.
- [84] Eliot Bolduc, Nicolas Bent, Enrico Santamato, Ebrahim Karimi, and Robert W. Boyd. “Exact solution to simultaneous intensity and phase encryption with a single phase-only hologram.” In: *Optics Letters* 38.18 (2013), p. 3546. ISSN: 0146-9592. DOI: [10.1364/ol.38.003546](https://doi.org/10.1364/ol.38.003546).



- [85] Andreas Eckstein, Benjamin Brecht, and Christine Silberhorn. “A quantum pulse gate based on spectrally engineered sum frequency generation.” In: *Opt. Express* 19.15 (2011), pp. 13770–13778. DOI: [10.1364/OE.19.013770](https://doi.org/10.1364/OE.19.013770). URL: <http://opg.optica.org/oe/abstract.cfm?URI=oe-19-15-13770>.
- [86] Baghdasar Baghdasaryan, Fabian Steinlechner, and Stephan Fritzsche. “Characterization of opening angle correlations of a biphoton state decomposed in Bessel modes.” In: *Phys. Rev. A* 101 (4 2020), p. 043844. DOI: [10.1103/PhysRevA.101.043844](https://doi.org/10.1103/PhysRevA.101.043844). URL: <https://link.aps.org/doi/10.1103/PhysRevA.101.043844>.
- [87] S. P. Walborn, S. Pádua, and C. H. Monken. “Conservation and entanglement of Hermite-Gaussian modes in parametric down-conversion.” In: *Phys. Rev. A* 71 (5 2005), p. 053812. DOI: [10.1103/PhysRevA.71.053812](https://doi.org/10.1103/PhysRevA.71.053812). URL: <https://link.aps.org/doi/10.1103/PhysRevA.71.053812>.
- [88] Xi-Feng Ren, Guo-Ping Guo, Jian Li, and Guang-Can Guo. “Entanglement of the Hermite-Gaussian modes states of photons.” In: *Physics Letters A* 341.1 (2005), pp. 81–86. ISSN: 0375-9601. DOI: <https://doi.org/10.1016/j.physleta.2005.04.060>. URL: <http://www.sciencedirect.com/science/article/pii/S0375960105006213>.
- [89] S P Walborn and A H Pimentel. “Generalized Hermite-Gauss decomposition of the two-photon state produced by spontaneous parametric down conversion.” In: *Journal of Physics B: Atomic, Molecular and Optical Physics* 45.16 (2012), p. 165502. DOI: [10.1088/0953-4075/45/16/165502](https://doi.org/10.1088/0953-4075/45/16/165502). URL: <https://dx.doi.org/10.1088/0953-4075/45/16/165502>.
- [90] V. D. Salakhutdinov, E. R. Eliel, and W. Löffler. “Full-Field Quantum Correlations of Spatially Entangled Photons.” In: *Phys. Rev. Lett.* 108 (17 2012), p. 173604. DOI: [10.1103/PhysRevLett.108.173604](https://doi.org/10.1103/PhysRevLett.108.173604). URL: <https://link.aps.org/doi/10.1103/PhysRevLett.108.173604>.
- [91] Filippo M. Miatto, Alison M. Yao, and Stephen M. Barnett. “Full characterization of the quantum spiral bandwidth of entangled biphotons.” In: *Phys. Rev. A* 83 (3 2011), p. 033816. DOI: [10.1103/PhysRevA.83.033816](https://doi.org/10.1103/PhysRevA.83.033816). URL: <https://link.aps.org/doi/10.1103/PhysRevA.83.033816>.
- [92] J. P. Torres, A. Alexandrescu, and Lluís Torner. “Quantum spiral bandwidth of entangled two-photon states.” In: *Phys. Rev. A* 68 (5 2003), 050301(R). DOI: [10.1103/PhysRevA.68.050301](https://doi.org/10.1103/PhysRevA.68.050301). URL: <https://link.aps.org/doi/10.1103/PhysRevA.68.050301>.

- [93] Mario Krenn, Robert Fickler, Marcus Huber, Radek Lapkiewicz, William Plick, Sven Ramelow, and Anton Zeilinger. “Entangled singularity patterns of photons in Ince-Gauss modes.” In: *Phys. Rev. A* 87 (1 2013), p. 012326. DOI: [10.1103/PhysRevA.87.012326](https://doi.org/10.1103/PhysRevA.87.012326). URL: <https://link.aps.org/doi/10.1103/PhysRevA.87.012326>.
- [94] Robert Fickler, Radek Lapkiewicz, William N. Plick, Mario Krenn, Christoph Schaeff, Sven Ramelow, and Anton Zeilinger. “Quantum Entanglement of High Angular Momenta.” In: *Science* 338.6107 (2012), pp. 640–643. DOI: [10.1126/science.1227193](https://doi.org/10.1126/science.1227193). eprint: <https://www.science.org/doi/pdf/10.1126/science.1227193>. URL: <https://www.science.org/doi/abs/10.1126/science.1227193>.
- [95] Mario Krenn, Mehul Malik, Manuel Erhard, and Anton Zeilinger. “Orbital angular momentum of photons and the entanglement of Laguerre–Gaussian modes.” In: *Philosophical Transactions of the Royal Society A: Mathematical, Physical and Engineering Sciences* 375.2087 (2017), p. 20150442. DOI: [10.1098/rsta.2015.0442](https://doi.org/10.1098/rsta.2015.0442). eprint: <https://royalsocietypublishing.org/doi/pdf/10.1098/rsta.2015.0442>. URL: <https://royalsocietypublishing.org/doi/abs/10.1098/rsta.2015.0442>.
- [96] Natalia Herrera Valencia, Vatshal Srivastav, Saroch Leedumrongwatthanakun, Will McCutcheon, and Mehul Malik. “Entangled ripples and twists of light: radial and azimuthal Laguerre–Gaussian mode entanglement.” In: *Journal of Optics* 23.10 (2021), p. 104001. DOI: [10.1088/2040-8986/ac213c](https://doi.org/10.1088/2040-8986/ac213c). URL: <https://dx.doi.org/10.1088/2040-8986/ac213c>.
- [97] Jano Gil-Lopez, Yong Siah Teo, Syamsundar De, Benjamin Brecht, Hyunseok Jeong, Christine Silberhorn, and Luis L. Sánchez-Soto. “Universal compressive tomography in the time-frequency domain.” In: *Optica* 8.10 (2021), pp. 1296–1305. DOI: [10.1364/OPTICA.427645](https://doi.org/10.1364/OPTICA.427645). URL: <https://opg.optica.org/optica/abstract.cfm?URI=optica-8-10-1296>.
- [98] Gabriel Molina-Terriza, Juan P. Torres, and Lluís Torner. “Orbital angular momentum of photons in noncollinear parametric downconversion.” In: *Optics Communications* 228.1 (2003), pp. 155–160. ISSN: 0030-4018. DOI: <https://doi.org/10.1016/j.optcom.2003.09.071>. URL: <https://www.sciencedirect.com/science/article/pii/S0030401803020285>.
- [99] Baghdasar Baghdasaryan, Birger Böning, Willi Paufler, and Stephan Fritzsche. “Dichroism in two-color above-threshold ionization with twisted XUV beams and intense infrared laser fields.” In: *Phys. Rev. A* 99 (2 2019), p. 023403. DOI:

- 10.1103/PhysRevA.99.023403. URL: <https://link.aps.org/doi/10.1103/PhysRevA.99.023403>.
- [100] Hashim A. Yousif and Richard Melka. "Bessel function of the first kind with complex argument." In: *Computer Physics Communications* 106.3 (1997), pp. 199–206. ISSN: 0010-4655. DOI: [https://doi.org/10.1016/S0010-4655\(97\)00087-8](https://doi.org/10.1016/S0010-4655(97)00087-8). URL: <http://www.sciencedirect.com/science/article/pii/S0010465597000878>.
- [101] Wolfram Research, Inc. *Gauss Hypergeometric function*. URL: <https://functions.wolfram.com/PDF/Hypergeometric2F1Regularized.pdf>.
- [102] Carlos Sevilla-Gutiérrez, Varun Raj Kaipalath, Baghdasar Baghdasaryan, Markus Gräfe, Stephan Fritzsche, and Fabian Steinlechner. *Spectral Properties of Transverse Laguerre-Gauss Modes in Parametric Down-Conversion*. 2022. DOI: [10.48550/ARXIV.2209.01913](https://arxiv.org/abs/2209.01913). URL: <https://arxiv.org/abs/2209.01913>.
- [103] Clara I Osorio, Alejandra Valencia, and Juan P Torres. "Spatiotemporal correlations in entangled photons generated by spontaneous parametric down conversion." In: *New Journal of Physics* 10.11 (2008), p. 113012. DOI: [10.1088/1367-2630/10/11/113012](https://doi.org/10.1088/1367-2630/10/11/113012). URL: <https://doi.org/10.1088/1367-2630/10/11/113012>.
- [104] Daisuke Kawase, Yoko Miyamoto, Mitsuo Takeda, Keiji Sasaki, and Shigeki Takeuchi. "Observing Quantum Correlation of Photons in Laguerre-Gauss Modes Using the Gouy Phase." In: *Phys. Rev. Lett.* 101 (5 2008), p. 050501. DOI: [10.1103/PhysRevLett.101.050501](https://link.aps.org/doi/10.1103/PhysRevLett.101.050501). URL: <https://link.aps.org/doi/10.1103/PhysRevLett.101.050501>.
- [105] F.C.V. de Brito, I.G. da Paz, Brigitte Hiller, Jonas B. Araujo, and Marcos Sampaio. "Gouy phase of type-I SPDC-generated biphotons." In: *Physics Letters A* 386 (2021), p. 126989. ISSN: 0375-9601. DOI: <https://doi.org/10.1016/j.physleta.2020.126989>. URL: <https://www.sciencedirect.com/science/article/pii/S0375960120308562>.
- [106] Rachel F. Offer, Andrew Daffurn, Erling Riis, Paul F. Griffin, Aidan S. Arnold, and Sonja Franke-Arnold. "Gouy phase-matched angular and radial mode conversion in four-wave mixing." In: *Phys. Rev. A* 103 (2 2021), p. L021502. DOI: [10.1103/PhysRevA.103.L021502](https://link.aps.org/doi/10.1103/PhysRevA.103.L021502). URL: <https://link.aps.org/doi/10.1103/PhysRevA.103.L021502>.
- [107] Juan P. Torres, Yana Deyanova, Lluís Torner, and Gabriel Molina-Terriza. "Preparation of engineered two-photon entangled states for multidimensional quantum information." In: *Phys. Rev. A* 67 (5 2003), p. 052313. DOI: [10.1103/PhysRevA.67.052313](https://doi.org/10.1103/PhysRevA.67.052313).

- PhysRevA.67.052313. URL: <https://link.aps.org/doi/10.1103/PhysRevA.67.052313>.
- [108] Nicholas Bornman, Wagner Tavares Bueno, Michael Lovemore, and Andrew Forbes. “Optimal Pump Shaping for Entanglement Control in Any Countable Basis.” In: *Advanced Quantum Technologies* 4.10 (2021), p. 2100066. DOI: <https://doi.org/10.1002/qute.202100066>. eprint: <https://onlinelibrary.wiley.com/doi/pdf/10.1002/qute.202100066>. URL: <https://onlinelibrary.wiley.com/doi/abs/10.1002/qute.202100066>.
- [109] E. V. Kovalkov, S. S. Straupe, and S. P. Kulik. “Quantum state engineering with twisted photons via adaptive shaping of the pump beam.” In: *Phys. Rev. A* 98 (6 2018), 060301(R). DOI: [10.1103/PhysRevA.98.060301](https://doi.org/10.1103/PhysRevA.98.060301). URL: <https://link.aps.org/doi/10.1103/PhysRevA.98.060301>.
- [110] J.C. Spall. “Implementation of the simultaneous perturbation algorithm for stochastic optimization.” In: *IEEE Transactions on Aerospace and Electronic Systems* 34.3 (1998), pp. 817–823. DOI: [10.1109/7.705889](https://doi.org/10.1109/7.705889).
- [111] C. H. Monken, P. H. Souto Ribeiro, and S. Pádua. “Transfer of angular spectrum and image formation in spontaneous parametric down-conversion.” In: *Phys. Rev. A* 57 (4 1998), pp. 3123–3126. DOI: [10.1103/PhysRevA.57.3123](https://doi.org/10.1103/PhysRevA.57.3123). URL: <https://link.aps.org/doi/10.1103/PhysRevA.57.3123>.
- [112] Bahaa E. A. Saleh, Ayman F. Abouraddy, Alexander V. Sergienko, and Malvin C. Teich. “Duality between partial coherence and partial entanglement.” In: *Phys. Rev. A* 62 (4 2000), p. 043816. DOI: [10.1103/PhysRevA.62.043816](https://doi.org/10.1103/PhysRevA.62.043816). URL: <https://link.aps.org/doi/10.1103/PhysRevA.62.043816>.
- [113] Silvana Palacios, R. de J. León-Montiel, Martin Hendrych, Alejandra Valencia, and Juan P. Torres. “Flux enhancement of photons entangled in orbital angular momentum.” In: *Opt. Express* 19.15 (2011), pp. 14108–14120. DOI: [10.1364/OE.19.014108](https://doi.org/10.1364/OE.19.014108). URL: <https://opg.optica.org/oe/abstract.cfm?URI=oe-19-15-14108>.
- [114] Daniel Ljunggren and Maria Tengner. “Optimal focusing for maximal collection of entangled narrow-band photon pairs into single-mode fibers.” In: *Phys. Rev. A* 72 (6 2005), p. 062301. DOI: [10.1103/PhysRevA.72.062301](https://doi.org/10.1103/PhysRevA.72.062301). URL: <https://link.aps.org/doi/10.1103/PhysRevA.72.062301>.
- [115] Baghdasar Baghdasaryan, Carlos Sevilla-Gutiérrez, Fabian Steinlechner, and Stephan Fritzsche. “Generalized description of the spatio-temporal biphoton state in spontaneous parametric down-conversion.” In: *Phys. Rev. A* 106 (6 2022), p. 063711. DOI: [10.1103/PhysRevA.106.063711](https://doi.org/10.1103/PhysRevA.106.063711). URL: <https://link.aps.org/doi/10.1103/PhysRevA.106.063711>.

- [116] Pauline Boucher, Hugo Defienne, and Sylvain Gigan. “Engineering spatial correlations of entangled photon pairs by pump beam shaping.” In: *Opt. Lett.* 46.17 (2021), pp. 4200–4203. DOI: [10.1364/OL.425372](https://doi.org/10.1364/OL.425372). URL: <https://opg.optica.org/ol/abstract.cfm?URI=ol-46-17-4200>.
- [117] Eyal Rozenberg, Aviv Karnieli, Ofir Yesharim, Joshua Foley-Comer, Sivan Trajtenberg-Mills, Daniel Freedman, Alex M. Bronstein, and Ady Arie. “Inverse design of spontaneous parametric downconversion for generation of high-dimensional qudits.” In: *Optica* 9.6 (2022), pp. 602–615. DOI: [10.1364/OPTICA.451115](https://doi.org/10.1364/OPTICA.451115). URL: <https://opg.optica.org/optica/abstract.cfm?URI=optica-9-6-602>.
- [118] Nicolas K. Fontaine, Roland Ryf, Haoshuo Chen, David T. Neilson, Kwangwoong Kim, and Joel Carpenter. “Laguerre-Gaussian mode sorter.” In: *Nature Communications* 10.1 (2019), p. 1865. ISSN: 2041-1723. DOI: [10.1038/s41467-019-09840-4](https://doi.org/10.1038/s41467-019-09840-4). URL: <https://doi.org/10.1038/s41467-019-09840-4>.
- [119] Markus Hiekkamäki, Shashi Prabhakar, and Robert Fickler. “Near-perfect measuring of full-field transverse-spatial modes of light.” In: *Opt. Express* 27.22 (2019), pp. 31456–31464. DOI: [10.1364/OE.27.031456](https://doi.org/10.1364/OE.27.031456). URL: <https://opg.optica.org/oe/abstract.cfm?URI=oe-27-22-31456>.
- [120] *The Angular Momentum of Light*. Cambridge University Press, 2012. DOI: [10.1017/CB09780511795213](https://doi.org/10.1017/CB09780511795213).
- [121] Chaitali Joshi, Alessandro Farsi, Stéphane Clemmen, Sven Ramelow, and Alexander L. Gaeta. “Frequency multiplexing for quasi-deterministic heralded single-photon sources.” In: *Nature Communications* 9.1 (2018), p. 847. ISSN: 2041-1723. DOI: [10.1038/s41467-018-03254-4](https://doi.org/10.1038/s41467-018-03254-4). URL: <https://doi.org/10.1038/s41467-018-03254-4>.
- [122] William N. Plick and Mario Krenn. “Physical meaning of the radial index of Laguerre-Gauss beams.” In: *Phys. Rev. A* 92 (6 2015), p. 063841. DOI: [10.1103/PhysRevA.92.063841](https://doi.org/10.1103/PhysRevA.92.063841). URL: <https://link.aps.org/doi/10.1103/PhysRevA.92.063841>.



---

## EHRENWÖRTLICHE ERKLÄRUNG

---

Ich erkläre hiermit ehrenwörtlich, dass ich die vorliegende Arbeit selbstständig, ohne unzulässige Hilfe dritter und ohne Benutzung anderer als der angegebenen Hilfsmittel und Literatur angefertigt habe. Die aus anderen Quellen direkt oder indirekt übernommenen Daten und Konzepte sind unter Angabe der Quelle gekennzeichnet. Bei der Anfertigung dieser Arbeit haben mir meine Betreuer und die Koautoren oben genannter Publikationen geholfen.

Weitere Personen waren an der inhaltlich-materiellen Erstellung der vorliegenden Arbeit nicht beteiligt. Insbesondere habe ich hierfür nicht die entgeltliche Hilfe von Vermittlungs- bzw. Beratungsdiensten (Promotionsberater oder andere Personen) in Anspruch genommen.

Niemand hat von mir unmittelbar oder mittelbar geldwerte Leistungen für Arbeiten erhalten, die im Zusammenhang mit dem Inhalt der vorgelegten Dissertation stehen. Die Arbeit wurde bisher weder im In- noch im Ausland in gleicher oder ähnlicher Form einer anderen Prüfungsbehörde vorgelegt. Die geltende Promotionsordnung der Physikalisch-Astronomischen Fakultät ist mir bekannt.

Ich versichere ehrenwörtlich, dass ich nach bestem Wissen die reine Wahrheit gesagt und nichts verschwiegen habe.

*Jena,*

---

Baghdasar Baghdasaryan